University of Alberta

Characterization of Chemically Bound Thin Films on Carbon Electrodes

By

James Keffa Kariuki

A thesis submitted to the faculty of Graduate studies and Research in Partial fulfillment of the requirements for the degree of Doctor of Philosophy

Department of Chemistry
Edmonton, Alberta, Canada

Fall 2001

National Library of Canada
Acquisitions and Bibliographic Services
395 Wellington Street
Ottawa ON K1A 0N4
Canada

Bibliothèque nationale du Canada
Acquisitions et services bibliographiques
395, rue Wellington
Ottawa ON K1A 0N4
Canada

Your file Votre référence

Our file Notre référence

The author has granted a non-exclusive licence allowing the National Library of Canada to reproduce, loan, distribute or sell copies of this thesis in microform, paper or electronic formats.

L'auteur a accordé une licence non exclusive permettant à la Bibliothèque nationale du Canada de reproduire, prêter, distribuer ou vendre des copies de cette thèse sous la forme de microfiche/film, de reproduction sur papier ou sur format électronique.

The author retains ownership of the copyright in this thesis. Neither the thesis nor substantial extracts from it may be printed or otherwise reproduced without the author's permission.

L'auteur conserve la propriété du droit d'auteur qui protège cette thèse. Ni la thèse ni des extraits substantiels de celle-ci ne doivent être imprimés ou autrement reproduits sans son autorisation.

0-612-68955-7

Canada

University of Alberta

Library Release Form

Name of Author:	James Keffa Kariuki
Title of Thesis:	Characterization of Chemically Bound Thin Films on Carbon Electrodes
Degree:	Doctor of Philosophy
Year this Degree Granted:	2001

Permission is hereby granted to the University of Alberta Library to reproduce single copies of this thesis and to lend or sell such copies for private, scholarly or scientific research purposes only.

The author reserves all other publication and other rights in association with the copyright in the thesis, and except as herein before provided, neither the thesis nor any substantial portion thereof may be printed or otherwise reproduced in any material form whatever without the author's prior written permission.

112 RH, Michener Park
Edmonton, Alberta
Canada T6H 4M4

June 14, 2001

"Mtaka cha mvunguni huinama."
(He who wants what is under the bed must stoop for it.)

University of Alberta

Faculty of Graduate Studies and Research

The undersigned certify that they have read, and recommended to the Faculty of Graduate Studies and Research for acceptance, a thesis entitled "Characterization of Chemically Bound Thin Films on Carbon Electrodes" submitted by James Keffa Kariuki in partial fulfillment of the requirements for the Degree of Doctor of Philosophy.

Dr. Mark T. McDermott

Dr. Fred F. Cantwell

Dr. Charles A. Lucy

Dr. Rik R. Tykwinski

Dr. Doug G. Ivey

Dr. Daniel Bélanger
External Examiner, University of Québec at Montréal

30/04/01
Date

Dedicated to my wife Dolly...
to my children Nancy, Ken, and Naomi...
and to my grandfather for having the vision.

ABSTRACT

Modification of carbon surfaces is of interest to several fields of electrochemistry and material science. A lot of research has been directed towards covalently modified electrodes in order to gain better control as well as a deeper understanding of interfacial reactivity. One of the most versatile methods for modifying carbon surfaces involves the electrochemical reduction of diazonium salts which leads to covalent attachment of aryl radicals onto the carbon surface.

In this work, we utilized scanning force microscopy (SFM), electrochemical studies, and infrared reflectance absorbance spectroscopy (IRRAS) to characterize the thin films formed on carbon from the reduction of diazoniums salts. Studies carried out on highly oriented pyrolytic graphite (HOPG) showed that the initial nucleation of the films started at cleavage steps. Continued deposition resulted in growth onto the supposedly non-reactive basal plane. Features with more than monolayer heights were observed at longer deposition times or at high concentrations of the diazonium salt. The formation of these multilayers was attributed to a polymerization type reaction between the bound monolayer and the free radicals in solution. The multilayers could also be formed on glassy carbon (GC) under certain conditions.

In view of the importance of carbon as a biomaterial, our work was also directed towards the application of the films formed on carbon for controlling protein adsorption. By the use of SFM and IRRAS, it was found that the

conformation of human fibrinogen was dependent on the chemistry of the underlying film. Due to the inherent difficulties of working with carbon electrodes especially for IRRAS studies, these types of studies are usually carried out on metal substrates. However, our studies were carried on a carbon substrate, a more important biomaterial. Importantly, we extended the same modification scheme to a real carbon heart valve. This has important implications toward the production of more biocompatible carbon heart valves.

Acknowledgements

Yes! I did it! However, the preparation of this thesis would not have been possible without the assistance of many people who I wish to thank. I am grateful in measure beyond words to my Ph.D. supervisor, Dr. Mark McDermott. His invaluable guidance, advice, suggestions, and encouragement throughout my stay in his group are greatly acknowledged. Mark guided me through all the carbon "jargon" there is to know and taught me how to see the big picture. Importantly he was there offering support even during those times when I felt I did not deserve any. Thank you Mark for all the reference letters and all those useful suggestions you gave me on "stuff" outside chemistry. It has been a real joy to be part of your group.

I wish to thank all the McDermott group members who traveled with me during this intellectual safari and made my stay in the group enjoyable. I am grateful to the "old guys", Michael, Truong, and Gregory. Your suggestions helped me over a variety of humps, large and small. The memories of the good times will linger with me for a long time. More so, I will not forget that the TSE and the DOW are not for the faint hearted. As well I wish to thank Mirwais, Vishal, Aaron, Francis, and Solomon. Thank you all for useful discussions during my research.

I am indebted to the Department of Chemistry for financial support, and the Natural Science and Engineering Research Council of Canada (NSERC) for funding our research.

I am grateful to the members of my Ph.D. committee for taking the time off their busy schedules to sit in my committee. As well, I thank the faculty, and staff in the Chemistry Department for their assistance in various ways. I would like to thank the staff at the glass, electronic and machine shops in the Chemistry Department, and at the MicroFab, University of Alberta, for their technical support.

It is my greatest pleasure to acknowledge my family without whose love and support I would never have made it this far. I owe much to my wife Dolly, for her constant encouragement and patience throughout my studies. My children Nancy, Ken, and Naomi somehow put up with my busy schedule especially during exam sessions, and for their forbearance, I thank and owe them a lot. Despite all the hard times my mum made sure I become the person I am today. Though she is not here today to share in this moment, this proud moment is hers nevertheless. I wish to thank all my relatives in Kenya and in the USA for offering moral and financial support during my early days. There are too many to mention but I acknowledge the following for their support during my early days; Karis, Rachel, Maingi, Mugambi, Njoroge, Sylvia, John, and especially Lizzie Wanyoike for her unwavering support. I thank my grandparents and my parents-in-law for their unending love, support, and prayers as well as for reminding me always that this accomplishment would not have being possible without God's blessing. I thank many royal friends for their true friendship over the years. At the risk of being incomplete, I would like to mention George (gathee) and Kuria for many years of true friendship. Thank you all.

Last but not least, I wish to thank the following. Dr. Robert More (Medical Carbon Research Institute) for the gift of carbon heart valve samples, Dr. Author Moore (Advanced Ceramics) for the gift of HOPG, and Dr. Arthur Mar (Chemistry Department, University of Alberta) for the use of his furnace to prepare my carbon samples. I also wish to thank Ryan Chowdhury, for his work on the modification of photo resist derived carbon surfaces. I acknowledge Jomo Kenyatta University of Agriculture and Technology for granting me a study leave to undertake my Ph.D. studies. My acknowledgement list is by no means exhaustive. If I forgot your name, please bear with me and accept my thanks.

TABLE OF CONTENTS

CHAPTER I: INTRODUCTION

General Introduction	1
Chemically Modified Electrodes	2
Polymers	4
Monolayers	7
Carbon Electrodes	11
Chemically Modified Carbon Electrodes	15
Modification Carbon Electrodes via Reduction of Diazonium Salts	21
Research Objectives	29
References	30

CHAPTER II: NUCLEATION AND GROWTH OF FUNCTIONALIZED ARYL FILMS ON GRAPHITE ELECTRODES

Introduction	36
Experimental Section	38
Results and Discussion	40
Conclusions	62
References	63

CHAPTER III: FORMATION OF MULTILAYERS ON GLASSY CARBON VIA THE REDUCTION OF DIAZONIUM SALTS

Introduction 66

Experimental 69

Results and Discussion 72

Conclusions 87

References 88

CHAPTER IV: CONTROLLING PROTEIN ADSORPTION AT CARBON SURFACES VIA CHEMICAL MODIFICATION

Introduction 90

Experimental Section 95

Results and Discussion 97

Conclusions 117

References 117

CHAPTER V: APPLICATION OF IRRAS TO STUDY THE EFFECT OF ELECTROCHEMICAL MODIFICATION OF GLASSY CARBON SURFACES ON PROTEIN ADSORPTION

Introduction	120
Experimental Section	122
Results and Discussion	124
Conclusions	134
References	134

CHAPTER VI: ELECTROCHEMICAL STUDIES OF CARBON FILMS FROM PYROLYZED PHOTORESIST AND THEIR APPLICATION AS MODEL BIOMATERIALS

Introduction	137
Experimental Section	140
Results and Discussion	143
Conclusions	165
References	166

CHAPTER VII: CONCLUSIONS AND FUTURE WORK

Overall Conclusions 170

Suggestions for Future Work 172

References 174

LIST OF TABLES

Table 3.1	Band assignments and intensities from the IRRAS spectra of DEA films on GC .	75
Table 3.2	Cyclic voltammetric peak separations for three redox systems at DEA modified GC electrodes.	82
Table 4.1	Results of SFM studies comparing protein aggregate size, number and density on an unmodified HOPG surface and on HOPG surfaces modified by one cycle in 5 mM solutions of NB, PAA, and DDEA respectively.	111
Table 5.1	Table of Amide I and Amide II peak position of HFG adsorbed on various GC surfaces.	128
Table 5.2	Table of Amide I/Amide II ratio of HFG adsorbed on various GC surfaces.	133
Table 6.1	Results from electrochemical characterizations of photoresist-derived carbon films.	157

LIST OF FIGURES

Figure 1.1	A schematic view of a self-assembled monolayer on a gold surface.	8
Figure 1.2	Schematic representations of (A) HOPG, and (B) GC.	12
Figure 2.1	A schematic illustration of the predicted two step attachment process. The first involves the electrochemical generation of aryl radicals followed by their attachment to a carbon surface.	37
Figure 2.2	Cyclic Voltammograms for the reduction of 0.5 mM DDEA.	41
Figure 2.3	Cyclic voltammetry of 1mM $Fe(CN)_6^{-3/-4}$ (1 M KCl) on HOPG.	43
Figure 2.4	Plot of the log of the heterogeneous rate constant, k^0, for $Fe(CN)_6^{-3/-4}$ vs. the number of cycles on HOPG modified in 0.5 mM DDEA.	44
Figure 2.5	Topographic *in situ* SFM images of a HOPG substrate collected in 0.5 mM DDEA.	46
Figure 2.6	Lateral force image of the same region as in Figure 2.5-C.	51
Figure 2.7	Constant current STM image of a HOPG substrate collected in air following 2 deposition cycles from -0.1 V to –0.9 V vs Ag/AgCl in 0.5mM DDEA.	53
Figure 2.8	A schematic illustration of the predicted mode of attachment of free aryl radicals in solution to the aryl moieties attached to the HOPG surface.	55
Figure 2.9	Contact mode SPM image collected in air of a HOPG surface modified using one cycle from -0.1 V to –0.9 V vs Ag/AgCl in 5 mM DDEA.	57

Figure 2.10	Topographic SFM image of a HOPG substrate modified by one cycle from -0.1 V to –0.9 V vs Ag/AgCl in 5 mM DDEA.	59
Figure 2.11	SFM topographic image of a HOPG substrate modified by one cycle from 0.6 V to –0.4 V vs Ag/AgCl in 5 mM NB.	61
Figure 3.1	A schematic illustration of a possible mode of attachment of free aryl radicals in solution to the aryl moieties attached to the HOPG surface.	68
Figure 3.2	IRRAS spectra of a GC electrode modified with a DEA film.	73
Figure 3.3	Topographic SFM image of a GC electrode. The surface contains regions modified with DEA (lighter contrast) adjacent to unmodified polished GC (darker contrast).	78
Figure 3.4	Plot of film thickness against attachment time for DEA films formed on GC with potential steps of 5 mM DDEA.	79
Figure 3.5	Topographic SFM images of a GC electrode. (A) Surface modified with a PAA film. (B) Surface modified with a NB film .	80
Figure 3.6	(A) Topographic image of a polished GC electrode. (B). Topographic image of a GC electrode modified with a DEA film.	85
Figure 4.1	SFM topographic image of an unmodified HOPG substrate. The image was collected in 1mM PBS.(z-scale = 10 nm).	98
Figure 4.2	SFM topographic image of a HOPG substrate modified by one cycle in 5 mM NB	100
Figure 4.3	SFM topographic image of a HOPG substrate modified by one cycle in 5 mM PAA.	101

Figure 4.4	SFM topographic image of HOPG substrate after adsorbing 20 µg/ml BFG for 1 hour.	104
Figure 4.5	SFM topographic images of a HOPG substrate. (A) Surface modified by one cycle in 5 mM NB (B) Same surface after adsorbing 20 µg/mL BFG for one hour.	106
Figure 4.6	SFM topographic images of a HOPG substrate (A) Surface modified by one cycle in 5 mM DDEA (B) Same surface after adsorbing 20 µg/mL BFG for one hour.	107
Figure 4.7	SFM topographic images of a HOPG substrate. (A) Surface modified by one cycle in 5 mM PAA. (B) Same surface after adsorbing 20 µg/mL BFG for one hour.	109
Figure 4.8	Photograph of a carbon heart valve made from LTIC.	113
Figure 4.9	Cyclic voltammogram for the reduction of 5 mM PAA on a heart valve fabricated from LTIC.	114
Figure 4.10	Topographic SFM images. (A). Carbon heart valve. (B). GC electrode.	116
Figure 5.1	IRRAS spectra of various carbon surfaces.	125
Figure 5.2	IRRAS spectra of HFG on GC surfaces modified with a Potential step at –0.6 V in a solution of 5 mM PAA. Spectrum A is after adsorption of 20 µg/mL of HFG. Spectrum B is after adsorption of anti-HFG.	129
Figure 5.3	Bar graph depicting surface chemistry effect on amount of corrected specific binding of anti-HFG to adsorbed HFG.	131
Figure 6.1	Photographs of PDC film substrates.	145
Figure 6.2	SFM images of a PDC substrate obtained in 1 mM PBS. (A): Topographic image (B): Corresponding lateral force image.	146

Figure 6.3	Raman spectra (515 nm) of a PDC film substrate.	148
Figure 6.4	Cyclic voltammogram for the reduction of 5mM PAA on a PDC surface.	150
Figure 6.5	Cyclic voltammetry of 1mM $Fe(CN)_6^{3-/4-}$ (1 M KCl) on PDC.	151
Figure 6.6	Cyclic voltammetry of 1 mM $Ru(NH_3)_6^{2+/3+}$ (1 M KCl) on PDC	153
Figure 6.7	Cyclic voltammetry of 1 mM $Eu^{2+/3+}$ (1 M KCl) on PDC	155
Figure 6.8	SFM images of a PDC substrate obtained in ambient air. (A): Topographic image (B): Corresponding lateral force image.	159
Figure 6.9	SFM topographic image of a PDC substrate obtained following adsorption 0f 20 µg/mL BSA for one hour.	161
Figure 6.10	IRRAS spectra of a PDC substrate following adsorption of 20 µg/mL HFG.	163
Figure 6.11	IRRAS spectra of a PDC substrate following adsorption of 20 µg/mL HFG for one hour.	164

LIST OF SYMBOLS

ν_{aI}	Wavenumber (cm^{-1}) of amide I band
ν_{aII}	Wavenumber (cm^{-1}) of amide II band
ΔE_p	E_{pa} - E_{pc} in cyclic voltammetry
Å	A distance unit (angstroms)
d	Distance
D	Vibrational band in Raman spectroscopy
D_O	Diffusion coefficient for oxidized species
D_R	Diffusion coefficient for reduced species
E_{2g}	Vibrational band in Raman spectroscopy
k	Spring constant
k^0	Heterogeneous rate constant
$k_{app}{}^0$	Apparent heterogeneous rate constant
L_a	Intraplanar microcrystallite size
L_c	Interplanar microcrystallite size
α	Transfer coefficient
β	Tunneling parameter

LIST OF ABBREVIATIONS

AFM	Atomic force microscopy
anti-FN	antibody to fibronectin
anti-HFG	antibody to human fibrinogen
BFG	Bovine fibrinogen
BOE	Buffered oxide etch
BSA	Bovine serum albumin
Bu_4NBF_4	Tetrabutyl ammonium tetrafluoroborate
CH_3CN	Acetonitrile
CMEs	Chemically modified electrodes
DDEA	4-diazo-N,N-diethylaniline tetrafluoroborate
DEA	Diethylaniline
DOPAC	3,4-dihydroxyphenyl acetate
ET	Electron-transfer
FN	Fibronectin
FTIR	Fourier transform infrared spectroscopy
GC	Glassy carbon
HFG	Human fibrinogen
HOPG	Highly oriented pyrolytic graphite
IC	Integrated circuit
IR	Infrared spectroscopy

IRRAS	Infrared reflectance absorbance spectroscopy
LB	Langmuir-Blodgett
LTIC	Low temperature isotropic carbon
MCT	Mercury-cadmium-telluride
MEMS	Microelectromechanical systems
NADH	Nicotinamide adenine dinucleotide
NB	p-nitro benzenediazonium tetrafluoroborate
NHS	N-hydroxysuccinimide
PAA	4-aminophenylacetic acid tetrafluoroborate
PBS	Phosphate buffered saline
PDC	Photoresist-derived carbon
PPY	Polypyrrole
PS	Polystyrene
RBS	Rutherford backscattering
rms	root mean square
SAM	Self-assembled monolayer
SEM	Scanning electron microscopy
SFM	Scanning force microscopy
STM	Scanning tunneling microscopy
TEM	Transmission electron microscopy
XPS	x-ray photoelectron spectroscopy

Chapter I

Introduction

General Introduction

The modification of material interfaces via chemical reactions is crucial to the growth of many areas of importance, including electronics, sensors, biocompatibility, composite materials, chromatography, and chemical and wear resistance. A common goal in all these areas is to develop well-defined chemical reactions, which will form a basis on which new surfaces can be designed rationally for specific tasks. Key to achieving this goal will be to develop methods for surface modification that cleanly and reproducibly introduce well defined chemical entities onto surfaces. In so doing, we can use well-established chemical principles to design surfaces, and then create these surfaces by attaching appropriate molecules [1, 2].

Chemically modified electrodes (CMEs) are prepared by attaching or coating chemicals onto conducting or semiconducting electrodes to give the electrode some desired property. This is important in a number of electrochemically related devices because it is possible to convert, modify, or improve an existing electrode. This is usually desirable because a number of useful properties of a solid material depend upon the nature of the ambient surface layer. These include adhesion, wetting, friction, biocompatibilty, charge and mass transport, and chemical reactivity. Often these properties can be dramatically

altered by the attachment of one or more layers of organic functional groups at the material surface. The variety of possible structures ranges from random arrangements of attached organic functional groups to highly organized, densely packed, ordered molecular assemblies [3].

My thesis describes work carried out to chemically modify carbon electrodes by grafting aryl moieties generated from the reduction of diazonium salts. Electrochemical, scanning force microscopic (SFM) and infrared spectroscopic techniques were utilized to track film formation. The resulting films were used in studies geared towards controlling adsorption of proteins onto the electrodes. Similar studies were also carried out on carbon surfaces generated from the pyrolysis of photoresist. Due to their smooth nature, these electrodes were used as model biomaterial surfaces for protein adsorption studies. Initial studies towards chemically modifying a carbon heart valve were also demonstrated. This may eventually lead to the manufacture of more biocompatible carbon heart valves.

Chemically Modified Electrodes

Three routes to immobilization of reactive substances have been traditionally applied. These routes can be grouped as chemisorption, covalent modification, and attachment of a thin polymer film by chemical or physical deposition routes. Most of the initial work on these modification schemes is covered in a review article by Murray [2]. Since then, several more electrode

modification schemes have been developed. For example, the advent of self-assembled thiol monolayers on gold has also created numerous new possibilities. Multiple modification schemes have also become more common. Current efforts often involve multiple step modification procedures, and synthetic methods, that result in the immobilization of enzymes, proteins, DNA, or other biologically active molecules. Such methods may consist of adsorption followed by derivatization, or application of a thin polymer film. My discussion will include several examples of the methods mentioned above.

Chemisorption refers to strong or irreversible attachment of a substance on an electrode surface. The first demonstrations of such modification were by Lane and Hubbard [4, 5]. The authors demonstrated the tendency of olefins to chemisorb irreversibly on platinum electrodes. This tendency was then exploited to attach a variety of reactive entities to the electrode surface. For example, chelates connected to the electrode surface through an olefinic side chain allowed metals to be selectively chemisorbed at the electrode surface. The influence of chemisorbed olefins having ionic substituents on the rates of electrode reactions of metal complexes was also investigated.

Thin conductive films on various substrates have been widely employed as electrodes. These films have been made from vapor deposited or evaporated noble metals or from thermally decomposed and deposited metal oxides. It is common to surface-modify these oxides by organic compounds or organosilicon

compounds in order to further improve their performance in many applications. Moses and coworkers used silane chemistry to attach amine, pyridine, and ethylenediamine ligands to tin oxide electrodes [6]. Their results demonstrated that tin oxide surfaces exhibited reactivity towards organosilanes quite analogous to that of silica surfaces. The modified surfaces were shown to retain activity toward solution reactants. Electrochemical characteristics of heavily doped tin oxide and indium oxide electrodes have been correlated with results of surface analysis by XPS and Auger spectroscopy. From measurements of current, capacitance, and surface conductance as a function of applied electrode potential, regions where surface reactions were occurring could be delineated [7].

(a) Polymers

Chemically modified electrodes have been prepared by coating electrodes with polymers. If the reagent of interest is incorporated into a polymer matrix, the equivalent of many monolayers of reagent can be immobilized. The polymer adheres on the surface by some combination of adsorption and low solubility in the contacting solvent or by covalent bonding. Polymers have been coated on electrodes by dip [8] and spin coating [9], organosilane bonding [10], electrochemical precipitation [11] and polymerization adsorption from solutions [12], and plasma discharge polymerization [13]. Polymer coatings have been appealing on several accounts. First, immobilization experiments are less demanding than working with monolayers. Secondly, electrochemical responses

are larger since multiple layers of redox sites react. Thirdly, it has been surmised that improved stability results from incorporating reagents into polymers [14]. Polymer films with redox sites called redox polymers conduct electricity via electron hopping between oxidized and reduced states. This is the case with the o-quinone, pyrrole substituted porphyrin, and ferrocene polymers. Electronically conducting polymers, also called organic metals, conduct electricity more efficiently than do redox polymers via delocalized metal-like band structures. One of these, polypyrrole, is quite popular because it is easily formed by electrochemical polymerization, and it can be used to entrap electrocataylsts such as enzymes. Ion-exchange polymer films are made electroactive by exchange of some of their charge-compensating counterions for electroactive ones. An example is exchanging $Fe(CN)_6^{-3}$ for the ClO_4^- counterion of a protonated polyvinylpyridine film [15]. Another example is Nafion which is a perfluorinated ion-exchange polymer which can incorporate large amounts of electroactive species such as ruthenium bypyridine $Ru(bpy)_3^{2+}$ by electrostatic binding and extraction [16]. In the following discussion some of the procedures used to immobilize polymers on various electrodes will be discussed.

Nakahama and Murray have described the effect of composition of a ferrocene-containing redox polymer on the electrochemistry of its thin film coatings on electrodes [17]. A copolymer of vinylferrocene and δ-(methacrylylpropyltrimethoxysilane) was formed as an electroactive, insoluble

film on Pt electrodes by droplet evaporation followed by siloxane cross-linking. The well behaved cyclic voltammetry of these films in acetonitrile depended on the copolymer composition which was varied from 38% to 88% vinylferrocene. A lower percentage of vinylferrocene caused a lower ionic mobility in the films and was manifested by a larger peak potential separation.

Polypyrrole (PPY) is a conducting polymer with a high stability that offers a big field for technical applications. PPY has been one of the most studied polymers because of its physical and electrical properties that have led to several applications such as solid state devices and electronics [18]. It has been found that electrochemically produced PPY films show different structures depending on the preparation methods. Froeck *et al.* have investigated the properties of PPY by use of scanning tunneling microscopy (STM) as well as by atomic force microscopy (AFM) [19]. They showed that different preparation methods of PPY films lead to different surface properties. Films which were polymerized at high current densities showed a rougher microstructure of the surface. Under electrochemical potential controlled conditions, the surface roughness increases when the anodic potential is also increased. The STM and AFM surface structure analysis could be used to explain the polymerization condition from the PPY structures where the preparation method was not known. The electrodeposition of PPY on a platinum (Pt) film on mica has been investigated using *in situ* STM [20]. The changes in surface topography of a Pt electrode during electropolymerization of pyrrole in

acetonitrile were investigated. The electropolymerization of pyrrole was shown to involve cluster formation on the bare Pt substrate and to follow a nucleation-and growth mechanism rather than a layer-by-layer growth of smooth films.

(b) Monolayers

Organized monolayers are single molecular layers in which the constituents share a common orientation. A classic picture of an organized monolayer consists of molecules with identifiable head and tail groups, aligned perfectly on a smooth surface. Monolayers approaching this idealized picture can be deposited by two methods. These are the Langmuir-Blodgett (LB) and self assembly methods [21]. The LB monolayer is transferred to a substrate by contacting the substrate with a compressed organized layer spread on the air-water interface. The head group is generally hydrophilic and the tail group is hydrophobic, so that the orientation of the molecules is achieved prior to the transfer step. A self-assembled monolayer (SAM) is formed by adsorption of molecules onto the substrate from a homogenous solution. Figure 1.1 is a schematic view of a self-assembled monolayer consisting of alkyl chains on a gold surface. The organization is obtained from the affinity of the head group for the substrate combined with the favorable interactions between closed-packed tail groups. Interest in such monolayers stems largely from their characteristic of good structural definition, which provides a needed platform for probing relationships between molecular microstructure on electrode surfaces and macroscopic

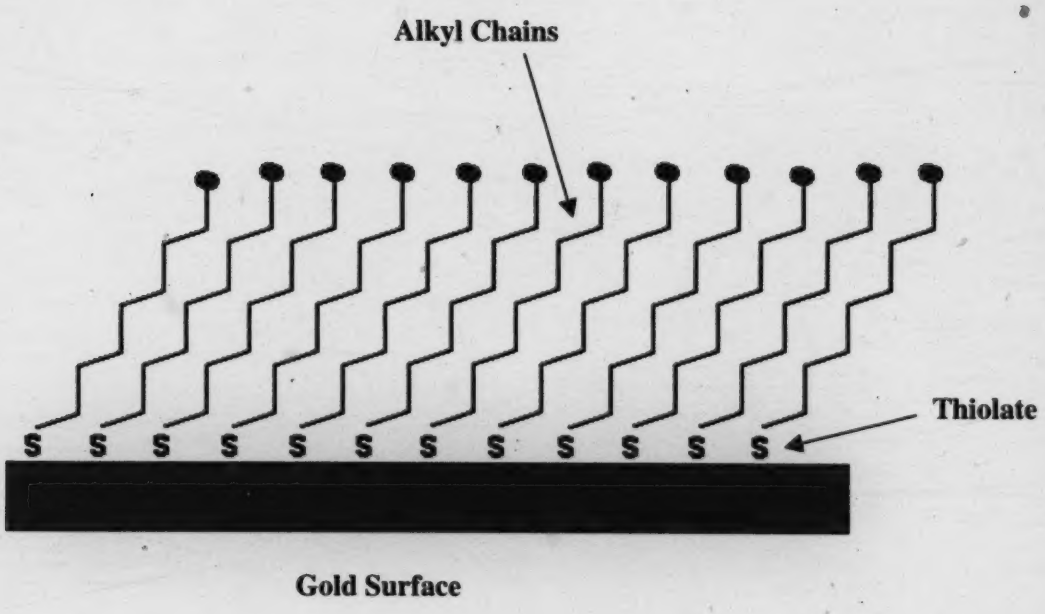

Figure 1.1: A schematic view of a self-assembled monolayer on a gold surface.

electrochemical observables such as electrocatalytic effect and analytical selectivity [22]. The control of molecular microstructure also allows research that addresses the limitations of predicting chemical and physical behavior at interfaces by extrapolation of bulk-phase properties. Importantly, the microstructural definition allowed by self-assembled monolayers has already provided fresh insights into electron-transfer reactions at electrodes and in other areas of interfacial science like adhesion, corrosion inhibition, friction and wear, and microelectrodes [21, 23]. Scientific studies of molecular interactions in thin-film structures have led to an understanding of the collective properties of ordered arrays. Detailed characterization of organic films has only recently been possible by use of a number of the newer surface science techniques. Biological lipid membranes exhibit a variety of different functions, and attempts to produce synthetic thin-film analogues have created a lot of ongoing research. As a result, the physical, chemical, biological and theoretical aspects of thin molecular films have been reviewed [3].

The phenomenon of self-assembly has been known for a long time, but it has not enjoyed the popularity of LB layers until more recently. Work by Sagiv [24, 25] revived interest in SAMs by demonstrating that alkylsilanes could be used to form very stable monolayers on glass or aluminum oxide. Monolayers varying in the degree of their perfection, in terms of a controllable density of uniformly distributed molecular holes, could be easily prepared by this simple adsorption-desorption method. The electrical properties of the organic films were also

investigated. The electrochemical and structural properties of octadecyltrichlorosilane monolayer on gold and platinum electrodes have been studied. Lateral covalent bonding between silanes was shown to be a likely contributor to the stability of the silane monolayer [26].

In recent years, there have been many studies that have explored the applications of monolayers formed by the chemisorption of alkanethiols at gold electrodes. This adsorbate-substrate combination presents a versatile route to creating interfaces that, in comparison with the compositional and morphological heterogeneity of polymers, have a well defined composition, thickness, and spatial arrangement. The system also offers the opportunity to tailor electrode surface structures by varying the length of the alkyl chain and/or altering the tail group. The high affinity of gold and other metals towards sulfur adsorption allows a diverse range of functional groups to be incorporated into the SAM or onto the exposed surface of the SAM. This fact combined with the greater ease of synthesizing and handling molecules with sulfur moieties compared with the hydrolytically sensitive silanes, has led to an extensive research on SAMs [21]. Recognition of this versatile approach can be credited to Allara and Nuzzo [27]. In their work, they showed that gold surfaces could be easily functionalized by disulfide adsorption. Many workers thereafter reported the formation and characterization of thiol SAMs on gold electrodes. They include Whitesides and coworkers [28], Nuzzo and coworkers [29, 30], and Porter and coworkers [31].

In summary self-assembled, chemisorbed monolayers of alkanethiols on metal substrates open exciting new possibilities of engineering smooth surfaces with their chemical properties fine-tuned at the molecular level. These novel systems exhibit a rich variety of packing and ordering phenomena, as a result of competing steric, dispersive, chemisorption, and intramolecular elastic potentials. Hence, these thin films can serve as excellent model systems for evaluating modern theories of wetting, spreading, adhesion, friction, molecular recognition, and related phenomena [32].

Carbon Electrodes

Carbon has been studied extensively as an electrode material for electrosynthesis, electroanalysis, and electrochemical energy conversions for a variety of reasons [33, 34]. The low cost, rich surface chemistry, wide potential range, and compatibility with a variety of electrolytes make carbon an attractive alternative to metals for electrochemistry. Various sp^2 hybridized carbons exist. These include carbon black, glassy carbon (GC), pyrolytic graphite, highly oriented pyrolytic graphite (HOPG), etc. Although the carbon-carbon bonding of all these materials is similar, the bulk properties of the materials vary greatly due to the size and orientation of graphitic crystallites [34]. The microcrystallite size of sp^2 hybridized carbon can be defined by the intraplanar microcrystallite size, L_a, and the interplanar microcrystallite size, L_c. Figure 1.2-A is a schematic representation of a single crystal of graphite. Strictly speaking, L_a is the mean

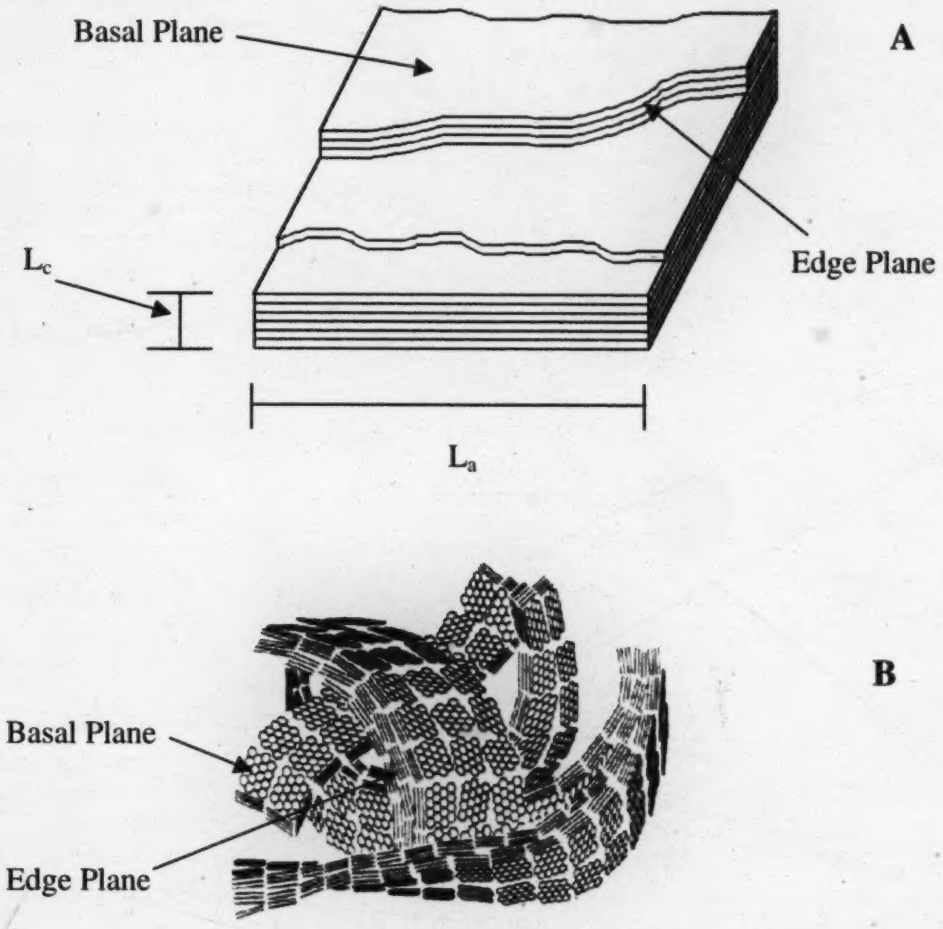

Figure 1.2: Schematic representations of (A) HOPG, and (B) GC.

crystallite size along the basal plane, while L_c is a measure of the thickness of the stacked hexagonal ring layers. My discussion will include properties of GC, HOPG, and of carbon materials that are fabricated from the pyrolysis of photoresist. These three types of carbon were used in my research.

In 1962, starting from phenolic resins, Yamada and Sato, [35] prepared a gas-permeable carbon which they called GC. In their method, a phenol-formaldehyde resin was heated in an inert atmosphere. At temperatures above 300^0C, a carbonization process starts. Hydrogen is gradually eliminated in the temperature range between 500°C and 1200°C and only carbon is left. The carbonization process is accompanied by shrinkage of volume of about 50%. Once the carbonization process is complete, the material is heated slowly under pressure to elevated temperatures, typically in the range of 1000 to 3000^0C. The formation of the final structure of GC has been extensively studied by Jenkins and Kawamura [36] by means of X-ray diffraction, infrared spectroscopy, and by the determination of hardness, Young's modulus and the tensile strength. They concluded from their studies that GC is composed of a ribbon structure which is oriented randomly and are tangled in a complicated manner as shown in Figure 1.1-B. The GC material exhibited low oxidation rate at high temperatures, suggesting a greater inertness to chemical attack than other types of carbon. The use of GC as an electrode material in voltammetric and other studies is widespread due to its wide potential range, relatively low cost, low porosity, and availability

[34, 37, 38]. Figure 1.2-B is a schematic presentation of the structure of GC showing the basal and edge planes.

The importance of the basal and edge plane graphite regions to electrochemical behavior has been identified [39-42]. It has been noted that the distribution of edge and basal plane sites on a carbon surface varies greatly for different carbon substrates and surface preparations. The difficult problem of relating surface structure to electrochemical behavior is significantly simplified by examining a nearly ideal surface, namely, the basal plane of HOPG [43]. The basal plane has a known distribution of carbon atoms and provides a single-crystal analogue of more disordered materials. HOPG is a highly anisotropic material, exhibiting different properties on its basal and edge planes. Physical properties of HOPG such as resistivity, thermal conductivity, thermal expansion, and Young's modulus, display anisotropy with sometimes large differences between the in-plane (a-axis) and out-of-plane (c-axis) directions [34]. Raman spectroscopy of HOPG also depends on this anisotropy with the ratio of 1360 cm^{-1}/1582 cm^{-1} band intensities correlating with the graphitic edge plane density [40].

Recently several studies have been initiated to evaluate thin carbon films produced by the pyrolysis of photoresist as electrode materials and in microelectromechanical systems (MEMS). The first example of fabricating carbon films by pyrolyzing photoresist was reported by Lyons [44]. The advantage of starting with a photoresist is the availability of a wealth of knowledge on forming well-defined microstructures by photolithography techniques. After the

photoresist microstructures are formed, they can be pyrolyzed to produce carbon microstructures which can then serve as microelectrodes. Several studies have been carried out to gauge the utility of pyrolyzed carbon in electrochemical studies. Kinoshita and co-workers first reported the electrochemical properties of pyrolyzed photoresist [45], and Ranganathan, *et al.* have also described several of their electrochemical properties [46]. The surface structure of the films has been characterized using atomic force microscopy (AFM), Raman spectroscopy, X-ray photoelectron spectroscopy (XPS), and cyclic voltammetry [47]. Overall, the surface of the films produced from pyrolysis of the photoresist yielded an electrode surface with properties similar to a very smooth version of GC, but with differences in surface chemistry. Surface functional groups, mainly chemically bound oxygen and oxide species, are known to exist at GC electrode surfaces. These functional groups include phenols, carbonyl, carboxylic acids, and quinones [34].

Chemically Modified Carbon Electrodes

In the following section, methods that have been employed to chemically modify carbon electrodes will be discussed. The discussion will include methods that were developed in the past and the more current ones. However, modification of carbon electrodes via the reduction of diazonium salts will be discussed separately.

The importance of surface chemistry to the electrochemical behavior of carbon electrodes is well established and has been reviewed extensively [33, 34]. The low cost and broad applicability of carbon electrodes, particularly in electroanalysis and electrosynthesis, have driven years of research to find the relationship between surface structure and electrochemical phenomena, particularly adsorption, heterogeneous electron transfer, and surface stability. Because the carbon surface varies greatly with origin, it is often desirable to modify the surface with an aim of producing a well-defined reproducible electrode [34]. Procedures for immobilizing reagents on carbon electrodes have been devised at a steady pace and now include several types of covalent attachment. These result in the formation of a covalent bond between the electrode surface and the modifier of interest. Two methods of covalent attachment have been employed in the chemical modification of carbon electrodes. These are derivatization of existing functional groups, and covalent attachment directly to the carbon backbone via a carbon-carbon bond. Several derivatization methods have been described for the modification of carbon surfaces. These methods include amidation, esterification, silanization, and ether bond formation. However these methods are not exclusive to carbon electrodes as the derivitazation of tin-oxide, titanium oxide, and ruthenium oxide electrodes by silanization have also been investigated [14].

Watkins *et al.* were the first to demonstrate the principle of covalently modified carbon electrodes. They reported the binding of optically active amino

acids on graphite via amide bonds, producing a stable, chiral interfacial region for electrochemical reactions [48]. Thereafter, Elliot and Murray chemically employed organosilane chemistry to prepare chemically modified carbon and graphite electrodes with surface bound amine, ethylenediamine, pyridine, and alkyl chloride groups. The resulting surfaces were studied by X-ray photoelectron spectroscopy (XPS) as well as by the chemical properties of the functional groups such as protonation, Cu(II) coordination, and amidization reactions. The modified electrodes retained electrochemical reactivity toward solution reactants and were themselves electrochemically stable [49].

Glassy carbon (GC) surfaces can be oxidized to produce interfacial carbonyl or carboxyl groups. The occurrence of these carboxyl groups forms the basis of a class of chemically modified electrodes introduced by Lennox and Murray [50]. In a preliminary report, they used thionyl chloride activation of a thermally oxidized GC electrode to chemically bind electrochemically reactive reagents to GC surfaces. Using this method, they attached a tetraphenylporphyrin ring to a GC surface. Due to the well-behaved non-aqueous solution electrochemistry of the ring, subsequent metallation of the immobilized porphyrin and similar molecular systems are known to exert potentially useful electrocatalytic effects.

Other redox systems attached to carbon by surface amide bonds include ruthenium pyridine complexes described by Anson and co-workers [51]. Cyclic voltammetry was used to compare the electrochemical behavior of the attached

complexes and to measure their concentrations. Murray and co-workers have demonstrated the activation of GC by mechanical abrasion and by etching with a radio-frequency argon plasma. In both cases the surface oxides were removed and, at the same time, the reactivity of the surface carbon was increased so that ferrocene or pyridine could be attached directly via a vinyl coupling [13].

One of the more chemically innovative modified electrodes was directed towards the four-electron reduction of dioxygen to water. Collman and co-workers [52] synthesized a series of dimeric metalloporphyrins in which the two porphyrin rings were constrained to lie parallel to one another by amide bridges of varying lengths that linked the rings together. These co-facial metalloporphyrins were then applied to the surface of graphite electrodes and all showed catalytic activity.

Among the numerous composite materials involving an organic matrix, those obtained from carbon fibers and epoxy resins are of particular interest, especially in the fabrication of components for the aerospace industry. The mechanical properties of composite materials depend not only on the components, but also on the interface. Therefore, the chemical modification of carbon fibers is an important step in the fabrication process. Recently a novel method has been devised for modifying carbon fibers [53]. The method is based on the electrooxidation of amine-containing compounds. The method proceeds via a one-electron oxidation of an amine functionality to its corresponding cation radical, which subsequently forms a carbon-nitrogen linkage at the carbon surface.

Antoniadou *et al.* have examined the grafting of ethylenediamine to carbon fibers [54]. They titrated a ground sample of ethylenediamine modified carbon fiber with hydrochloric acid to establish the amount of amine on the surface. Based on the electrochemically active surface area, they deduced that more than a monolayer of ethylenediamine molecules is attached during modification. Park and Donnet have examined the effect of amine modification on the acid-base interactions between carbon fibers and an epoxy matrix [55]. Modification with ethylenediamine and triethylene tetramine significantly increased the basicity of the fibers and strengthened their acid-base interaction with the matrix. This was in turn reflected in increases in the interfacial shear strength of the fibers and the interlaminar shear strength of the composites.

Deinhammer and co-workers have employed the oxidation of amines to modify GC electrodes for electrocatalytic and biosensor purposes [56]. They immobilized dopamine on the GC surface, which facilitated the oxidation of β-nicotinamide adenine dinucleotide (β-NADH). The applicability of the method for the construction of biosensors that are based on biotin-avidin complexation was also demonstrated. Downard and Mohamed utilized the method to suppress protein adsorption at GC electrodes [57]. They modified the electrodes with tetraethylene glycol diamine. The modified surfaces showed resistance to protein adsorption while retaining electrochemical properties.

Anodic oxidation of GC electrodes in 1-alkanol containing sulfuric acid has been demonstrated. The method allows the alkanol molecules to be confined on

the electrode via an ether linkage [58-60]. Such modified GC surfaces have been used to suppress electrode fouling originating from adsorbed proteins in electrochemical measurements of biological fluids. Andrieux and co-workers have shown that the anodic oxidation of aryl acetic acids on carbon electrodes leads to attachment of an aryl radical onto the carbon surface [61]. The starting materials are easily accessible, and the presence of appropriate substituents on the phenyl ring makes this type of derivatization a convenient starting point for further chemical modifications. Chemical modification of carbon electrodes via the reaction of N-hydroxysuccinimide (NHS) esters with freshly polished GC surfaces has been demonstrated [62]. It was shown that the derivatization results from the formation of a covalent peptide linkage by reaction of the NHS ester with superficial amino groups on the GC surface. Since many NHS esters of biomolecules are available or can be easily prepared, the method affords a strategy that could be used to bind biomolecules directly to the carbon surface.

Derivatization of carbon electrodes using biotin hydrazide has recently been reported [63, 64]. The method indicates that hydrazines may be another class of compounds which on electrolysis, lead to covalently attached monolayers. In this work, it was shown that biotin could be covalently attached to GC surfaces from pH 9.0 borate buffer by using the scanning electrochemical microscope probe tip as an electrochemical pen [64]. Hayes and Kuhr attached biotin to a carbon fiber surface via reduction of biotin hydrazide in phosphate buffer [63]. Although the nature of the surface attachment had not been characterized, after considering the

impact of modification on NADH voltammetry, it was concluded that reaction between the hydrazide and a surface carbonyl was not likely and a covalent bond with a surface carbon was a possibility.

Modification of Carbon Electrodes via Reduction of Diazonium Salts

The following discussion will focus on applications of carbon surfaces modified via electrochemical reduction of diazonium salts. This modification scheme was used in my work. Delamar *et al.* recently reported a method that allows for covalent attachment of a wide variety of functionalized aryl groups on carbon through the electrochemical reduction of the corresponding diazonium salt [65]. Once attached to the carbon surface, the functionalized aryl groups can be modified by classical chemical reactions. Hence the method presents a facile and versatile means to derivatize carbon electrodes. Various carbon materials including HOPG, GC and carbon fibers have been derivatized using this method. Aryl films exposing a variety of functional groups have been utilized in diverse applications that include controlling protein adsorption, controlling electron transfer, and improving the mechanical properties of carbon-epoxy composites. A recent review by Downard summarizes the various applications of the method [66].

Carbon electrodes modified via the reduction of diazonium salts method have been investigated and characterized. X-ray photoelectron spectroscopy (XPS) [65, 67-75], Rutherford backscattering (RBS) [68], infrared reflectance

absorbance spectroscopy (IRRAS) [68], Auger spectroscopy [68], unenhanced Raman spectroscopy [72-76], scanning tunneling microscopy (STM) [68, 77, 78], and scanning force microscopy (SFM) [77] have been used for surface analysis.

Electrodes modified via the electrochemical reduction of diazonium salts have been found to be stable to long term storage in air and to sonication in various organic solvents. Basal plane HOPG modified with 4-nitrophenyl moieties showed the N peak in the Auger spectrum even after the HOPG was heated to 700 K. It disappeared only at 1400 K [68]. The stability of the thin films can be attributed to the formation of a covalent bond between the carbon electrode and the aryl group. Raman spectroscopy has provided evidence for freely rotating surface groups, consistent with a single C-C bond between the surface and the modifier [73].

Evidence has been presented that indicates that edge plane carbons are more reactive towards diazonium radicals coupling than basal plane carbons. For example Allongue *et al.* have used cyclic voltammetry to show that on GC, which has a higher density of edge planes, about 84% of electrochemically generated radicals couple to the surface compared with about 56% at basal plane HOPG [68]. A faster rate of derivatization at edge plane HOPG has also been reported by McCreery and co-workers using unenhanced Raman spectroscopy, cyclic voltammetry, and XPS to study modified carbon surfaces [72, 76]. Spatially resolved Raman spectra established the location and density of nitrobenzene modifiers on GC and HOPG surfaces [76]. An even coverage was observed at the

GC electrode surface, whereas at basal plane HOPG, a short reduction time of the diazonium salt resulted in nitrobenzene attached predominantly at basal plane defects. Longer electrolysis times resulted in attachment to the basal plane but at a lower coverage than at edge plane sites.

Modification of H-terminated GC (HGC) via reduction of 4-nitrobenzene diazonium in anhydrous conditions has been reported [75]. HGC was produced by exposing GC to a hydrogen plasma, thus generating a low O: C ratio and, presumably, surface C-H bonds. The proposed mechanism for nitrophenyl modification involves abstraction of a H-atom by a nitrophenyl radical forming a surface carbon radical and nitrobenzene. A second nitrophenyl radical could then couple to the surface via reaction with the surface radical. Kuo *et al.* have demonstrated that boron doped diamond electrodes can also be covalently modified with aryl groups using the diazonium reduction strategy [74]. Surface coverages were estimated to be 50-70% of a close packed monolayer consistent with modification involving sp^3 hybridized surface carbon.

The reductive electrochemistry of 4–nitrophenyl modified electrodes in protic solvents has been examined by several workers [65, 68-70, 72, 79]. For example, in aqueous acid, Saby *et al.* observed that in addition to reduction of the nitro substituent to the amine, the intermediate NHOH/NO redox couple was also formed [70]. XPS investigations indicated that only a fraction of the nitro groups were reduced. Yang and McCreery showed that a nitrophenyl monolayer chemisorbed on GC decreased the heterogeneous rate constant (k°), of

phenothiazine derivatives by 50%. A through-bond electron-tunneling mechanism for electron transfer was adduced to explain the observation [79].

The importance of surface chemistry to the electrochemical behavior of carbon electrodes is well established and has been reviewed extensively [33, 34]. In order to relate carbon structure to electron transfer activity, Chen and McCreery grafted nitrophenyl groups to GC and examined the effect on the electrochemistry of a variety of solution species [80]. Nitrophenyl was assumed to be a nonspecific adsorber which increased the distance for electron transfer, but not react preferentially with surface oxides. Based on results obtained at several different modified electrodes, redox couples could be categorized according to the effects of surface modification on their kinetics. McCreery and co-workers have also utilized a nitrophenyl monolayer on GC to help elucidate the mechanism of oxygen reduction at different carbon surfaces [81]. Surface modification was found to decrease the reduction rate, presumably by decreasing the amount of $O_2^{\cdot}$ reduction.

Saby *et al.* compared the barrier properties of 4-carboxyphenyl and 4-nitrophenyl modified GC electrodes [70]. The background currents at the modified electrodes were very small, consistent, with a compact, poorly solvated layer on the electrode. This film structure was proposed to account for the barrier properties of both types of modification toward ferrocene and $Fe(CN)_6^{3-}$. In aqueous media, the 4-carboxyphenyl coating is expected to be neutral at low pH, and to have an increasing negative charge with increasing pH. The responses of

$Fe(CN)_6^{3-}$ and $Ru(NH_3)_6^{3+}$ reflected these changes in surface charge and hydrophobicity. Investigation of the barrier properties of a reduced 4-nitrophenyl layer in aqueous acid was undertaken by the same workers [71]. After reduction of the nitro moiety to the NH_2/NHOH/NO functionalities, the barrier properties with respect to $Fe(CN)_6^{3-}$, $Ru(NH_3)_6^{3+}$, and hydroquinone were consistent with increased hydrophobicity and a positive surface charge.

Yang and McCreery have carried out studies on electron transfer across hydrophobic, insulating layers of varying thickness [79]. The redox systems studied were methyl viologen and four phenothiazine derivatives. Several different monolayers were attached to yield estimated thicknesses ranging from 5.9 Å to 14.0 Å. From their work a tunneling parameter β, of 0.2 Å consistent with values of 0.14-0.57 Å which have been estimated for through-bond tunneling in conjugated, unsaturated monolayers on metal electrodes was obtained.

The barrier properties of 4-phenylacetic modified electrodes have been examined at pH 7.4 where the layer bears a negative charge [82]. The voltammetric behaviors of the catechol derivatives, dopamine, 4-methylcatechol, and 3,4-dihydroxyphenyl acetate (DOPAC) were compared at polished and modified GC electrodes. Phenyl acetate modification increased the apparent rate of electron transfer for dopamine, decreased the rate for DOPAC and had no effect on the cyclic voltammetric response for 4-methylcatechol. Electrostatic interactions between the modifying layer and the solution species appeared to influence the electrode kinetics. Downard and Roddick have investigated the

influence of hydrophobic electrode coatings on carbon [83]. Modification of GC with p-methylphenyl monolayers had little influence on the voltammetry of outer-sphere, hydrophobic analytes chlorpromazine and iron(II)-tris-2,2′-bipyridine, but drastically retarded the apparent electron transfer kinetics of $Fe(CN)_6^{3-}$, ascorbic acid and uric acid.

Chemical modification of silicon surfaces via the reduction of diazonium salts has been carried out. For example, reduction of diazonium salts in aqueous 0.1 M H_2SO_4/HF mixture at H-terminated Si(111) surfaces resulted in the formation of a covalently attached layer of aryl groups [84, 85]. Characterization of the appropriate modified surfaces by XPS, RBS, voltammetry, FTIR, and STM pointed to monolayer coverage of groups attached via Si-C bonds. The proposed mechanism was the same as that for H-terminated GC surfaces. It proceeds via formation of an aryl radical which abstracts H from the surface producing a Si radical which couples with a second aryl radical giving a Si-C bond.

The adsorption of proteins onto electrode surfaces complicates the application of voltammetric techniques to clinical samples. Downard and Roddick modified GC electrodes by covalently binding p-substituted aryl groups via the reduction of the corresponding diazonium salt [86]. Their findings showed that hydrophilic groups attached to the surface reduced bovine serum albumin (BSA) adsorption. Voltammetry of hydroxymethylferrocene was used as a probe of surface fouling. Modification of GC electrodes with phenylacetate showed little impact on the voltammetry of hydroxymethylferrocene but significantly reduced

the impact of BSA adsorption. By examining the effects of a range of surface modifications, the authors concluded that hydrophilic groups that extend a sufficient distance from the electrode surface reduce protein adsorption while surface hydrophobicity promoted protein adsorption. The modified electrode could be used for analysis of clinical samples with reduced electrode fouling.

Bourdillon *et al.* have utilized phenylacetate modified electrodes for the immobilization of glucose oxidase onto GC electrodes [67]. After grafting of the phenylacetate layer by reduction of the corresponding diazonium salt, the enzyme was coupled via amide bond formation. The coverage of active enzyme per unit of effective area was similar to that achieved by a method based on oxidative generation of carboxylate groups on the carbon surface. An advantage of the method compared to oxidative treatment is that diazonium reduction does not lead to surface roughening and large background currents. Hence it should allow for the design of customized enzyme linkages. Dequaire *et al.* have used this approach to attach p-benzoyl biocytin to a screen-printed graphite electrode by reduction of a diazonium derivative [87]. The modified electrodes were reacted with extravidin followed by biotinylated alkaline phosphatase. Biotinylated screen-printed electrodes could be regenerated by removal of avidin in a solution of guanidine hydrochloride, thus allowing reuse of the electrodes.

Amperometric detection is commonly utilized with flow analytical techniques such as flow injection analysis, ion chromatography, and high performance liquid chromatography. Amperometric flow detectors with

selectivity based on hydrophobicity and charge have been prepared using the electrochemical reduction of diazonium salts [83]. At p-alkylphenyl monolayers, the sensitivity ratio for chlorpromazine to uric acid obtained from amperometric measurements was significantly enhanced over that observed at the polished electrode. At the phenylacetate monolayers, the sensitivity ratios for acetaminophen to uric acid and acetaminophen to ascorbic acid are enhanced over the polished electrode values. These results were explained by considering the impact of the hydrophobicity and charge of the monolayer and analyte. The ability of phenylacetate monolayers to protect surfaces from protein adsorption was also used by Parker and co-workers [88]. The aim of their work was to study electron transfer between redox proteins and redox mediators by analyzing the changes in the voltammetric response of the mediators in the presence of the protein. Use of phenylacetate modified electrodes prevented unwanted adsorption of ferri- and ferro-cytochrome c, while enabling well-defined voltammograms to be obtained for the mediator couple.

Liu *et al.* used the diazonium reduction method as a first step to constructing stable heteropolyanion-modifed electrodes [78, 89]. Nitrophenyl modified GC, HOPG and carbon fiber microdisk array electrodes were reduced to give aminophenyl modified surfaces. Potential scanning in an acidic solution of 12-tungstosilicic acid resulted in formation of SiW_{12}/aminophenyl modified electrodes, in which electrostatic interactions were proposed to lead to electrodeposition of the inorganic layer. At pH less than 2, the modified electrode

showed good stability and catalyzed the reduction of nitrite. Thus this strategy may be useful for the construction of other heteropolyanion modified electrodes with applications in catalysis-based sensing.

Research Objectives.

The modification of carbon electrodes via the reduction of diazonium salts is now commonly used, due its simplicity and flexibility. Previously films formed on carbon surfaces were characterized using voltammetry or spectroscopy. The goal of my research is to extend these film characterizations to a more local scale. I utilized SFM, STM, electrochemical studies, and IRRAS to provide both a macroscopic and microscopic picture of the development of the films on carbon surfaces. My initial research was to characterize the formation of the thin films on a well-ordered HOPG surface, and then extend the same to the more widely used GC surface.

Blood compatibility of the carbon surfaces is a widely studied subject. It is believed that the interaction of plasma proteins with a surface is critical in determining the biocompatibility of materials. In view of this, I applied the reduction of diazonium salts to modify carbon surfaces for controlling protein adsorption. The goal is to develop a methodology to produce surfaces that in future can be used in the manufacture of prosthetic implants, or as electrochemical probes that show limited protein adsorption in biological fluids. The well-established methods of SFM and IRRAS are used to probe surface-protein

interactions both at a microscopic and at a macroscopic scale. The work described in the following chapters describes my efforts toward these goals.

References

1. M. S. Wrighton, *Science* 231: 32 (1986).

2. R. W. Murray, in *Electroanalytical Chemistry*, Vol. 13 (A. J. Bard, ed.), Marcel Dekker, New York, 1984, p. 191.

3. J. D. Swalen, D. L. Allara, J. D. Andrade, E. A. Chandross, S. Garoff, J. Israelachvili, T. J. McCarthy, R. Murray, R. F. Pease, J. F. Rabolt, K. J. Wynne, and H. Yu, *Langmuir* 3 : 932 (1987).

4. R. F. Lane and A. T. Hubbard, *J. Phys. Chem.* 77 : 1401 (1973).

5. R. F. Lane and A. T. Hubbard, *J. Phys. Chem.* 77: 1411 (1973).

6. P. R. Moses, L. Wier, and R. W. Murray, *Anal. Chem.* 47: 1882 (1975).

7. N. R. Armstrong, A. W. C. Lin, M. Fujihira, and T. Kuwana, *Anal. Chem.* 48: 741 (1976).

8. L. L. Miller and M. R. Van De Mark, *J. Am. Chem. Soc.* 100: 639 (1978).

9. H. Tachikawa and L. R. Faulkner, *J. Am. Chem. Soc.* 100: 4379 (1978).

10. K. Itaya and A. J. Bard, *Anal. Chem.* 50: 1487 (1978).

11. A. Merz and A. J. Bard, *J. Am. Chem. Soc.* 100: 3222 (1978).

12. N. Oyama and F. C. Anson, *J. Am. Chem. Soc.* 101: 739 (1979).

13. R. Nowak, F. A. Schultz, M. Umana, H. Abruna, and R. W. Murray, *J. Electroanal. Chem.* 94: 219 (1978).

14. R. W. Murray, *Acc. Chem. Res.* 13: 135 (1980).

15. R. W. Murray, A. G. Ewing, and R. A. Durst, *Anal. Chem.* 59: 379A (1987).

16. H. S. White, J. Leddy, and A. J. Bard, *J. Am. Chem. Soc.* 104: 4811 (1982).

17. S. Nakahama and R. W. Murray, *J. Electroanal. Chem.* 158: 303 (1983).

18. M. C. Montemayor, L. Vazquez, and E. Fatas, *J. Appl. Phys.* 75: 1849 (1994).

19. C. Froeck, A. Bartl, and L. Dunsch, *Electrochimica Acta* 40: 1421 (1995).

20. F.-R. F. Fan and A. J. Bard, *J. Electrochem. Soc.* 136: 3216 (1989).

21. H. O. Finklea, in *Electroanalytical Chemistry: A series of Advances*, Vol. 19 (A. J. Bard and I. Rubenstein, eds.), Marcel Dekker, Inc., New York, 1996, p. 110.

22. A. Ulman, *Chem. Rev.* 96: 1533 (1996).

23. A. J. Bard, H. D. Abruna, C. E. Chidsey, L. R. Faulkner, S. W. Feldberg, K. Itaya, M. Majda, O. Melroy, R. W. Murray, M. D. Porter, M. P. Soriaga, and H. S. White, *J. Phys. Chem.* 97: 7147 (1993).

24. J. Sagiv and E. E. Polymeropoulos, *J. Chem. Phys.* 69: 1836 (1978).

25. J. Sagiv, *J. Am. Chem. Soc.* 102: 92 (1980).

26. H. O. Finklea, L. R. Robinson, A. Blackburn, and B. Richter, *Langmuir* 2: 239 (1986).

27. R. G. Nuzzo and D. L. Allara, *J. Am. Chem. Soc.* 105: 4481 (1983).

28. G. M. Whitesides and P. E. Laibinis, *Langmuir* 6: 87 (1990).

29. L. H. Dubois and R. G. Nuzzo, *Annu. Rev. Phys. Chem.* 43: 437 (1992).

30. R. G. Nuzzo, F. A. Fusco, and D. L. Allara, *J. Am. Chem. Soc.* 109: 2358 (1987).

31. M. D. Porter, T. B. Bright, D. L. Allara, and C. E. D. Chidsey, *J. Am. Chem. Soc.* 109: 3559 (1987).

32. A. Ulman, *An Introduction to Ultrathin Organic Films from Lagmuir-Blodgett to Self-Assembly*, Academic Press, Inc., New York, 1991.

33. K. Kinoshita, *Carbon: Electrochemical and Physicochemical Properties*, Wiley, New York, 1988.

34. R. L. McCreery, In *Electronalytical Chemistry*, Vol. 17 (A. J. Bard, ed.), Marcel Dekker, New York, 1991, p. 221.

35. S. Yamada and H. Sato, *Nature* 193: 261 (1962).

36. G. M. Jenkins and K. Kawamura, *Nature* 231: 175 (1971).

37. W. E. Linden Van Der and J. W. Dieker, *Anal. Chim. Acta* 119: 1 (1980).

38. H. E. Zittel and F. J. Miller, *Anal. Chem.* 37: 200 (1965).

39. J.-P. Randin and E. Yeager, *J. Electroanal. Chem.* 58: 313 (1975).

40. R. J. Bowling, R. T. Packard, and R. L. McCreery, *J. Am. Chem. Soc.* 111: 1217 (1989).

41. R. J. Rice and R. L. McCreery, *Anal. Chem.* 61: 1637 (1989).

42. R. M. Wightman, M. R. Deakin, P. M. Kovach, W. G. Kuhr, and K. J. Sturts, *J. Electrochem. Soc.* 131: 1578 (1984).

43. M. T. McDermott, K. Kneten, and R. L. McCreery, *J. Phys. Chem.* 96: 3124 (1992).

44. A. M. Lyons, L. P. Hale, and C. W. Wilkins, *J. Vac. Sci. Technol.* B 3 (1): 447 (1984).

45. J. Kim, X. Song, K. Kinoshita, M. Madou, and R. White, *J. Electrochem. Soc.* 145: 2314 (1998).

46. S. Ranganathan, R. L. McCreery, S. M. Majji, and M. Madou, *J. Electrochem. Soc.* 147(1): 277 (2000).

47. S. Ranganathan and R. L. McCreery, *Anal. Chem.* 73: 893 (2001).

48. B. F. Watkins, J. R. Behling, E. Kariv, and L. L. Miller, *J. Am. Chem. Soc.* 97: 3549 (1975).

49. C. M. Elliott and R. W. Murray, *Anal. Chem.* 48: 1247 (1976).

50. J. C. Lennox and R. W. Murray, *J. Electroanal. Chem.* 78: 395 (1977).

51. C. A. Koval and F. C. Anson, *Anal. Chem.* 50: 223 (1978).

52. J. P. Collman, P. Denisevish, Y. Konai, M. Marrocco, C. Koval, and F. Anson, *J. Am. Chem. Soc.* 102: 6027 (1980).

53. B. Barbier, J. Pinson, G. Desarmot, and M. Sanchez, *J. Electrochem. Soc.* 137: 1757 (1990).

54. S. Antoniadou, A. D. Jannakoudakis, and P. D. Jannakoudakis, *J. Appl. Electrochem.* 22: 1060 (1992).

55. S. J. Park and J. P. Donnet, *J. Colloid Interface Sci.* 206: 29 (1998).

56. R. S. Deinhammer, M. Ho, J. W. Anderegg, and M. D. Porter, *Langmuir* 10: 1306 (1994).

57. A. J. Downard and A. B. Mohamed, *Electroanalysis* 11: 418 (1999).

58. H. Maeda, Y. Yamauchi, M. Hosoe, T.-X. Li, E. Yamaguchi, M. Kasamatsu, and H. Ohmori, *Chem. Pharm. Bull.* 42: 1870 (1994).

59. H. Maeda, T. Kitano, C. Z. Huang, K. Katayama, Y. Yamauchi, and H. Ohmori, *Anal. Sci.:* 531 (1999).

60. H. Maeda, M. Itami, K. Katayama, Y. Yamauchi, and H. Ohmori, *Anal. Sci.* 13(5): 721 (1997).

61. C. P. Andrieux, F. Gonzalez, and J. M. Saveant, *J. Am. Chem. Soc.* 119: 4292 (1997).

62. A. Anne, B. Blanc, J. Moiroux, and J.-M. Saveant, *Langmuir* 14: 2368 (1998).

63. M. A. Hayes and W. G. Kuhr, *Anal. Chem.* 71: 1720 (1999).

64. W. B. Nowall, D. O. Wipf, and W. G. Kuhr, *Anal. Chem.* 70: 2601 (1998).

65. M. Delamar, R. Hitmi, J. Pinson, and J.-M. Saveant, *J. Am. Chem. Soc.* 114: 5883 (1992).

66. A. J. Downard, *Electroanalysis* 12(14): 1085 (2000).

67. C. Bourdillon, M. Delamar, C. Demaille, R. Hitmi, J. Moiroux, and J. Pinson, *J. Electroanal. Chem.* 336: 113 (1992).

68. P. Allongue, M. Delamar, B. Desbat, O. Fagebaume, R. Hitmi, J. Pinson, and J.-M. Saveant, *J. Am. Chem. Soc.* 119: 201 (1997).

69. M. Delamar, G. Desarmot, O. Fagebaume, R. Hitmi, J. Pinson, and J.-M. Saveant, *Carbon* 35: 801 (1997).

70. C. Saby, B. Ortiz, G. Y. Champagne, and D. Belanger, *Langmuir* 13: 6805 (1997).

71. B. Ortiz, C. Saby, G. Y. Champagne, and D. Belanger, *J. Electroanal. Chem.* 455: 75 (1998).

72. Y.-C. Liu and R. L. McCreery, *J. Am. Chem. Soc.* 117: 11254 (1995).

73. Y.-C. Liu and R. L. McCreery, *Anal. Chem.* 69: 2091 (1997).

74. T.-C. Kuo, R. L. McCreery, and G. M. Swain, *Electrochem. & Solid-State Lett.* 2: 288 (1999).

75. C.-T. Kuo and R. L. McCreery, *Anal. Chem.* 71: 1553 (1999).

76. K. Ray and R. L. McCreery, *Anal. Chem.* 69: 4680 (1997).

77. J. K. Kariuki and M. T. McDermott, *Langmuir* 15: 6534 (1999).

78. S. Liu, Z. Tang, Z. Shi, L. Niu, E. Wang, and S. Dong, *Langmuir* 15: 7268 (1999).

79. H.-H. Yang and R. L. McCreery, *Anal. Chem.* 71: 4081 (1999).

80. P. Chen and R. L. McCreery, *Anal. Chem.* 68: 3958 (1996).

81. J. Xu, W. Huang, and R. L. McCreery, *J. Electroanal. Chem.* 410 (1996).

82. A. J. Downard, A. D. Roddick, and A. M. Bond, *Anal. Chim. Acta* 317: 303 (1995).

83. A. J. Downard and A. D. Roddick, *Electroanalysis* 9: 693 (1997).

84. C. Henry de Villeneuve, *J. Phys. Chem. B* 101: 2415 (1997).

85. P. Allongue, C. Henry deVilleneuve, J. Pinson, F. Ozanan, J. N. Chazalviel, and X. Wallart, *Electrochimica Acta.* 43: 2791 (1998).

86. A. J. Downard and A. D. Roddick, *Electroanalysis* 7: 376 (1995).

87. M. Dequaire, C. Degrand, and B. Limoges, *J. Am. Chem. Soc.* 121: 6946 (1999).

88. V. D. Parker, A. Roddick, L. C. Seefeldt, H. Wang, and G. Zheng, *Anal. Biochem.:* 212 (1997).

89. S. Liu, Z. Shi, and S. Dond, *Electroanalysis* 10: 891 (1998).

Chapter II

Nucleation and Growth of Functionalized Aryl Films on Graphite Electrodes*

Introduction

This chapter describes the nucleation and growth of functionalized aryl films on ordered graphite. The attachment of aryl groups to carbon surfaces is induced by the electrochemical reduction of the corresponding diazonium salt.

The binding of aryl groups to carbon electrodes is likely a two step process involving the electrochemical generation of aryl radicals which subsequently react with the surface as depicted in Figure 2.1. It is speculated that the aryl radicals may form through a diazenyl radical intermediate [1-4]. Electrochemical and spectroscopic characterizations indicate that the resulting layers are covalently bound at a coverage very close to a theoretical monolayer [5, 6]. The method in Figure 2.1 has been employed to derivatize the surfaces of glassy carbon (GC) [6], highly oriented pyrolytic graphite (HOPG) [5] and carbon fibers [7]. Aryl films exposing a variety of functional groups have been utilized in applications focused on controlling protein adsorption [8], controlling electron transfer [9, 10] and demonstrations of Raman spectroscopic instrumentation [11] and methodology [12].

---

* A form of this chapter has been published in *Langmuir*, **1999**, 15, 6534-6540

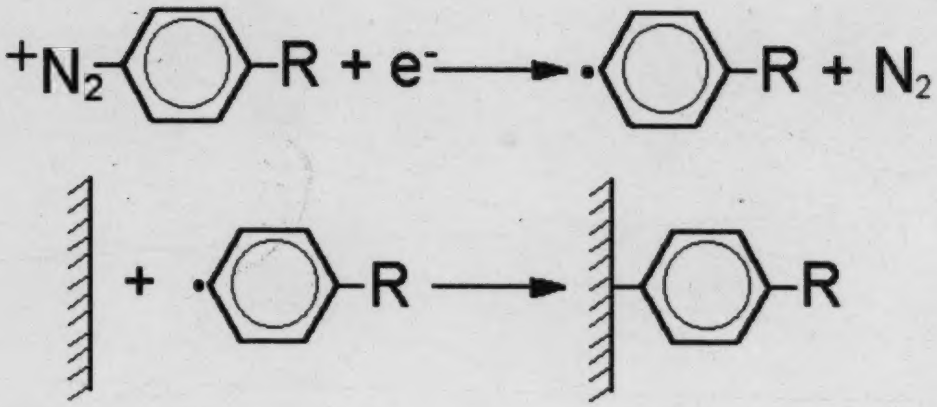

Figure 2.1: A schematic illustration of the predicted two step attachment process. The first involves the electrochemical generation of aryl radicals followed by their attachment to a carbon surface.

The work reported in this chapter extends the previous characterizations of layers formed from the reduction of diazonium salts to a more local scale. It has been reported that aryl radicals are able to attach to both edge plane and basal plane graphite [6, 13]. I will use electrochemical characterizations and scanning probe microscopy (SPM) to provide both a macroscopic and microscopic picture of the development of diethylaniline (DEA) films on HOPG. My findings show that these types of films do indeed nucleate on the basal plane, but their 2-dimensional growth is more consistent with aryl-aryl binding. In addition, I provide evidence for greater than monolayer coverage of DEA using standard deposition conditions.

Experimental

Reagents. The following reagents were all used as received: 4-Diazo-N,N-diethyl aniline fluoroborate (DDEA, Aldrich), p-nitro benzenediazonium tetrafluoroborate (NB, Sigma), tetrabutyl ammonium tetrafluoroborate (Bu_4NBF_4, Aldrich), potassium ferricyanide ($Fe(CN)_6^{3-/4-}$, Caledon), potassium chloride (Anachemia) and acetonitrile (CH_3CN, Fisher). Aqueous solutions were prepared using distilled/deionized water (18 MΩ/cm). All solutions were purged with nitrogen prior to use.

Electrode Preparation and Electrochemical Measurements. Fresh surfaces of highly oriented pyrolytic graphite (HOPG) (Advanced Ceramic Materials, Lakewood, OH) were generated by cleaving with adhesive tape before

each experiment. Cyclic voltammetric measurements were performed in a standard three-electrode cell in which the working electrode area was defined by an elastomeric o-ring (area = 0.5 cm^2). A platinum auxiliary electrode and a Ag/AgCl (sat'd $LiClO_4$) reference electrode were used. The cell was connected to either a Model CV-27 (Bioanalytical Systems Inc., W. Lafayette, IN), or model AFCBP1 potentiostat (Pine Instruments, Grove City, PA). Data was recorded with either an Omnigraphic (Houston Instruments, Bellaire, TX) X-Y recorder or with PineChem (version 2.5.2) software. Rate constants were calculated by the method of Nicholson [14]. Using the method, peak potential separation (ΔE_p) is used to estimate the heterogeneous rate constant (k°). The diffusion coefficients for $Fe(CN)_6^{3-/4-}$ were as follows [15]: $D_O = 7.63 \times 10^{-6}$ cm^2/s, $D_R = 6.32 \times 10^{-6}$ cm^2/s. In all cases, a value of $\alpha = 0.5$ was used.

SPM Imaging. SPM images were obtained with a Nanoscope III Multimode™ microscope (Digital Instruments, Santa Barbara, CA). Scanning force microscopy (SFM) was performed in contact mode with Si_3N_4 cantilevers, k ~ 0.06 N/m (Digital Instruments, NanoProbes,) using the electrochemical fluid cell. All SFM images were collected in CH_3CN. The substrate (working electrode), a Pt wire auxiliary and a Ag/AgCl wire reference electrode were connected to the CV-27 potentiostat to affect deposition in the SFM electrochemical fluid cell. Before collecting the images, the fluid cell was allowed to equilibrate for 30 minutes to reduce drift. Topographic and lateral force images

were collected simultaneously, but in most cases, only topographic images are shown. Images were software flattened and are shown unfiltered. Scanning tunneling microscopy was performed with a cut Pt/Ir tip. Bias voltages and tunneling currents are listed in the figure captions.

Results and Discussion

The deposition of diethylaniline (DEA) films on HOPG was affected by repetitive potential cycles in 0.5 mM 4-diazo-N,N-diethylaniline fluoroborate (DDEA) in CH_3CN (0.1 M Bu_4NBF_4). Cyclic voltammetric current-potential curves for 5 cycles between –0.1 and –1.0 V vs. Ag/AgCl are shown in Figure 2.2. These chemically irreversible cathodic waves correspond to the reduction of DDEA to a DEA radical as depicted in Figure 2.1 and are qualitatively similar to those for the reduction of a variety of other aryl diazonium salts at carbon electrodes [6, 7, 10]. Wave 1, exhibiting the largest peak current at –0.76 V, corresponds to the initial cycle. The peak current of each subsequent cycle decreases due to a progressive passivation mechanism as described previously [6]. The observation of current in cycles 2 through 5 implies that the formation of the DEA layer is not complete after one cycle and growth can be studied as a function of deposition cycle.

The nucleation and growth of DEA films on HOPG was probed both macroscopically, with electron transfer blocking analysis, and microscopically

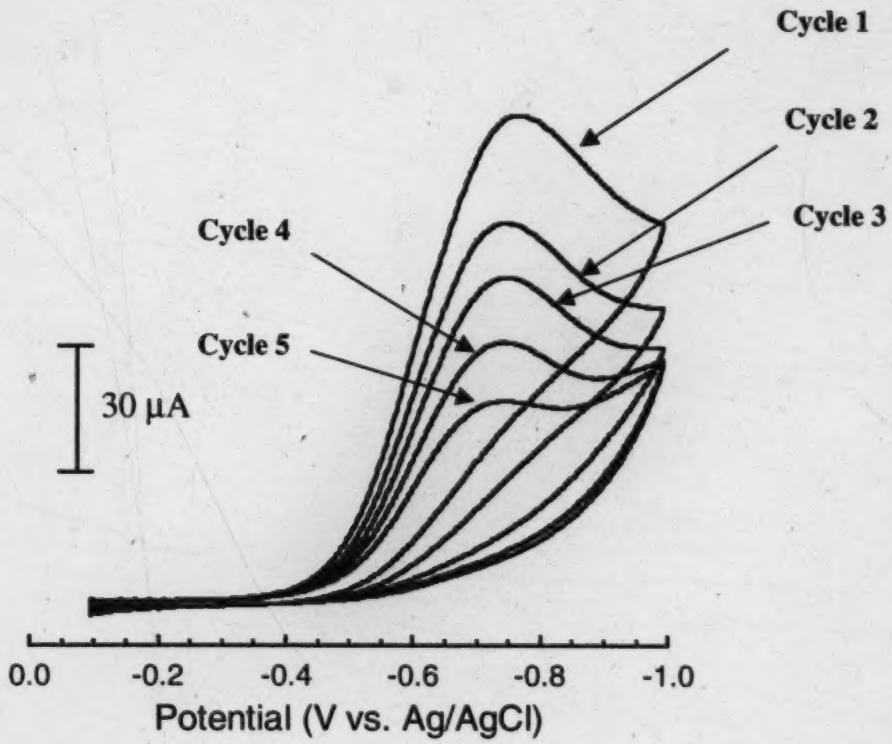

Figure 2.2: Cyclic voltammograms for the reduction of 0.5 mM DDEA in 0.1 M Bu_4NBF_4/CH_3CN on HOPG. Cycles 1 to 5 are indicated. Scan rate: 100mV/s.

with SPM. Figures 2.3 and 2.4 summarize experiments that describe the effect of DEA deposition on $Fe(CN)_6^{3-/4-}$ electron transfer. A number of reports have shown that the electron transfer rate for $Fe(CN)_6^{3-/4-}$ is controlled by edge plane defects at HOPG electrodes and that electron transfer at "pure" basal plane HOPG is anomalously slow [16-18]. This predictable electrochemical behavior will allow me to make assessments as to the sites for initial DEA attachment based on the blocking characteristics of the film.

Figure 2.3 contains cyclic voltammetric current-potential curves for 1 mM $Fe(CN)_6^{3-}$ (1 M KCl). Curve (a) of Figure 2.3 is the voltammogram at a freshly cleaved HOPG electrode. The value for the voltammetric peak separation (ΔE_p) of 80 mV in curve (a) of Figure 2.3 is diagnostic of a HOPG electrode with a significant density of edge plane defects. After this voltammogram was collected, the cell was rinsed and filled with 0.5 mM DDEA. The potential was cycled once in the manner of Figure 2.2 to induce the deposition of DEA. Curve (b) of Figure 2.3 is the $Fe(CN)_6^{3-/4-}$ voltammogram on the resultant HOPG surface. The measured ΔE_p value of 360 mV reflects a significant decrease in the electron transfer rate from the unmodified HOPG electrode due to blocking by the bound DEA.

The effect of continued DEA film growth on the blocking of $Fe(CN)_6^{3-/4-}$ was examined as a function of deposition cycle. In Figure 2.4, ΔE_p values were converted to heterogeneous electron transfer rate constants (k^o) via the method of

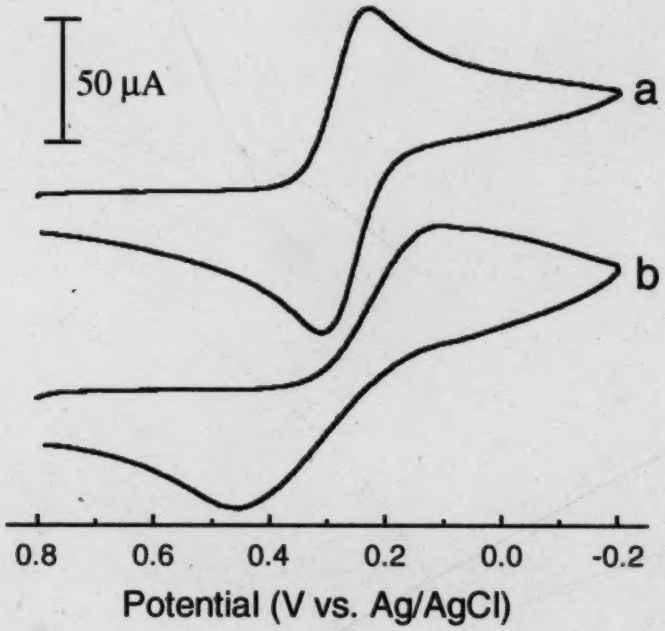

Figure 2.3: Cyclic voltammetry of 1mM $Fe(CN)_6^{-3/-4}$ (1 M KCl) on HOPG. Curve (a) corresponds to freshly cleaved HOPG. Curve (b) is on a HOPG substrate modified with one cycle from -0.1 V to –0.9 V vs Ag/AgCl in 0.5 mM DDEA (0.1 M Bu_4NBF_4/CH_3CN).

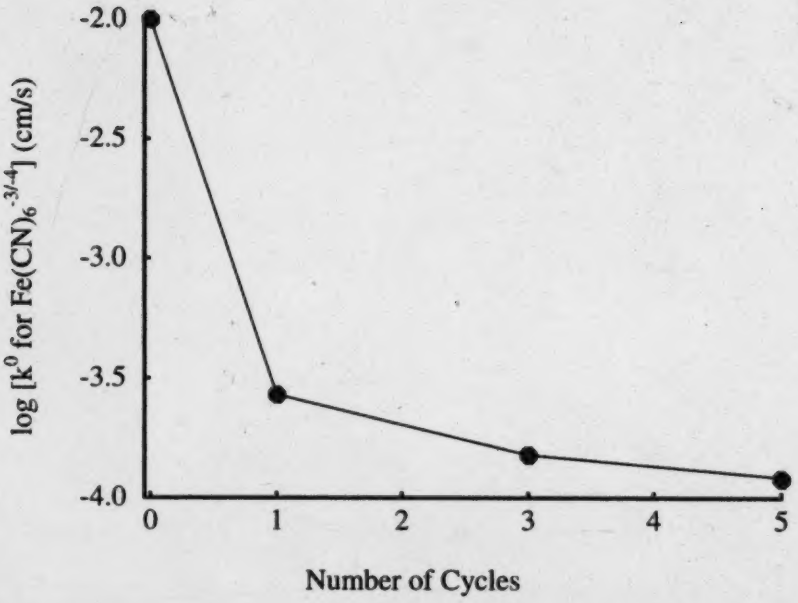

Figure 2.4: Plot of the log of the heterogeneous rate constant, k^0, for $Fe(CN)_6^{-3/-4}$ vs. number of cycles on HOPG modified in 0.5 mM DDEA (0.1M Bu_4NBF_4/CH_3CN). The line through the points does not represent a functional dependence. It is merely a guide to the eye.

Nicholson [14] and plotted versus cycle number. Apparently, the electron transfer blocking capability of the DEA film is maximized following one cycle which induces a decrease in k^o by a factor of ~40 fold (0.01 to 2.7 × 10^{-4} cm/s). Subsequent cycles have relatively little effect, reducing k^o of $Fe(CN)_6^{3-/4-}$ by only an additional factor of 2. This observation implies that one potential cycle in 0.5 mM DDEA initiates film growth at the defect sites that control k^o for $Fe(CN)_6^{3-/4-}$ on HOPG. Spatially resolved Raman spectroscopic experiments show that deposition of nitrophenyl groups for short times results in more material at defects than at basal plane HOPG [12]., consistent with our observations. It is noted that k^o values of $<10^{-6}$ cm/s for $Fe(CN)_6^{3-/4-}$ have been measured on defect free basal plane HOPG. The lowest k^o values measured here after 7 cycles is ~10^{-4} cm/s implying that the DEA layer does not completely block $Fe(CN)_6^{3-/4-}$ reduction at defect sites.

The evolution of a DEA film formed on HOPG by repetitive cycling of DDEA was probed on a more local scale with *in situ* SFM. Figure 2.5 is comprised of 5 × 5 μm topographic SFM images collected in CH_3CN containing 0.5 mM DDEA and 0.1 M Bu_4NBF_4. Figure 2.5-A is the image of the HOPG substrate at open circuit. Observed in the image are terraces of atomically flat basal plane graphite separated by several diagonally running step defects that result from cleaving [19-21]. The face of each step is composed of edge plane graphite and is a site for facile $Fe(CN)_6^{3-/4-}$ electron transfer [20]. Higher resolution

Figure 2.5: 5×5 µm topographic *in situ* SFM images of a HOPG substrate collected in 0.5 mM DDEA (0.1 M Bu_4NBF_4/CH_3CN). (A). Open circuit. (B). Following one cycle between –0.1 to –0.9 V vs Ag/AgCl. Parts C, D, E, and F are following two, three, four, and five cycles, respectively. Z-scale is 5 nm for all images.

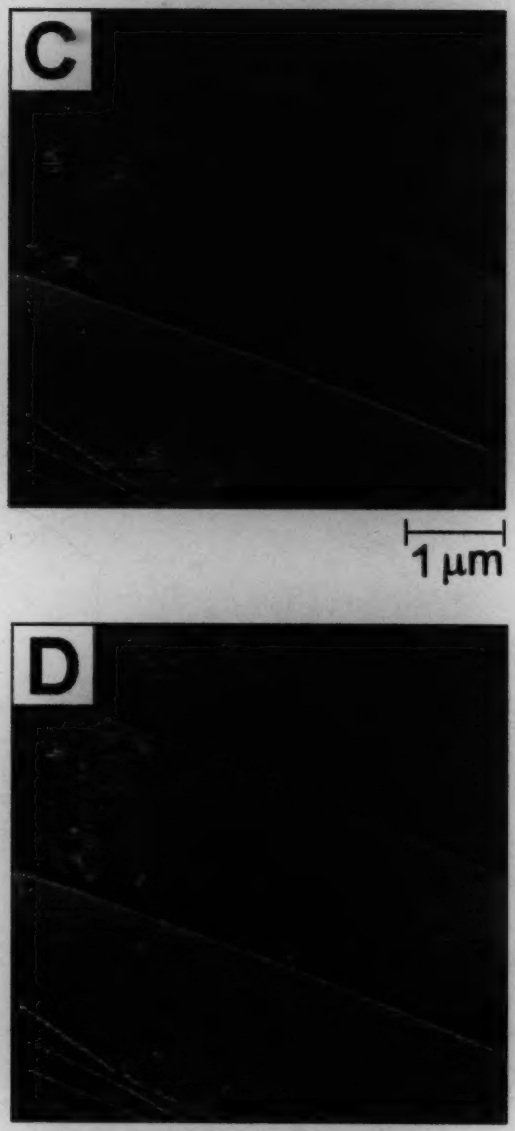

Figure 2.5: (continued)

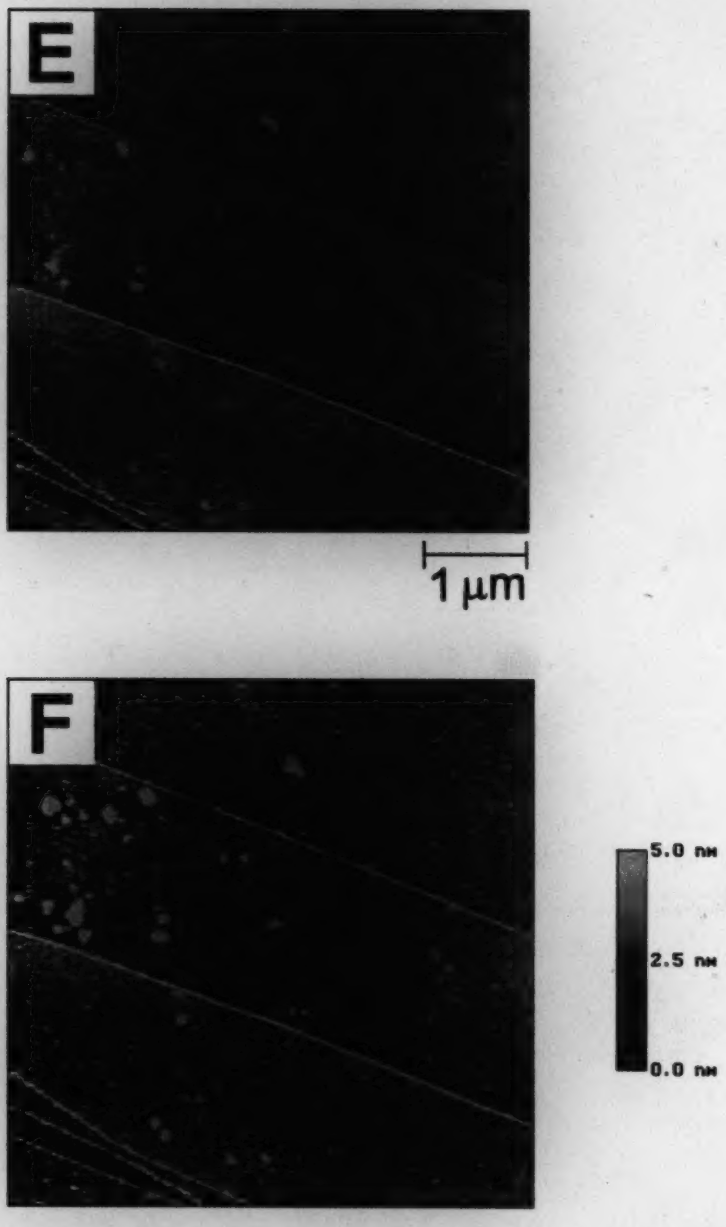

Figure 2.5: (continued)

images do not reveal physisorption of any solution components either on the basal plane or on cleavage defects. After thorough characterization of the unmodified HOPG substrate, the tip was retracted and the potential of the HOPG was cycled to affect the reduction of DDEA.

Parts B through F of Figure 2.5 provide an overview of the nucleation and growth of the DEA film at the same location as Figure 2.5-A. Figure 2.5-B depicts the surface after 1 cycle. In this image, the basal plane appears relatively unchanged while the topography of the steps now consists of a ~1.5 nm high "hump". The observation of material solely at the step defects implies that the aryl radicals initially attach to these sites, consistent with the $Fe(CN)_6^{3-/4-}$ voltammetry in Figure 2.3. This type of nucleation is not surprising considering the number of examples of electrochemical nucleation at defects on HOPG electrodes in the literature. For example, surface oxidation [22] as well as metal [23, 24] and polymer [25] deposition have been shown to initiate at cleavage steps. In this case, the nucleation of the DEA film at steps is likely the result of the high reactivity of edge plane graphite for both the electrochemical and chemical processes involved in film formation. That is, because of the high electrochemical reactivity of cleavage steps, the production of aryl radicals will be kinetically enhanced at these sites. In addition, the step defects will also contain sites for more facile attachment of the radicals relative to basal plane [16].

The electrode surface following cycles 2 through 5 is shown in parts C to F in Figure 2.5. Nucleation of the DEA film initiates on the basal plane during the

second cycle, as several regions of increased height appear. Further growth of the film on the basal plane is evident in images D and E following 3 and 4 cycles respectively. Because the SFM probe-tip is withdrawn from the surface during the potential cycle, I do not believe the tip is perturbing film formation. Following 5 cycles, a continuous layer is observed as shown in Figure 2.5-F. After this point there are no significant variations in film structure with further cycling. The majority of the final film structure in Figure 2.5-F is of uniform height, consistent with recent scanning tunneling microscopy (STM) images [6]. However, several 3-dimensional features are apparent which exhibit a larger height than the surrounding layer. The development of these structures can be tracked in Figure 2.5 where their height increases from 2.2 nm in Figure 2.5-C to 7.6 nm in Figure 2.5-F. In addition, the height of the material bound at the cleavage steps continues to increase throughout the deposition and measures 3.8 nm in Figure 2.5-F.

Consideration of the images of Figure 2.5 draws out two issues of interest. The first is the nature of the nucleation sites for aryl radical attachment to basal plane HOPG. The second is the mechanism of formation of the 3-dimensional structures in the DEA film. A snapshot of nucleation on the basal plane is shown more clearly in Figure 2.6 which contains a 3 × 3 μm lateral (or friction) force image of the same region as in Figure 2.5C; that is, after 2 deposition cycles. Considering that, at this point, the cleavage steps are covered with bound DEA, the signature at these sites in Figure 2.6 implies that the grafted DEA induces a higher frictional signal than the surrounding basal plane HOPG. This signal is

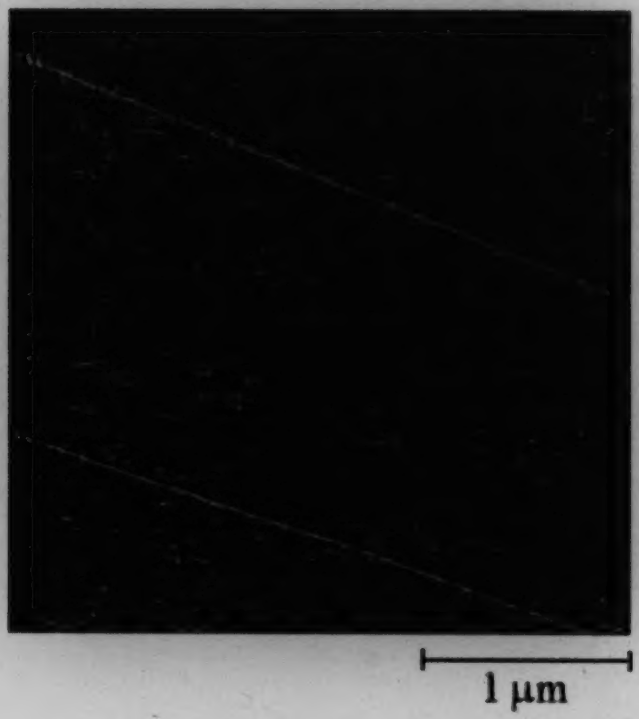

Figure 2.6: 3 × 3 μm *in situ* lateral force image of the same region as in Figure 2.5-C (after 2 cycles). Z-scale = 0.1V.

either the result of a chemical difference, or simply due to a mechanical "tripping" of the tip. Along with the high friction observed at the cleavage steps, numerous localized nucleation sites are evenly distributed on the basal plane away from the steps. These sites are more apparent in lateral force images because of the higher sensitivity of laser-based SFM systems to torsional cantilever motion compared to bending normal to the surface [26]. It is apparent from Figure 2.6 that DEA film formation on the basal plane of HOPG nucleates at sites distinct from the cleavage steps. Thus, although the aryl radicals initially attach at cleavage defects on HOPG, further film growth on basal plane does not extend solely from these sites.

A higher resolution depiction of DEA nucleation on basal plane HOPG is afforded by scanning tunneling microscopy (STM). Figure 2.7 is a 650 × 650 nm STM image of a HOPG substrate following 2 deposition cycles in 0.5 mM DDEA. Isolated structures are visible against an atomically flat basal plane background. These structures are too large to consist of individual DEA molecules and are likely composed of a cluster of molecules. The observation of isolated features in Figure 2.7 implies one of two scenarios. Either an sp^2 hybridized carbon atom in the basal plane lattice reacts with an aryl radical to produce an sp^3 surface carbon atom or that unoccupied sp^2 sites pre-exist on the basal plane capable of forming a covalent bond with the aryl moieties. Observations in the literature suggest the presence of atomic scale defects on basal plane HOPG. Chang and Bard have reported the formation of monolayer deep etch pits in the basal plane of HOPG following heat treatment in the presence of oxygen [27, 28]. The nucleation sites

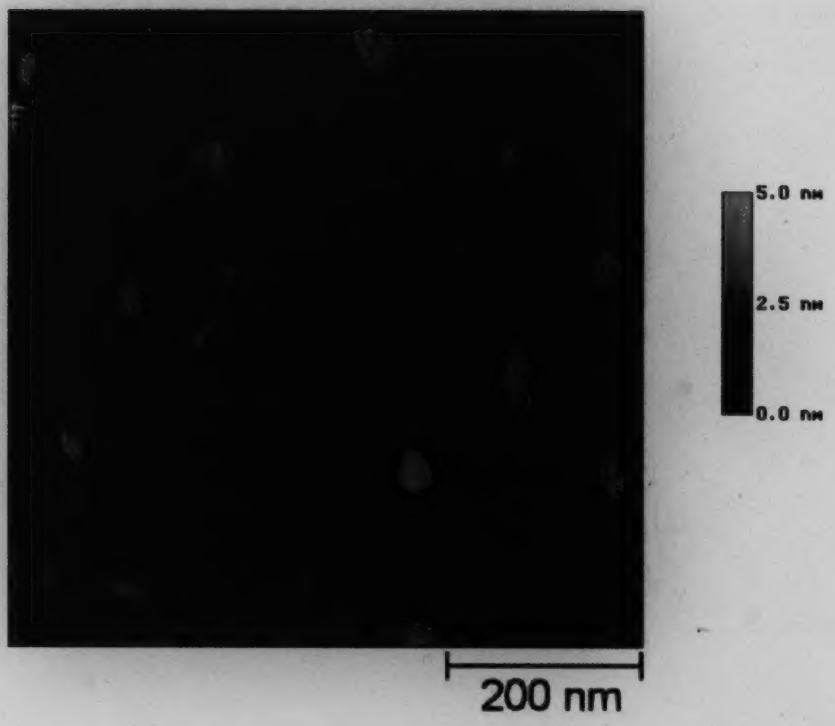

Figure 2.7: 650 × 650 nm constant current STM image of a HOPG substrate collected in air following 2 deposition cycles from -0.1 V to –0.9 V vs Ag/ AgCl in 0.5mM DDEA. Bias voltage = 100mV, tunneling current = 100 pA.

for pit formation were ascribed to atomic vacancies in the basal plane. Zoval *et al.* have observed the presence of silver and platinum nanocrystallites on basal plane HOPG following electrochemical reduction of the corresponding metal cation [29, 30]. The sites responsible for nucleation were attributed to defects on the basal plane terraces that were invisible to their SFM imaging. It is likely then, that hidden defect sites on the supposed defect free basal plane are also responsible for the DEA nucleation illustrated in Figure 2.7. These hidden sites may be point defects, such as atomic vacancies [31].

Following the establishment of nucleation sites on the basal plane, DEA film growth can proceed through one of two mechanisms. The first involves continued binding of DEA radicals to the basal plane. This could occur if the graphitic structure near the nucleation site was distorted as a result of the initial radical attachment thus exposing additional carbon atoms with unoccupied sp^2 orbitals. I believe this mechanism is unlikely because it essentially involves the propagation of defect sites across the basal plane as the film forms. Another possibility involves growth of the film through intermolecular binding. That is, the attachment of DEA radicals to DEA molecules already attached to the surface.

Several observations suggest the possibility of aryl-aryl bond formation as depicted in Figure 2.8. This type of reaction is well known from the organic synthesis literature and likely competes for aryl radicals with hydrogen abstraction from the solvent [32-34]. The first observation in support of the mechanism in Figure 2.8 derives from consideration of the nucleated clusters in Figure 2.5 that

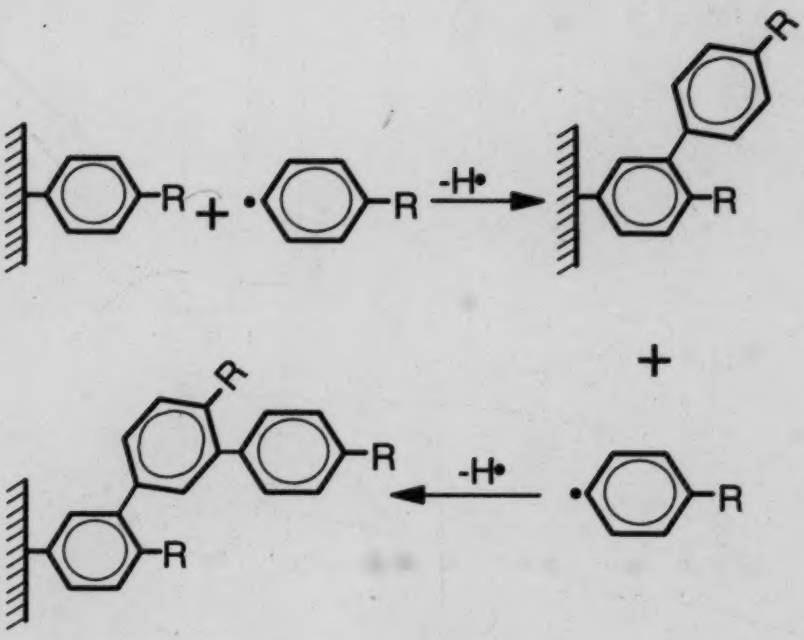

Figure 2.8: A schematic illustration of the predicted mode of attachment of free aryl radicals in solution to the aryl moieties attached to the HOPG surface. The hydrogen atoms produced in this mechanism can react with solvent or other radicals.

range in height from 0.7 to 2.5 nm. Compared with the length of a single DEA molecule (~0.8 nm), the observed heights imply that several of the structures are likely composed of more than one DEA molecule. In other cases, I have observed a single cluster exhibiting different height levels. Secondly, the observation of the 3-dimensional structures in Figure 2.5-F argues for multilayer formation, possibly localized at the nucleation sites. The increase in the height of these structures as well as the material at cleavage defects following each voltammetric sweep suggests continued deposition of DEA. In a previous study, higher quantities of nitrophenyl groups were consistently observed at defects relative to basal plane HOPG with spatially resolved Raman spectroscopy [12]. Taken together, these observations provide strong evidence for aryl-aryl polymerization.

A growth mechanism across the basal plane governed by aryl-aryl bond formation would result in a final film structure anchored to the basal plane only at the nucleation sites. This type of film structure should be easily manipulated by an SFM tip. The images in Figure 2.5 were collected in CH_3CN at a low normal force (~1-2 nN), which are conditions suitable for imaging weakly bound species. SFM images of a complete DEA film collected in air are shown in Figure 2.9. After imaging in a certain region at a force of ~5 nN, the scan area was translated slightly. The boundary between these regions is noted with an arrow in Figure 2.9, with the lower part corresponding to the repeatedly scanned area. Significant tip induced perturbation of the film is observed in both the topographic (Figure

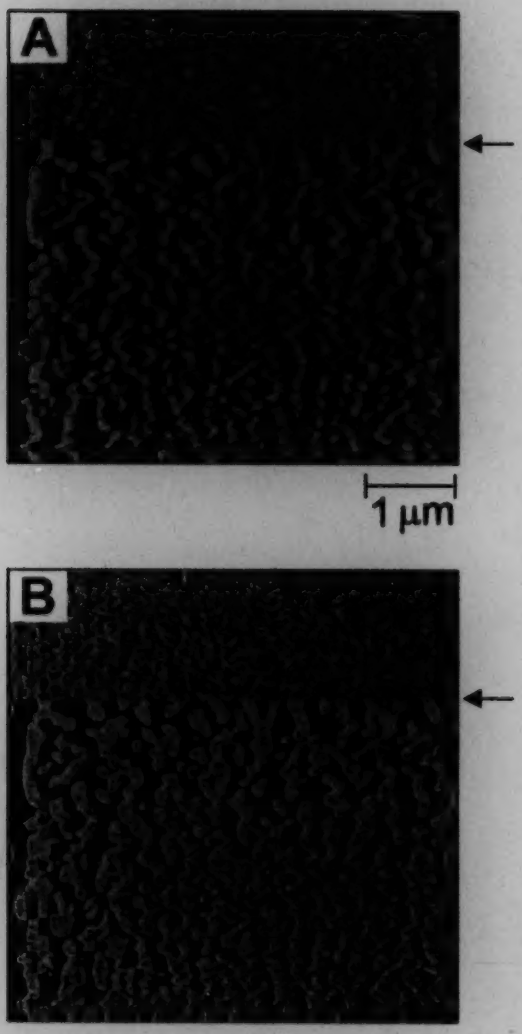

Figure 2.9: 5 × 5 μm contact mode SFM image collected in air of a HOPG surface modified using one cycle from -0.1 V to –0.9 V vs Ag/ AgCl in 5 mM DDEA (0.1 M Bu_4NBF_4/CH_3CN). (A) topography (z-scale = 10 nm) (B) lateral force image (z-scale = 0.1V). The arrow points to the boundary between regions imaged using different forces. The upper region was scanned at a low normal force (~ 1=2 nN), whereas the bottom region was scanned repeatedly at a force of ~ 5 nN.

2.9-A) and lateral force (Figure 2.9-B) images. The SFM tip has apparently displaced regions of the film and created domain-like structures. These domains are separated by unmodified basal plane which exhibits a characteristic low frictional signal in Figure 2.9-B [21].

Two points derived from Figure 2.9 lend support to a growth mechanism involving 2-dimensional polymerization of DEA from discrete nucleation sites. First, the facile manipulation of the layer with the SFM tip is consistent with a film structure that would result from this type of growth. This is especially true when one compares these aryl based films to spontaneously adsorbed alkanethiol monolayers on gold, which are considerably stable to SFM imaging in air [35]. The domain structures in Figure 2.9 may in fact be located at the nucleation sites where the film is anchored. Secondly, the height of the less perturbed region near the top of the images is 2.3 nm above the basal plane, which corresponds to ~4 times the molecular length of DEA. A growth process like that depicted in Figure 2.8 would likely result in films thicker than one monolayer.

Multilayer formation is strikingly apparent in the structure of complete aryl films when imaged under less perturbing conditions. Figure 2.10 is a 4×4 μm *in situ* topographic image of a HOPG substrate after modification with one potential cycle in a solution of 5 mM DDEA. In this case, cleavage defects and the basal plane are completely covered after one cycle because of the higher precursor concentration. Apparent in the topography image are uniformly distributed 3-

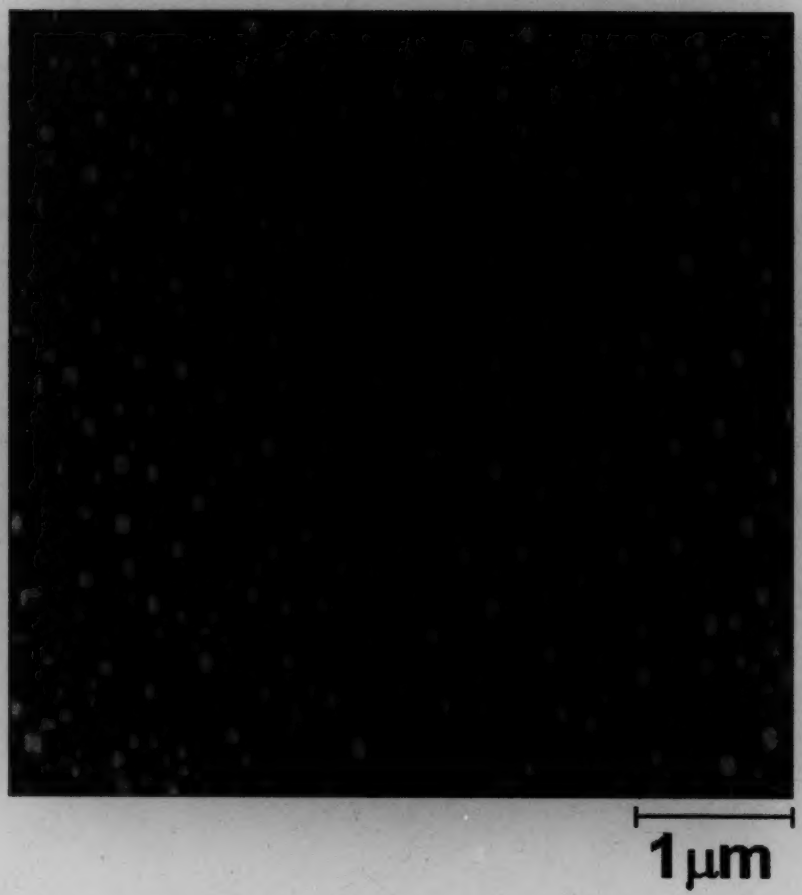

Figure 2.10: 4 × 4 μm topographic SFM image of a HOPG substrate modified by one cycle from -0.1 V to –0.9 V vs Ag/ AgCl in 5 mM DDEA (0.1 M Bu_4NBF_4/CH_3CN). (z-scale = 5 nm).

dimensional structures that range in height from 5 to 15 nm. These heights suggest numerous DEA layers.

I have also observed 3-dimensional structures in films formed from other diazonium salts implying that aryl-aryl polymerization is not specific to DDEA. For example, Figure 2.11 is 10 x 10 μm topographic image of a HOPG substrate after modification with one potential cycle in a solution of 5 mM 4-nitro benzene diazonium salt (NB). In agreement with the data obtained using DDEA modification, I observed high topographic features that range in height from 2 to 25 nm. The features are higher than the expected NB monolayer height of about 0.7 nm. I attribute the formation of these features to multilayer formation via the same mechanism described using DDEA. As well, coverage from partial monolayer to multilayer formation has been observed in films formed from the deposition of 4-phenylacetic acid diazonium tetrafluoroborate (PAA) on carbon electrodes. This data will be presented in Chapter III.

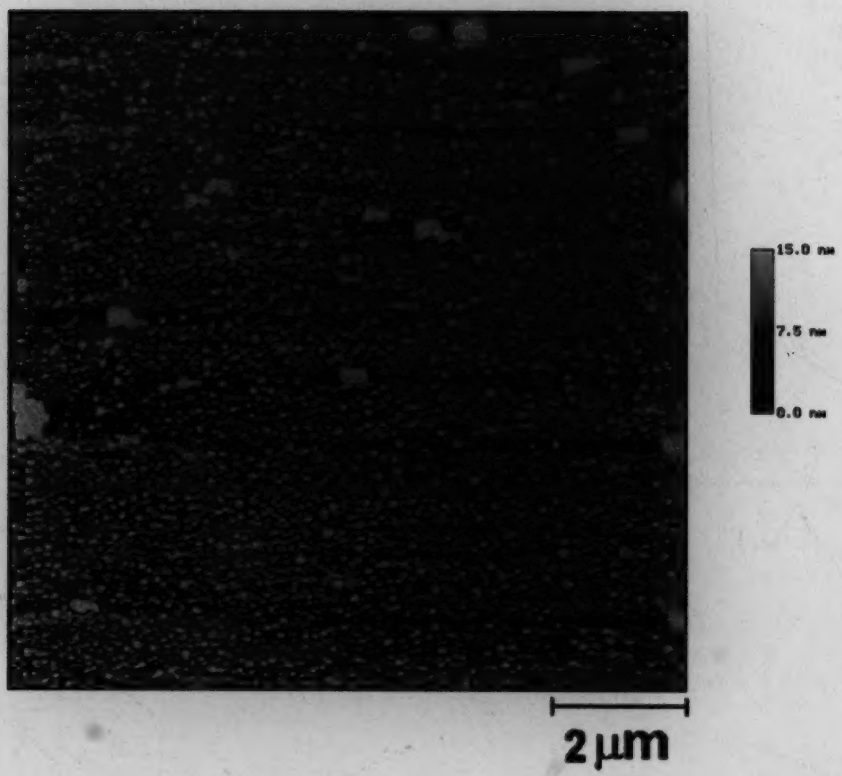

Figure 2.11: 10×10 µm SFM topographic image of a HOPG substrate modified by one cycle from 0.6 V to –0.4 V vs Ag/AgCl in 5 mM NB (0.1 M Bu_4NBF_4/CH_3CN). (z-scale = 15 nm).

Conclusions

Electrochemical blocking and SFM imaging both indicate that aryl films formed on HOPG from the electrochemical reduction of diazonium salts initiate at cleavage steps. Nucleation on the basal plane occurs at sites that are distinct from the cleavage defects. These sites are likely atomic scale defects (i.e., vacancies) on the otherwise pristine basal plane. My results indicate that continued film growth occurs in both 2- and 3-dimensions through the binding of electrochemically generated aryl radicals to aryl groups already bound to the surface. This mechanism implies a 2-dimensional structure where the film is anchored to the HOPG at a finite number of nucleation sites and extends across the surface via intermolecular binding. The evidence of 3-dimensional growth is on much stronger footing where structures exhibiting heights consistent with multilayer formation have been observed.

It would be risky to extend the nucleation and growth mechanism proposed here to more disordered carbon electrode materials, such as glassy carbon (GC). The much greater density of edge plane sites on GC likely provides ample nucleation sites for radical attachment across the entire surface. However, observation of 3-dimensional growth on HOPG may have implications for modified GC. My continuing experiments provide evidence for multilayer formation on GC as well, and will be presented in Chapter III.

References

1. C. Galli, *Chem. Rev.* 88: 765 (1988).

2. M. P. Doyle, J. K. Guy, K. C. Brown, S. N. Mahapatro, C. M. VanZyl, and J. R. Pladziewicz, *J. Am. Chem. Soc.* 109: 1536 (1987).

3. F. F. Gadallah and R. M. Elofson, *J. Org. Chem.* 34: 3335 (1969).

4. J. K. Kochi, *J. Am. Chem. Soc.* 77: 3208 (1955).

5. Y.-C. Liu and R. L. McCreery, *Anal. Chem.* 69: 2091 (1997).

6. P. Allongue, M. Delamar, B. Desbat, O. Fagebaume, R. Hitmi, J. Pinson, and J.-M. Saveant, *J. Am. Chem. Soc.* 119: 201 (1997).

7. M. Delamar, G. Desarmot, O. Fagebaume, R. Hitmi, J. Pinson, and J.-M. Saveant, *Carbon* 35: 801 (1997).

8. A. J. Downard, A. D. Roddick, and A. M. Bond, *Anal. Chim. Acta* 317: 303 (1995).

9. B. Ortiz, C. Saby, G. Y. Champagne, and D. Belanger, *J. Electroanal. Chem.* 455: 75 (1998).

10. C. Saby, B. Ortiz, G. Y. Champagne, and D. Belanger, *Langmuir* 13: 6805 (1997).

11. Y.-C. Liu and R. L. McCreery, *J. Am. Chem. Soc.* 117: 11254 (1995).

12. K. Ray and R. L. McCreery, *Anal. Chem.* 69: 4680 (1997).

13. M. Delamar, R. Hitmi, J. Pinson, and J.-M. Saveant, *J. Am. Chem. Soc.* 114: 5883 (1992).

14. R. S. Nicholson, *Anal. Chem.* 37: 1351 (1965).

15. K. R. Kneten and R. L. McCreery, *Anal. Chem.* 64: 2518 (1992).

16. R. J. Bowling, R. T. Packard, and R. L. McCreery, *J. Am. Chem. Soc.* 111: 1217 (1989).

17. M. T. McDermott, K. Kneten, and R. L. McCreery, *J. Phys. Chem.* 96: 3124 (1992).

18. R. J. Rice and R. L. McCreery, *Anal. Chem.* 61: 1637 (1989).

19. H. Chang and A. J. Bard, *Langmuir* 7: 1143 (1991).

20. M. T. McDermott and R. L. McCreeery, *Langmuir* 10: 4307 (1994).

21. D. R. Baselt and J. D. Baldeschwieler, *J. Vac. Sci. Technol. B* 10: 2316 (1992).

22. A. A. Gewirth and A. J. Bard, *J. Phys. Chem.* 92: 5563 (1988).

23. R. T. Potzschke, C. A. Gervasi, S. Vinzelberg, G. Staikov, and W. J. Lorenz, *Electrochim. Acta* 40: 1469 (1995).

24. Z. Li, L. Wang, T. Suzuki, A. Argoitia, P. Pirouz, and J. C. Angus, *J. Appl. Phys.* 73: 711 (1993).

25. S. R. Snyder, H. S. White, S. Lopez, and H. D. Abruna, *J. Am. Chem. Soc.* 112: 1333 (1990).

26. G. Meyer and N. M. Amer, *Appl. Phys. Lett.* 56: 2100 (1990).

27. H. Chang and A. J. Bard, *J. Am. Chem. Soc.* 112: 4598 (1990).

28. H. Chang and A. J. Bard, *J. Am. Chem. Soc.* 113: 5588 (1991).

29. J. V. Zoval, R. M. Stiger, P. R. Biernacki, and R. M. Penner, *J. Phys. Chem.* 100: 837 (1996).

30. J. V. Zoval, J. Lee, S. Gorer, and R. M. Penner, *J. Phys. Chem. B* 102: 1166 (1998).

31. H. A. Mizes and W. A. Harrison, *J. Vac. Sci. Technol. A* 6: 300 (1988).

32. R. M. Elofson and F. F. Gadallah, *J. Org. Chem.* 36: 1769 (1971).

33. D. H. Hey, in *Advances in Free Radical Chemistry*, Vol. II (G. H. Williams, ed.), Logos, London, 1967, p. 47.

34. R. Bolton and G. H. Williams, in *Advances in Free Radical Chemistry*, Vol. V (G. H. Williams, ed.), Logos, London, 1975, p. 1.

35. C. A. Alves, E. L. Smith, and M. D. Porter, *J. Am. Chem. Soc.* 114: 1222 (1992).

Chapter III

Formation of Multilayers on Glassy Carbon Electrodes via the Reduction of Diazonium Salts

Introduction

The functionalization of carbon electrodes with aryl films can be achieved via the electrochemical reduction of the corresponding diazonium salt. In Chapter II it was shown that this deposition procedure produced multilayer films on ordered graphite under certain conditions. This chapter presents results that show the formation of multilayer films on glassy carbon (GC) electrodes by potential step electrolysis of diazonium salts for longer times.

A significant amount of effort has been put forth recently to develop methods to covalently bind chemical groups to carbon electrodes [1]. A protocol initially examined by Delamar *et al.* has emerged and involves the grafting of functionalized aryl groups via the electrochemical reduction of diazonium salts [2]. The acceptance and application of this method by a number of researchers is primarily due the ease by which diazonium salts bearing a wide range of functional groups can be synthesized as well as the structure and stability of the resulting layer [3]. Functionalized phenyl films have been utilized in a number of fundamental studies at carbon electrodes including investigations of electrochemical reactions of surface bound layers [4] and long range electron tunneling studies [5]. Biological applications include their use as a platform to

link biomolecules [6] and as a layer to control protein adsorption [7]. The reduction of diazonium salts has also been employed to modify silicon and metal surfaces [8]. Considering the number of studies exploiting this attachment scheme thus far, it is clear that the use of this method to control the chemistry of carbon surfaces will become more widespread. Thus, a complete understanding of the deposition and structure of these films is required for their successful application.

The binding of aryl groups to carbon electrodes is likely a two step process. The first step involves the electrochemical reduction of the diazonium salt to generate aryl radicals. This is followed by the reaction of the radicals with the carbon surface. It was initially proposed that a covalently bound monolayer was formed from this procedure [2]. I have previously investigated the binding of diethylaniline (DEA) radicals to highly oriented pyrolytic graphite (HOPG) electrodes [9]. The results of this work were presented in Chapter II. It was shown that aryl multilayers could form by the reaction of an electrochemically generated radical with a surface bound phenyl group as illustrated in Figure 3.1.

The results reported here extend my previous work by identifying the conditions necessary to produce phenyl multilayers on glassy carbon (GC) and probing the resulting films. The structure and thickness of aryl films bound to polished GC electrodes are characterized as a function of deposition time. I employ infrared reflectance absorption spectroscopy (IRRAS) and scanning force microscopy (SFM) to show that the reduction of diazonium salts will form

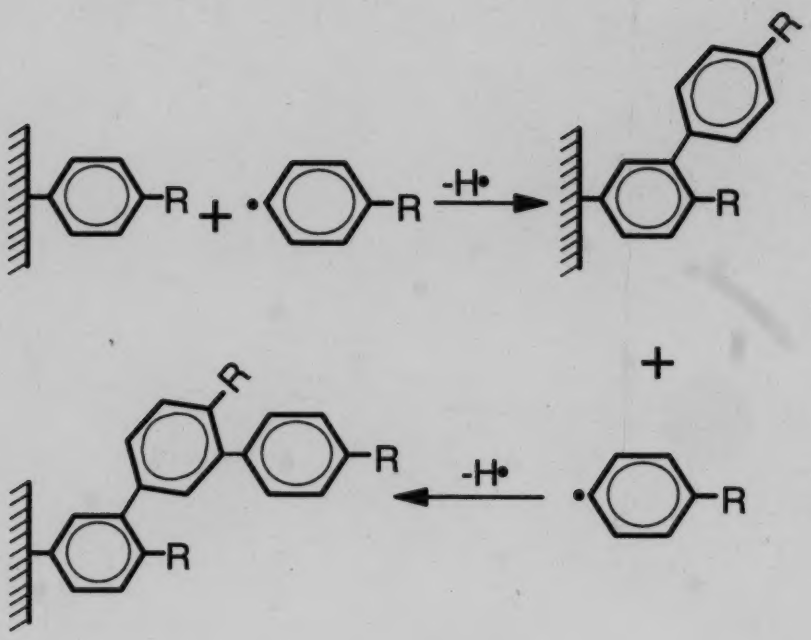

Figure 3.1: A schematic illustration of a possible mode of attachment of free aryl radicals in solution to the aryl moieties attached to the HOPG surface. The hydride radicals produced in this mechanism can react with solvent or other aryl radicals. A discussion of an alternative polymerization mode is included in the text.

multilayer films on GC under certain conditions; specifically, long deposition times (10-30 min.). The electrochemical barrier properties of phenyl multilayers are also explored to provide insights into the structural uniformity of the layers.

Experimental

Reagents. 4-Diazo-N,N-diethyl aniline tetrafluoroborate (DEA) and tetrabutyl ammonium tetrafluoroborate (Bu_4NBF_4) were purchased from Aldrich. 4-Diazo-nitrobenzene tetrafluoroborate (NB) was obtained from Sigma. 4-Diazo-phenylacetic acid tetrafluoroborate (PAA) was synthesized from 4-aminophenylacetic acid (Aldrich) according to a published procedure [10]. Reagent grade acetonitrile (CH_3CN) was purchased from Fisher. The redox systems studied were as follows: $Ru(NH_3)_6^{3+}$(aq) in 1 M KCl (pH = 5.7) and $Fe(CN)_6^{4-}$ (aq) in 1 M KCl (pH = 6.8) were prepared at 1mM concentrations from $Ru(NH_3)_3Cl_3$ (Strem Chemicals) and $K_4Fe(CN)_6$ (BDH Chemicals) respectively. Eu^{3+}(aq) in 0.2 M $HClO_4$ (pH = 1.3) was prepared at 5 mM concentrations from $Eu(NO_3).5H_2O$ (Aldrich). All reagents were used as received. All solutions were purged with argon prior to use.

Electrode Preparation and Electrochemical Measurements. Square, planar GC electrodes were cut from a larger, 3 mm thick plate of GC-20 (Tokai GC-20, Electrosynthesis Corp, NY). For SFM analysis, the electrodes measured ~1 × 1 cm. The GC electrodes used for IRRAS studies were 3 cm x 6 cm plates. The backside of these plates was coated with a thick (~1 mm) film of

poly(ethylene)/poly(vinylacetate) 60:40 (Aldrich) to block electroactivity. All GC electrodes were initially prepared by polishing with successive slurries of 1, 0.3, and 0.05 μm alumina in 18 MΩ deionized water on polishing microcloth (Buehler). The electrodes were sonicated in deionized water for 5 min. between polishing steps.

Regions of GC electrodes were blocked by spraying the surface with polystyrene (Aldrich, MW = 45,000 D) dissolved in CCl_4. About 0.005 g of polymer was dissolved in 50 mL CCl_4. A home-made nebulizer was used. After modification of these "patterned" GC electrodes, the polystyrene mask was removed by rinsing with CCl_4. Cyclic voltammetric measurements were performed in a standard three-electrode cell in which the electrode area of the GC was defined by an elastomeric o-ring (area = 0.5 cm^2). A platinum auxiliary electrode and a Ag/AgCl reference electrode were used. The scan rate was 100 mV/s for all voltammograms. The cell was connected to either a Model CV-27 (Bioanalytical Systems Inc.) or Pine Instruments, model AFCBP1 potentiostat. Data was recorded with either an Omnigraphic (Houston Instruments) X-Y recorder or with PineChem (version 2.5.2) software. Phenyl layers were deposited by potential-step electrolysis of the corresponding diazonium salt in CH_3CN (0.1 M Bu_4NBF_4) in the same cell described above. The cyclic voltammetric peak potentials for each diazonium salt are as follows: DEA, E_p = -0.75 V vs Ag/AgCl; PAA, E_p = -0.20 V; NB, E_p = 0.2 V. Cyclic voltammetric peak separations (ΔE_p)

were used to determine heterogeneous electron transfer rate constants (k^o) via the method of Nicholson [11].

SFM Imaging. SFM images were obtained with a Nanoscope III Multimode™ microscope (Digital Instruments, Santa Barbara, CA). Both contact and tapping-mode SFM were employed. For tapping-mode imaging, Si cantilevers were oscillated at their resonance frequency (~ 200-300 kHz). The parameter in tapping-mode imaging that determines tapping force is the ratio of the set point (or imaging) amplitude, A_{sp}, to the oscillation amplitude, A_o where $r_{sp} = A_{sp}/A_o$ [12]. All images shown here were collected with r_{sp} between 0.5 to 0.7 (moderate tapping force) at a scan rate of ~1 Hz. Contact mode imaging was performed with Si_3N_4 cantilevers, k~0.06 N/m (Digital Instruments, NanoProbes) at normal forces of <10 nN. Images were software flattened and are otherwise shown unfiltered.

IRRAS Studies. IRRAS spectra were obtained on an ATI Mattson Infinity Series FTIR (Madison, WI) spectrometer equipped with an external sample module and liquid nitrogen cooled mercury-cadmium-telluride (MCT) detector. The IR beam was incident on the GC surface at an angle of 60° with respect to the surface normal [13]. Spectra were taken at 4 cm^{-1} resolution with an interferometer mirror speed of 50 kHz. Typically, 1000 scans were averaged to yield spectra with an acceptable signal-to-noise ratio. The interferograms were

Fourier transformed using triangular apodization. Reference spectra were on an unmodified polished GC electrode.

Results and Discussion

Binding of aryl films to carbon electrodes via the electrochemical reduction of the corresponding diazonium salt can be achieved through either potential cycling or a potential step [3]. In Chapter II it was shown that films with greater than monolayer thickness can be deposited on ordered graphite. To investigate possible multilayer formation on GC, aryl films were deposited by potential-step electrolysis for various lengths of time. A deposition procedure commonly reported involves 2 or 3 potential cycles at 100 mV/s in 5 mM diazonium salt. I classify this procedure as producing monolayer coverage and use films deposited in this way as starting point for comparison. In the sections below, I investigate the growth and thickness of aryl films deposited on GC electrodes for long times.

Tracking diethylaniline (DEA) deposition with IRRAS. Figure 3.2 contains a series of spectra tracking DEA film growth as a function of deposition time. The bottom trace in Figure 3.2 is a spectrum of a film formed on polished GC from 2 cycles in 5 mM 4-diazo-N,N-diethyl aniline tetrafluoroborate. The upper spectra are from electrodes held at –1.2 V vs. Ag/AgCl for 10, 20 and 30 min. A band at ~2300 cm^{-1} due to the N≡N stretch of the diazonium salt is absent in all spectra as is expected for films formed by a radical attachment mechanism.

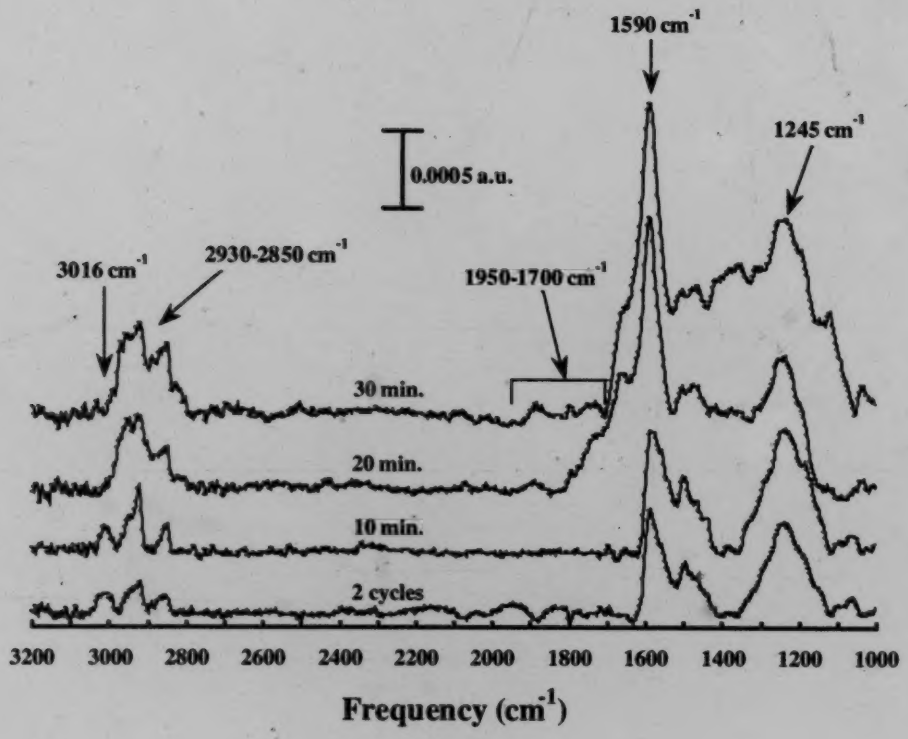

Figure 3.2: IRRAS spectra of a GC electrode modified with a DEA film. The bottom spectrum is following two cycles in 5 mM DDEA (0.1 M Bu_4NBF_4/CH_3CN) between –0.1 to –0.9 V vs Ag/AgCl. Other spectra are following modification with a potential step at –1.20 V Ag/AgCl for different time scales as labeled on each spectrum.

Assignments and intensities for the prominent bands are given in Table 3.1 [14]. Generally the absorbance of each band increases with deposition time, an observation consistent with the continual growth of the DEA film over the time-scale of the deposition.

Downard recently suggested that the applied overpotential is an important parameter in determining the structure of phenyl layers on GC [15]. My results along those lines agree with this claim. The potential used to deposit the films for Figure 3.2 (-1.2 V) represents an overpotential of –450 mV relative to the cyclic voltammetric peak for DEA deposition. Deposition of DEA at an overpotential of -150 mV (-0.9 V) resulted in IRRAS spectra with bands of roughly equal intensity for 10, 20 and 30 min. deposition times. I find that a deposition overpotential of –300 mV is required to observe continued film growth with IRRAS. The higher driving force required is consistent with the self-inhibiting nature of these films [3].

Several details from Figure 3.2 and Table 3.1 also support the mechanism illustrated in Figure 3.1. A band due to aromatic C-H stretching is observed at 3016 cm^{-1} for films formed for short times. However, films formed for longer times do not exhibit this peak. In this experiment, transition dipoles with a component perpendicular to the GC surface will be preferentially excited due to the IRRAS surface selection rule. The transition dipole of the aromatic C-H bonds in the first monolayer of DEA molecules likely contains a major component normal to the surface. The disappearance of the 3016 cm^{-1} band is consistent with

		Frequency (cm^{-1})				
		3016	2930-2850	1590	1480-1500	1245
Assignment		Aromatic C-H stretch	Aliphatic C-H stretch	Aromatic C=C stretch	Aromatic C=C stretch	phenyl-N stretch
Absorbance$\times 10^{-3}$	2 Cycles	0.13	0.19	0.66	0.32	0.56
	10 min.	0.15	0.40	0.76	0.48	0.76
	20 min.	—	0.46	1.7	0.66	0.81
	30 min.	—	0.57	2.0	0.77	1.2

Table 3.1: Band assignments and intensities from the IRRAS spectra of DEA films on GC in Figure 3.2.

these C-H bonds becoming replaced by phenyl-phenyl bonds during multilayer formation. The second and third layer of phenyl groups may be in an orientation that lessens the perpendicular component of phenyl C-H transition dipole to a degree below my detection limit.

The spectra for the films formed for longer times (20, 30 min.) contain several weak bands between 1950 and 1700 cm^{-1}. The positions of these bands (1890, 1800, 1730 cm^{-1}) are consistent with combination and overtone bands expected for multi-substituted aromatic rings. I note that bands in the region between 900 and 700 cm^{-1} characteristic of substituted aromatic compounds patterns are not observed due to the low frequency cut-off of my MCT-A detector at ~800 cm^{-1}. I also note the appearance of a shoulder at ~1660 cm^{-1} on the ring deformation band. I attribute this shoulder to the deformation of multiply substituted rings that comprise the structure of the multilayer. Thus, spectral details from Figure 3.2 in both the C-H and C=C stretching region are consistent with the multilayer attachment mechanism depicted in Figure 3.1.

Although the proposed mechanism is supported by the presented data, other pathways to multilayer formation cannot be ruled out. For example, a pathway of electrochemically initiated polymerization process via the reduction of diazonium salts was recently reported [16]. In this case the formation of a polymer occurs via an amine linkage. An example of a polymeric product resulting from such a mechanism is $(C_6H_5\text{-}NH\text{-}NH\text{-}C_6H_5)_n$.

SFM measurement of DEA film thickness. DEA film thickness can also be tracked with SFM by masking regions of polished GC electrodes with a polystyrene (PS) film. Following deposition of DEA, the PS mask is dissolved in CCl_4. The resulting surface contained regions modified with DEA adjacent to unmodified polished GC. An example of such an electrode is shown in the 30 × 30 μm topographic SFM image in Figure 3.3-A. The regions of higher topography in Figure 3.3-A correspond to the unmasked regions during deposition of DEA. A higher magnification image of the boundary between a modified and unmodified region is shown in Figure 3.3-B. The thickness measured at the boundaries is plotted vs. deposition time in Figure 3.4. Three conclusions can be drawn from Figure 3.4. The first is that DEA films thicker than a monolayer can be deposited on GC by employing long electrolysis times. Secondly, the thickness of the films can be controlled by deposition time. And thirdly, DEA films continue to grow throughout a 30 min. deposition. This indicates that aryl radicals are being generated through a 20 nm thick film. I believe this is due to the defective nature of DEA films formed for long times (*vide infra*).

I have also examined the thickness of films formed for other precursors. For example, 4-diazo-phenylacetic acid fluoroborate was used to produce films of phenylacetic acid (PAA) on a PS masked GC surface. Figure 3.5-A is a 20 × 20 μm contact mode topographic image of a PAA film deposited at –1.0 V for 30

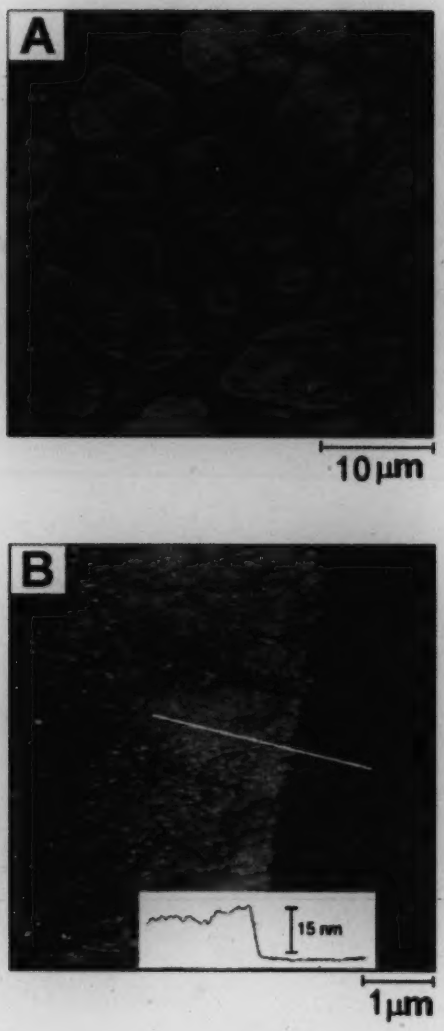

Figure 3.3: (A) 30 × 30 µm topographic SFM image of a GC electrode. The surface contains regions modified with DEA (lighter contrast) adjacent to unmodified polished GC (darker contrast). Experimental details regarding how these regions were obtained are outlined in the text. (B) A higher magnification image of the boundary between a modified and unmodified region. The thickness measured at the boundaries is plotted vs. deposition time in Figure 3.4. Z-scale is 40 nm in both images.

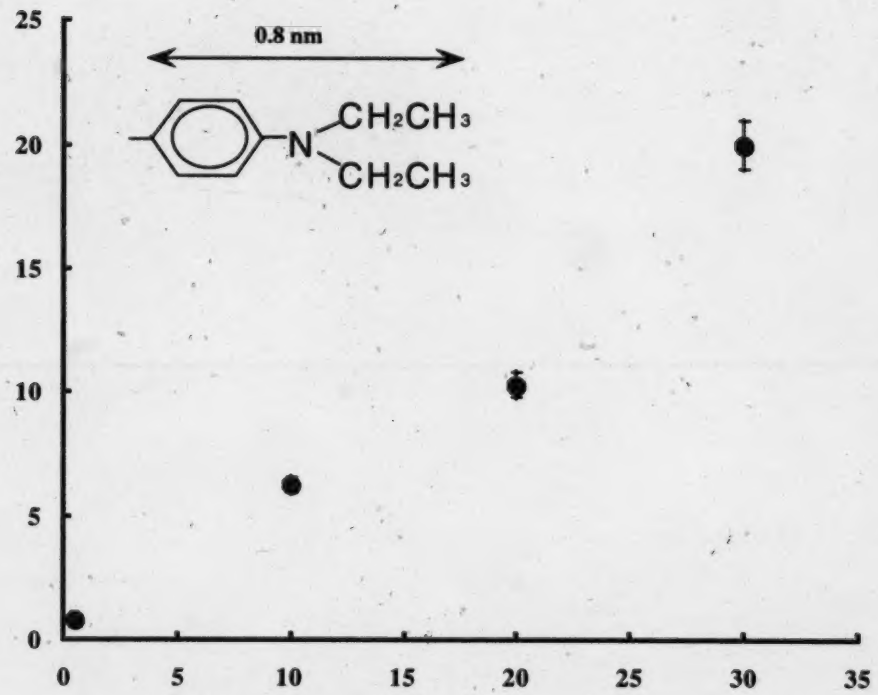

Figure 3.4: Plot of film thickness against attachment time for DEA films formed on GC with potential steps of 5 mM DDEA (0.1 M Bu_4NBF_4/CH_3CN) at different time scales.

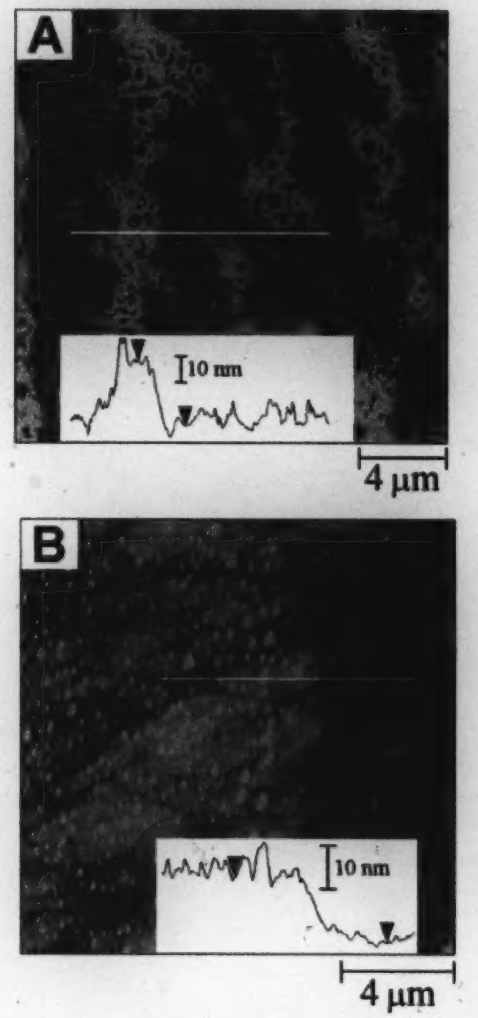

Figure 3.5: (A) 20 × 20 μm contact mode image of a PAA film deposited at –1.0 V for 30 min on a GC electrode. The surface contains regions modified with PAA (lighter contrast) adjacent to unmodified polished GC (darker contrast). For PAA deposition, CV peak potential is –0.2 V vs Ag/AgCl, while the deposition potential used to deposit the film was –1.0 V vs Ag/AgCl. (B) 15 × 15 μm image of a NB film formed at a PS masked electrode with a thickness of 15 nm. For NB deposition, CV peak potential is 0.2 V vs Ag/AgCl, while the deposition potential used to deposit the film was –0.5 V vs Ag/AgCl. Z-scale is 40 nm for both images.

min. The PS mask was removed by dissolving in CCl_4. The cross-sectional profile in the inset of Figure 3.5-A illustrates that a 30 min. deposition yields a 25 nm thick PAA film. Figure 3.5-B is a 15 × 15 μm image of a NB film formed at a PS masked electrode with a thickness of 15 nm. Thus, multilayer aryl films with a range of functional groups can be deposited on GC by reducing the corresponding diazonium salt for time-scales greater than 10 min.

Electrochemical properties of thick DEA films. The blocking ability of DEA films on GC was assessed by cyclic voltammetry of several redox systems. The $Fe(CN)_6^{3-/4-}$ redox couple is a common benchmark system with an electron transfer (ET) rate that is very sensitive to the state of the GC surface [17]. The ET rate of $Ru(NH_3)_6^{2+/3+}$ is relatively insensitive to the GC surface state [17]. Finally, $Eu^{2+/3+}$ is a system dependent on the presence of surface carbonyl groups [18]. Table 3.2 lists the cyclic voltammetric peak separation (ΔE_p) for the three systems on polished GC and DEA modified GC. Also listed is the DEA film thickness determined by SFM. All three systems show an increase in ΔE_p as the deposition time increases. This is consistent with the IRRAS and SFM results that indicate DEA deposition continues with time. For $Eu^{2+/3+}$, any deposition more extensive than 2 cycles completely blocks ET indicating that the attachment of DEA quickly and completely obstructs the surface carbonyl sites. However, the other two redox systems do not become completely blocked, even at 20 nm thick DEA films. In

Deposition time	ΔE_p(mV) for ν = 100 mV/s			
	$Fe(CN)_6^{-3/-4}$	$Ru(NH_3)^{+3/+2}$	$Eu^{+3/+2}$	SFM measured thickness (nm)
Polished GC	78 ± 10	80 ± 9	203 ± 21	0
2 cycles	115 ± 6	88 ± 3	408 ± 15	0.8 ± 0.1
10 min	170 ± 5	110 ± 4	> than 1200	6.2 ± 0.4
20 min	200 ± 9	115 ± 14	> than 1200	10.3 ± 0.9
30 min	230 ± 5	120 ± 4	> than 1200	20.0 ± 0.6

Table 3.2: Cyclic voltammetric peak separations for three redox systems at DEA modified GC electrodes.

fact, the heterogeneous electron transfer rate constants (k^o) for $Fe(CN)_6^{3-/4-}$ and $Ru(NH_3)_6^{2+/3+}$ are much higher than expected for the thicker DEA films. Electrostatic interactions with a partially protonated DEA layer can be discounted because both a positively and negatively charged redox species display similar behavior. For example, I do not observe any significant change in peak current of the cyclic voltammograms for the three redox systems. Hence, there does not appear to be any significant preconcentration of the redox species into the grafted film.

From long-range ET studies at metal/monolayer interfaces, the apparent (k^o_{app}) should exponentially decrease with the thickness of the layer, d, via

$$k^o_{app} = k^o \exp(-\beta d) \qquad (1)$$

where β is the tunneling parameter, and k^o is the heterogeneous rate constant. Yang and McCreery determined a β of 0.20 $Å^{-1}$ for through-bond tunneling at functionalized aryl monolayers on GC [5]. Assuming a similar tunneling mechanism and using k^o of 0.012 cm/s for $Fe(CN)_6^{3-/4-}$ at a polished GC surface, a 20 nm thick DEA film should yield a k^o_{app} of ~10^{-20} cm/s. The ΔE_p of 230 mV for $Fe(CN)_6^{3-/4-}$ on the 20 nm thick DEA film (30 min. electrolysis), however, corresponds to a k^o of 7.3×10^{-4} cm/s. It is clear that ET pathways other than through-bond tunneling are operative at DEA multilayers.

An alternative ET pathway to through-bond tunneling in thin organic films on electrodes is through defects. I investigated the possibility of this mechanism

by probing the uniformity of DEA multilayers on GC with SFM. Figure 3.6 compares the topography of a polished GC electrode (Figure 3.6-A) with that of a 30 min. DEA film (Figure 3.6-B). Scratches resulting from the polishing procedure characterize the topography of Figure 3.6-A. The DEA film topography in Figure 3. 6B is composed of groupings of 100-200 nm diameter cluster-like structures. Visually, the overall morphology of the DEA film appears less uniform than the original polished GC surface and it is apparent that the topography in Figure 3.6-B is not governed by the underlying GC substrate. Quantitative descriptions of the topography are obtained from analysis of cross-sectional profiles. The profile of Figure 3.6-B exhibits a root mean square (rms) of 9.0 nm and a maximum deviation in the z-direction of 19 nm. Similar results are obtained from roughness analysis of the image as a whole. Thus, while the average thickness of a DEA film deposited for 30 min. is 20 nm, the local topography varies over a length-scale comparable with the thickness.

Studies have shown that molecular scale defects can govern ET at organic monolayers adsorbed to metal electrodes [19]. Figure 3.6-B shows that the structure of DEA films deposited for longer times exhibit non-uniformity at micron length scales. It is likely that a significant number of molecular scale defects exist in the film as well. The electrochemical barrier properties of these films will be severely compromised by these defects. The low level of electrochemical blocking for $Fe(CN)_6^{3-/4-}$ and $Ru(NH_3)_6^{2+/3+}$ listed in Table 2 is

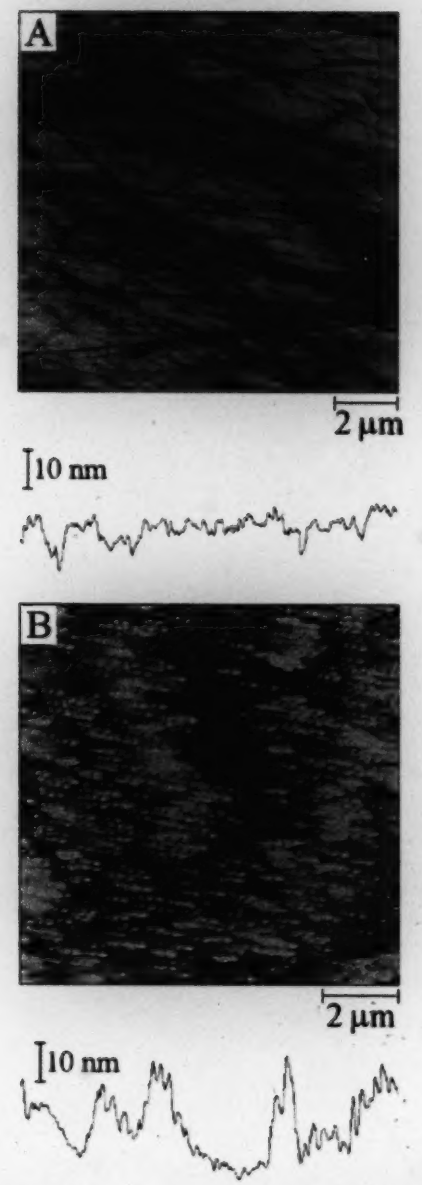

Figure 3.6: (A) 12 x 12 µm topographic image of a polished GC electrode. Surface roughness measurements were as follows: rms = 1.3 nm, maximum height = 5.2 nm. (B) 10 x 10 µm topographic image of a GC electrode modified with a DEA film obtained after a 30 min. deposition of DDEA at –1.0 V vs Ag/AgCl . rms = 9.0 nm, maximum height = 16.0 nm. Z-scale is 20 nm for both images.

consistent with a defective film structure. In addition, the prolonged film growth shown in Figure 3.3 implies that aryl radicals are continually generated. If the radicals are generated at defects, it is surprising that the defects do not "heal" during the 30 min. time-scale. I speculate that the defect sites may be efficient electron transfer sites for radical production but not favorable sites for binding and that more favorable binding sites exist at the film terminus.

It is important, at this point, to compare my results for the blocking capabilities of DEA films with those reported for phenyl films bearing other functionalities. Saby *et al.* observed complete blocking of $Ru(NH_3)_6^{2+/3+}$ at a nitrophenyl film formed for 4 min [4]. Downard [15] recently reported that an unsubstituted phenyl film, formed for 10 min. at sufficient overpotential, also completely blocks $Ru(NH_3)_6^{2+/3+}$. Direct comparison of these and my observations is difficult because of lab-to-lab differences in materials and electrode preparation procedure. For example, Saby *et al.* and Downard used GC-10 from different manufacturers (Saby: AIMCORE, Downard: Atomergic), while I use Tokai GC-20. It is known that the processing temperature (GC-10: 1000°C, GC-20: 2000°C) greatly influences the electrochemical reactivity of GC [20]. Despite these procedural inconsistencies, I believe the results reported by Saby *et al.* and Downard are consistent with multilayer formation. A monolayer of phenyl or nitrophenyl groups (0.59 nm and 0.68 nm thick, respectively [5]) would not be expected to completely block $Ru(NH_3)_6^{2+/3+}$ ET. For example, using my observed k^o = 0.01 cm/s for $Ru(NH_3)_6^{2+/3+}$ at polished GC and β = 0.2 $Å^{-1}$, k^o_{app} at a

complete nitrophenyl monolayer would be 0.0026 cm/s. This translates into a ΔE_p of 153 mV for ν = 200 mV/s.

Chen and McCreery noted a slight increase in ΔE_p (12 mV at 20 V/s) for $Ru(NH_3)_6^{2+/3+}$ relative to a polished GC surface, at a nitrophenyl film formed under monolayer-producing conditions [17]. Considering all of these results combined, it appears that the blocking capabilities and thus the structure of functionalized phenyl films on carbon electrodes depend on both the precursor molecule and the deposition procedure.

Conclusions

In this chapter, I have shown that multilayer films of substituted phenyl moieties can be formed by the electrolysis of diazonium salts. I find that DEA films continue to grow throughout a 30 min. electrolysis at an overpotential of -250 mV. SFM images show that this procedure can produce DEA films with an average thickness of 20 nm. I also show that 15-25 nm thick phenylacetic acid and nitrobenzene films can also be produced by 30 min. electrolysis. The DEA films produced at long electrolysis times do not display electron transfer blocking abilities that are characteristic of their thickness. SFM analysis reveals that the topography of these films is non-uniform implying a defective structure. This defective structure compromises the blocking ability of the films.

Although it has been shown that multilayer films can form on GC surfaces, the exact nature of the multilayer films has not been fully determined by the presented data. Hence, further studies geared towards the determination of the mechanism of the formation of the observed multilayers and eventually the exact nature of the multilayer films needs to be carried out.

References

1. A. J. Downard, *Electroanalysis* 12:1085 (2000).

2. M. Delamar, R. Hitmi, J. Pinson, and J.-M. Saveant, *J. Am. Chem. Soc.* 114:5883 (1992).

3. P. Allongue, M. Delamar, B. Desbat, O. Fagebaume, R. Hitmi, J. Pinson, and J.-M. Saveant, *J. Am. Chem. Soc.* 119:201 (1997).

4. C. Saby, B. Ortiz, G. Y. Champagne, and D. Belanger, *Langmuir* 13:6805 (1997).

5. H.-H. Yang and R. L. McCreery, *Anal. Chem.* 71:4081 (1999).

6. C. Bourdillon, M. Delamar, C. Demaille, R. Hitmi, J. Moiroux, and J. Pinson, *J. Electroanal. Chem.* 336:113 (1992).

7. A. J. Downard and A. D. Roddick, *Electroanalysis* 7:376 (1995).

8. C. Henry de Villeneuve, J. Pinson, F. Ozanam, J. N. Chazalviel, and P. Allongue, *Mat. Res.Soc. Symp. Proc.* 451:185 (1997).

9. J. K. Kariuki and M. T. McDermott, *Langmuir* 15:6534 (1999).

10. M. F. W. Dunker, E. B. Starkey, and G. L. Jenkins, *J. Am. Chem. Soc.* 58:2308 (1936).

11. R. S. Nicholson, *Anal. Chem.* 37:1351 (1965).

12. S. N. Magonov, V. Elings, and M.-H. Whangbo, *Surf. sci.* 375:L385 (1997).

13. M. D. Porter, T. B. Bright, and D. A. Allara, *Anal. Chem.* 58:2461 (1986).

14. J. B. Lambert, H. F. Shurvell, D. A. Lightner, and R. G. Cooks, *Introduction to Organic Spectroscopy*, Macmillan Publishing Company, New York, 1987.

15. A. J. Downard, *Langmuir* 16:9680 (2000).

16. E. P. Koval'chuk, Z. E. Kozlowska, J. L., and J. Blazejowski, *Polish J. Chem.* 74:67 (2000).

17. P. Chen and R. L. McCreery, *Anal. Chem.* 68:3958 (1996).

18. C. A. McDermott, K. R. Kneten, and R. L. McCreery, *J. Electrochem. Soc.* 140:2593 (1993).

19. H. O. Finklea, S. Avery, and M. Lynch, *Langmuir* 3:409 (1987).

20. R. L. McCreery, in *Electronalytical Chemistry*, Vol. 17 (A. J. Bard, ed.), Marcel Dekker, New York, 1991, p. 221.

Chapter IV

Controlling Protein Adsorption at Carbon Surfaces via Chemical Modification

Introduction

The electrochemical analysis of biological samples is often hampered by electrode fouling arising from non-specific protein adsorption. To circumvent this problem, there have been many efforts to develop modification methods that would increase surface hydrophilicity and thus decrease protein adsorption [1]. Coating with membranes such as cellulose film, Nafion or polyesters have proven to be feasible techniques for this purpose. However, membrane electrodes seem to have found only a few applications (e.g., stripping analysis of trace metals), probably due to the slow mass transport of organic analytes in thick polymeric membranes. Covalent modification with hydrophilic molecules has been shown to have possibilities as a tool for prevention of protein adsorption. Gold electrodes modified with a self-assembled monolayer of 2-mercaptoethane sulfonic acid were reported to resist protein adsorption quite effectively [1]. Polymers and oligomers of ethylene glycol are well known to confer protein resistance to surfaces and a considerable amount of work has focused on the properties of self-assembled monolayers of these species on gold substrates [2, 3]. In contrast, modification of carbon surfaces with ethylene glycol has received little attention. In one approach, poly(oxyethylene) diamines have been coupled to carbon surfaces via amide bond formation to form hydrophilic tethers for attachment of enzymes [4].

Dehydrogenase enzymes have also been immobilized onto carbon fiber microelectrode surfaces via avidin-biotin technology and a covalently linked hydrophilic tether [5]. In a second recent example, glassy carbon (GC) electrodes anodized in oligomers of ethylene glycol and their monomethyl ethers showed resistance to adsorption of bovine serum albumin (BSA) [6]. The study compared the properties of seven closely related species coupled to the electrodes using a standard procedure. Electrodes modified with triethylene glycol and its monomethyl ether were found to resist surface fouling by BSA and to retain adequate sensitivity to small analytes.

The ability to probe and control nonspecific protein adsorption at interfaces is also a key issue in the design of implant materials. Key issues for these applications are the type, amount and conformation/orientation of surface bound proteins [7]. For example, the biocompatibility of materials is generally governed by the state in which certain plasma proteins adsorb at the surface. In comparison to receptor-ligand binding, which involves a particular site on the biomolecule, nonspecific adsorption generally involves the interaction of a large fraction of the amino acid sequence with the surface. Because of the participation of a significant portion of the protein, adsorption often induces conformational changes from the solution state. Also, in some situations, a single binding mode will be favored over the many possible modes, producing a protein film with a preferred orientation of molecules [8].

It is now well accepted that the properties of surfaces will govern both the degree of conformational change and orientation of nonspecifically adsorbed proteins. The ability to rationally design interfaces for biosensors, implants, etc., with predefined control over protein adsorption will only be realized with the aid of techniques that can rapidly analyze surface induced variations in protein conformation and orientation. Furthermore, detailed studies using well-defined interfaces presenting a wide range of chemical groups will enable the evaluation of the effect of specific surface properties on protein adsorption. Because of the apparent importance of the interactions occurring between surfaces and blood proteins, there has been increasing interest in studies of the behavior of protein adsorption with respect to different surfaces. As well, chemical modification of surfaces has been carried out in order to control the chemical properties of the surface with a view of controlling protein adsorption.

Essential to understanding the fundamental role of the modified surfaces in both electrochemical and other applications is the ability to characterize the surface at a microscopic level and a macroscopic level. These type of studies have been mostly carried out using scanning force microscopy (SFM) and infrared reflectance absorbance spectroscopy respectively (IRRAS) [9]. The growth of SFM in both academic and industrial research can be attributed, in part, to its applicability for imaging biological samples. One of the unique features of SFM is its ability to image a biomolecular system under ambient conditions and in aqueous environments, thus opening up a way to follow biochemical reactions in

real time with nanometer resolution [10-12]. As well, SFM has been used to probe resistance to protein adsorption of many types of monolayers both on carbon and gold surfaces [13-15]. In this work I use SFM to study changes in protein conformation or orientation on highly oriented pyrolytic graphite (HOPG) surfaces before and after chemical modification. Although GC is the more widely used electrode, I used HOPG as the substrate in the SFM studies due to the ease of obtaining an atomically flat surface simply by cleaving the substrate with adhesive tape. Once the HOPG surface has been thoroughly characterized, similar studies could be extended to GC electrodes.

In this chapter, I will present my SFM studies on the nature of the thin films formed by the grafting of aryl groups containing different functional groups on carbon surfaces. Aryl films exposing a variety of functional groups have been utilized in applications focussed on controlling protein adsorption [16, 17]. The response of the modified electrodes for oxidation of ferrocenemethanol in the absence and presence of bovine serum albumin (BSA) was monitored to give a measure of protein adsorption. As well Bourdillion *et al.* have demonstrated the covalent attachment of glucose oxidase on a carbon surface using the same method [18]. I will characterize films obtained from the reduction of 4-diazo-N,N-diethylaniline tetrafluoroborate (DDEA), 4-nitrobenzene diazonium tetrafluoroborate (NB), and 4-phenylacetic acid diazonium tetrafluoroborate (PAA) on carbon surfaces. I will then investigate the utility of these films for controlling protein adsorption on carbon surfaces. Bovine fibrinogen (BFG) was

used as the study protein because fibrinogen is one of the plasma proteins that has received much attention due to its dual functionality in thrombosis (formation of a blood clot). The conversion of fibrinogen to fibrin and the subsequent polymerization of fibrin is a key step in blood clot formation. Fibrinogen also serves as an adhesive agent in the aggregation of platelets, which occurs simultaneously with fibrin polymerization in the development of a blood clot [19].

My second set of investigations involves applying my expertise with covalent modification of carbon electrodes to the area of carbon biomaterials. The valves of the heart are made up of very strong flaps of tissue called leaflets that open and close as the heart contracts and releases. When working properly, these leaflets keep blood flowing in the correct direction through the heart. Heart valve disease prevents the valves from opening or closing properly, thus interfering with the flow of blood. Valve repair surgery can be used to fix an improperly opening or closing valve. However, when a valve is too badly deformed, the old valve is removed and replaced with an artificial valve. Artificial heart valves are usually from animals or from human donors. Tissue valves from animals have the advantage of not requiring the long-term use of blood-thinning medications. However, since the durability of these valves is limited, they are less attractive option, especially in young patients. Human valves have the advantage of not being associated with rejection by the body and providing normal heart valve function. These valves, however, are in short supply [20].

The mechanical heart valve has the advantage of being very durable. It is not, however, a natural part of the body, and there is danger that blood clots may form on it. The vast majority of mechanical prosthetic heart valves are constructed either partially or wholly of low temperature isotropic carbon (LTIC). Similar to most artificial implant materials, LTIC devices are susceptible to complications due to thrombosis/thromboembolism [21]. Patients carrying mechanical heart valves are required to orally ingest anticoagulants on a daily basis in order to curb thromboembolism formation. These patients live with the danger of anticoagulant-related hemorrhaging. In this work, I employ the derivatization scheme used to modify both GC and HOPG electrodes to LTIC surfaces with an aim of developing methodologies for controlling aryl deposition on LTIC. The ability to control the chemistry of the LTIC surfaces is an important initial step in the design of LTIC heart valves with enhanced blood compatibility.

Experimental Section

Reagents. The following reagents were all used as received: 4-diazo-N,N-diethylaniline tetrafluoroborate (DDEA), and tetrabutylammonium tetrafluoroborate (Bu_4NBF_4) were obtained from Aldrich. 4-Nitro benzenediazonium tetrafluoroborate (NB) was obtained from Sigma. 4-phenylacetic acid diazonium tetrafluoroborate was synthesized from 4-aminophenylacetic acid (Aldrich) according to the procedure described by Dunker *et al* [22]. 0.1 mole of the corresponding amine precursor was dissolved in 44 mL

of 50% fluoroboric acid. The solution was placed in an ice bath and stirred with an efficient stirrer. Then a cold solution of 0.1 M of sodium nitrite in 14 mL of water was added dropwise. When the addition was complete, the mixture was stirred for several more minutes, and then suction filtered on a sintered-glass filter. The solid diazonium tetrafluoroborate was washed with cold ethanol, and then with diethyl ether. Reagent grade Acetonitrile (CH_3CN), 50 % fluoroboric acid, diethyl ether (anhydrous, 99.8%), were obtained from Fisher. Sodium nitrite was obtained from ACP Chemicals Inc., Montreal, QB). Ethanol (punctilious grade) was obtained from AAPER Alcohol & Chemical Company, Shelbyville, KY. Bovine fibrinogen solutions (BFG) (20 μg/mL) were prepared by weight, using fraction I, 95% clottable fibrinogen, obtained from Sigma (St. Louis, MO). Distilled/deionized water (18 MΩ/cm) was used in all solution preparations. All solutions were purged with pure argon before use.

Electrode Preparation. Fresh surfaces of highly oriented pyrolytic graphite (HOPG) (A gift from Dr. Arthur Moore of Advanced Ceramics Materials, Lakewood, OH) were generated by cleaving with adhesive tape before each experiment. Low temperature isotropic carbon (LTIC) was obtained in the form of heart valve leaflets and were a gift from Medical Carbon Research Institute (Austin, Texas).

SFM Imaging. SFM images were obtained with a Nanoscope III multimode microscope (Digital Instruments, Santa Barbara, CA). Scanning was performed in contact mode with Si_3N_4 cantilevers, k ~ 0.06 N/m (Digital

Instruments, Nanoprobes), both in ambient conditions and in a fluid cell. Unless otherwise stated, all images were collected in 1 mM phosphate buffered saline (PBS), prepared with reagent grade 0.2 mM KH_2PO_4 and 0.8 mM Na_2HPO_4, 1 mM KCl and 10 mM NaCl. All solutions that were to be introduced into the microscope were filtered with 0.22 μm millex-GV low protein-binding filter (Millipore, Bedford, MA) just before use. Topographic and lateral force images were collected simultaneously, but in most cases, only topographic images are shown. Images were software flattened and are shown unfiltered.

Results and Discussion

In the following sections, I report my SFM characterizations on the growth of aryl films on HOPG and GC surfaces. I then investigate the influence of aryl modification on the adsorption of bovine fibrinogen (BFG) on these carbon surfaces. I will use my results as a guide for studies on low temperature isotropic carbon (LTIC).

In order to study the effect of protein adsorption on aryl films, diazonium salts bearing different functionalities were used. I first used SFM to investigate the surface morphology of an unmodified HOPG surface. Figure 4.1 is a 5 x 5 μm SFM topographic image of an unmodified HOPG surface. Observed in the image are terraces of atomically flat basal plane graphite separated by several diagonally running step defects that results from cleaving of the HOPG with adhesive tape

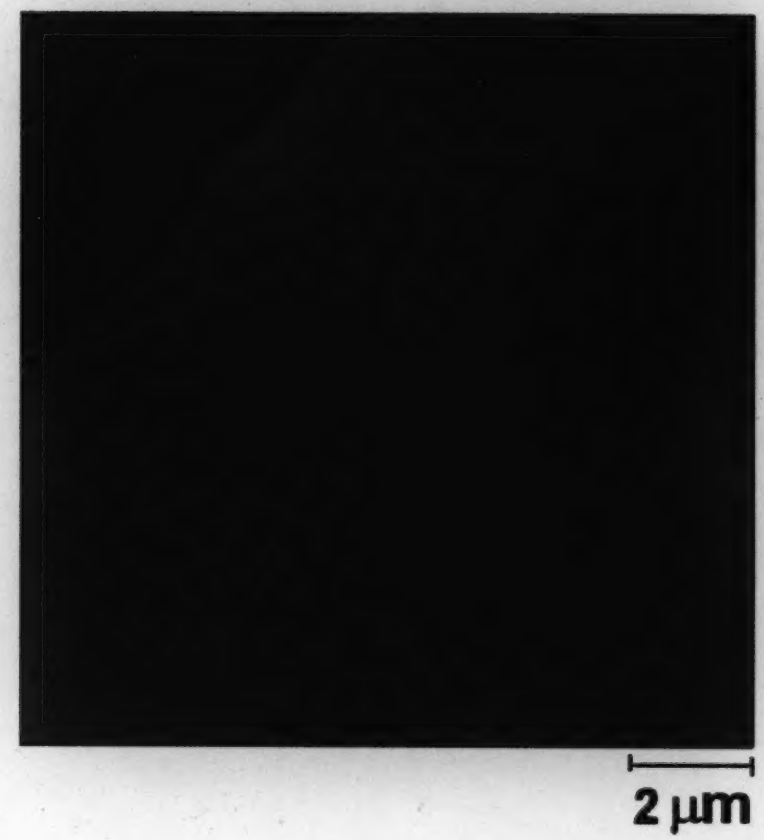

Figure 4.1: 10×10 μm SFM topographic image of an unmodified HOPG substrate. The image was collected in 1mM PBS.(z-scale = 10 nm).

[23-25]. After thorough characterization of the unmodified substrate, deposition of the diazonium salts was effected. Differences in surface structure of the films formed on HOPG as a result of electrochemical reduction of the three diazonium salts were investigated by use of SFM.

Figure 4.2 is a 10 x 10 μm SFM topographic image of a HOPG substrate modified by 1 cycle in 5 mM nitrobenzene diazonium tetrafluoroborate (NB) in 0.1 M Bu_4NBF_4/CH_3CN. The film morphology is comprised of uniformly distributed spherical structures. However, several three-dimensional structures exhibiting a larger height than the surrounding layer were also observed. The structures are due to multilayer formation. Details of the formation of the multilayers were presented in Chapter 2.

Figure 4.3 is a 10 x 10 μm SFM topographic image of a HOPG substrate modified by 1 cycle in 5 mM 4-phenylacetic acid diazonium tetrafluoroborate (PAA) in 0.1 M Bu_4NBF_4/CH_3CN. In contrast to the film structure formed from the DDEA and NB precursors, partial monolayer formation is observed in this case. The surface consists of several segregated modified and unmodified regions. The modified regions are high in topography (lighter contrast) when compared to the unmodified regions. Exposed basal plane can be seen in the unmodified regions. This type of structure is useful because it provides two well defined regions composed of the hydrophilic phenylacetic acid film regions and the hydrophobic HOPG basal plane. As an aside, this type of structure can be useful, for example, in several applications that require the ability to pattern biological

Figure 4.2: 10×10 µm SFM topographic image of a HOPG substrate modified by one cycle in 5 mM NB (0.1 M Bu_4NBF_4/CH_3CN). (z-scale = 10 nm).

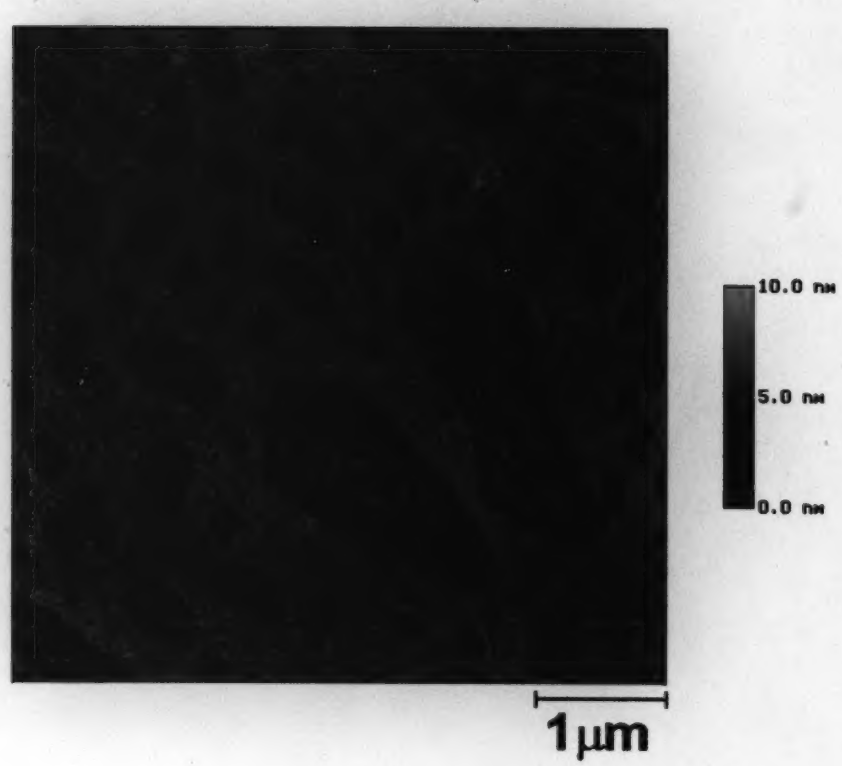

Figure 4.3: 5 × 5 μm SFM topographic image of a HOPG substrate modified by one cycle in 5 mM PAA (0.1 M Bu_4NBF_4/CH_3CN). (z-scale = 10 nm).

ligands onto surfaces [26]. For example, microphotolithographic techniques were used to devise silica surfaces bearing two types of microdomains with an average width of 40 μm. One of the microdomains was silanized in order to make it hydrophobic. SFM was used to correlate the topographic distribution of diluted human plasma to the specific chemistry of each type of microdomain.

When a foreign material comes into contact with blood, it is generally accepted that a complex biomolecular film containing plasma proteins forms at the interface. It is commonly agreed that interaction between a biomaterial and blood and/or tissues in general are governed by its surface characteristics in terms of physicochemical properties. In this respect, the surface free energy which is related to the residual binding capacity of the biomaterial surface, is expected to be an objective parameter of these interactions [27]. My objective is to prepare model surfaces with well-defined chemistry bearing either hydrophilic or hydrophobic groups. The pKa of DEA is about 6.6 [28]. Hence in a pH 7.4 buffer solution the surface terminated with a DEA film should be neutral and hydrophobic. The pKa of a PAA molecule is 4.3 [28]. In pH 7.4 buffer the surface carboxylates should be deprotonated resulting in a negatively charged and hydrophilic surface. The nitrobenzene terminated surface is charged but generally hydrophobic. It should be noted that the pKa's quoted above are for solution dissolved species and may not be necessarily the same as that of the surface-bound molecule. For example, the pKa's of several surface-bound groups have been found to shift by between 7-4 units when compared to values in aqueous solutions

[29, 30]. In this work it is presumed that the pKa's of the bound moieties are close to those in solution.

In order to compare the effect of protein adsorption on the three surfaces with different chemical properties, bovine fibrinogen (BFG) was adsorbed on the surfaces. To act as a control, BFG was also adsorbed on an unmodified HOPG surface. The following discussion illustrates the utility of SFM to probe surface-induced variations in adsorbed BFG film structure. The results presented compare film structures on unmodified and chemically modified HOPG surfaces. The surface morphology of an unmodified HOPG substrate was earlier shown in Figure 4.1. Figure 4.4 is a 5 x 5 μm SFM topographic image of a HOPG substrate, collected 1 mM PBS, after adsorbing 20 μg/ml BFG for one hour. The surface is comprised of fibrinogen aggregates that range in height between 4 to 13 nm. These type of aggregates have been seen previously using scanning electron microscopy (SEM) [31] and have been designated as macromolecular protein complexes [32]. The aggregates were stable to imaging at moderate normal forces (10 nN) for extended periods implying a robust structure. Aggregates in various shapes and dimensions were a common observation on the imaged surfaces. As a result, the morphology of the aggregates will be used as a diagnostic of the influence of each functional group on the adsorbed protein.

I next investigated the effect of protein film structure as a result of modifying the HOPG surfaces with aryl groups bearing different functional

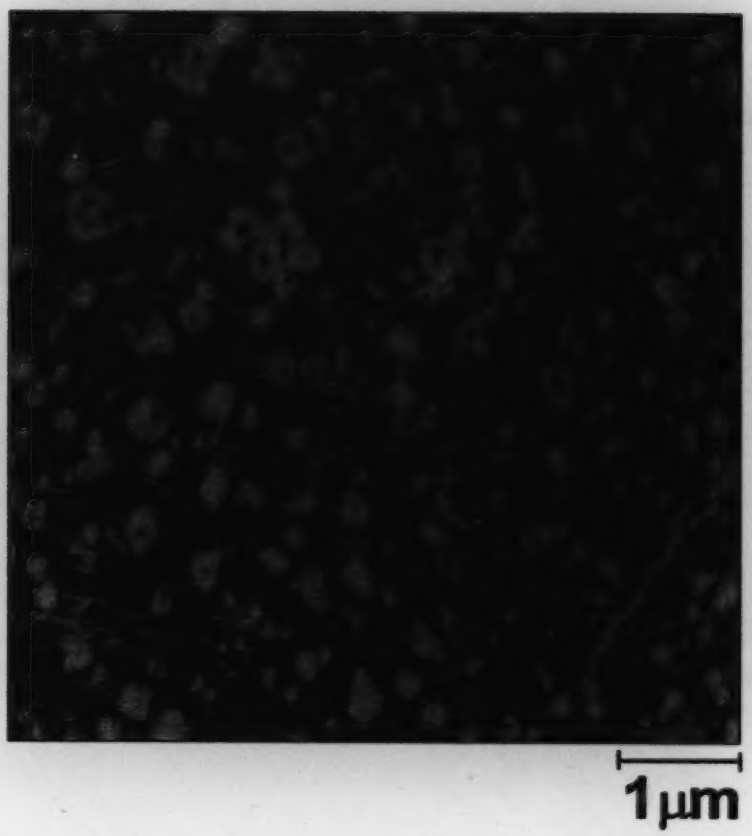

Figure 4.4: 5×5 µm SFM topographic image of HOPG substrate after adsorbing 20 µg/ml BFG for 1 hour. The image was collected in 1mM PBS. (z-scale = 10 nm).

groups. Figure 4.5-A is a 5 x 5 μm SFM topographic image of a HOPG substrate collected in 1mM PBS after modification by 1 cycle of 5mM NB in a 0.1 M Bu_4NBF_4/CH_3CN solution. The surface is fully covered by a continuous NB film. Figure 4.5-B shows the same surface after adsorption of 20 μg/ml BFG for one hour. The surface was imaged in 1 mM PBS. Observed on the surface are more closely packed protein aggregates than those obtained at an unmodified HOPG surface (Fig. 4.4). As well, the aggregates are smaller in size than those observed at the unmodified HOPG surface. The NB film is charged and less hydrophobic than the unmodified HOPG surface. It has been reported that reduction of the nitro to amine may occur for the grafted film at the deposition conditions [33, 34]. The film is however expected to retain significant hydrophobic character. Fibrinogen has a net charge of about –7 at a pH of 7.4 [19]. Adsorption of fibrinogen is favored on hydrophobic surfaces. It is thought that the D-domains of fibrinogen change conformation to maximize hydrophobic interactions [19]. This results in the formation of smaller protein aggregates on the less hydrophobic NB film when compared to the unmodified HOPG surface.

Figure 4.6-A is a 5 x 5 μm SFM topographic image of an HOPG substrate collected in 1 mM PBS after modification by 1 cycle of 5 mM DDEA in a 0.1 M Bu_4NBF_4/CH_3CN solution. A uniform DEA film covers the surface. Figure 4.6-B shows the same surface after adsorption of 20 μg/ml BFG for one hour. The surface was imaged in 1 mM PBS. Unlike the surface modified by the NB film, the surface morphology consists of larger macromolecular protein aggregates.

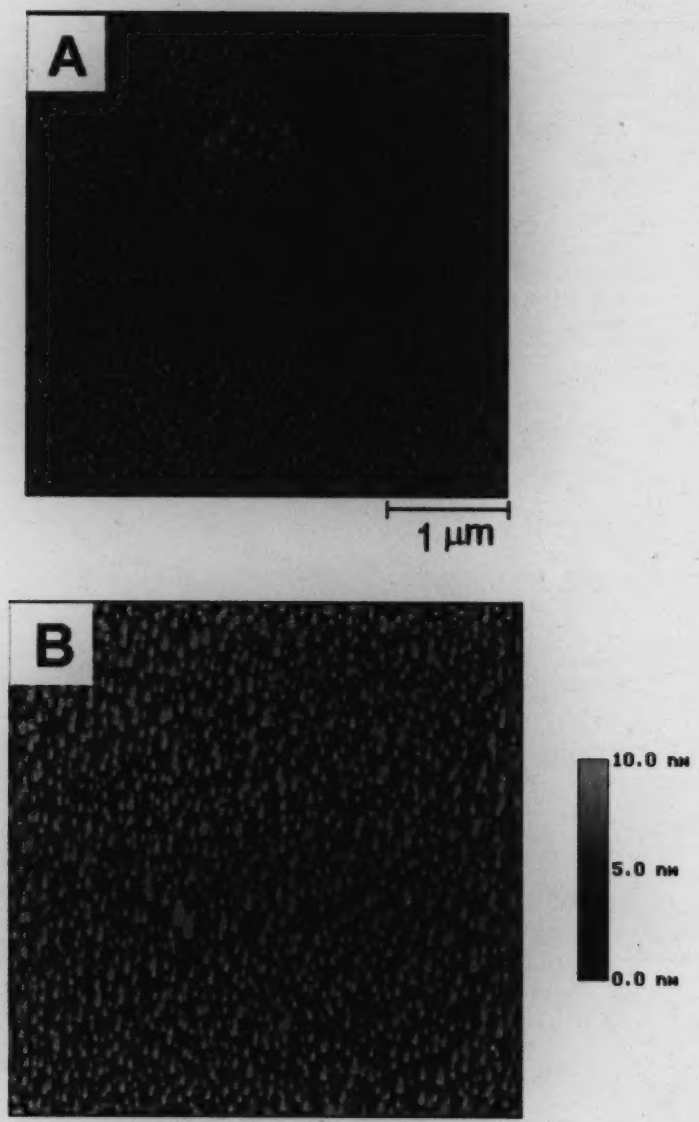

Figure 4.5: 5 × 5 μm SFM topographic images of a HOPG substrate. (A) Surface modified by one cycle in 5 mM NB (0.1 M Bu_4NBF_4/CH_3CN). (B) Same surface after adsorbing 20 μg/mL BFG for one hour. (z-scale = 10 nm).

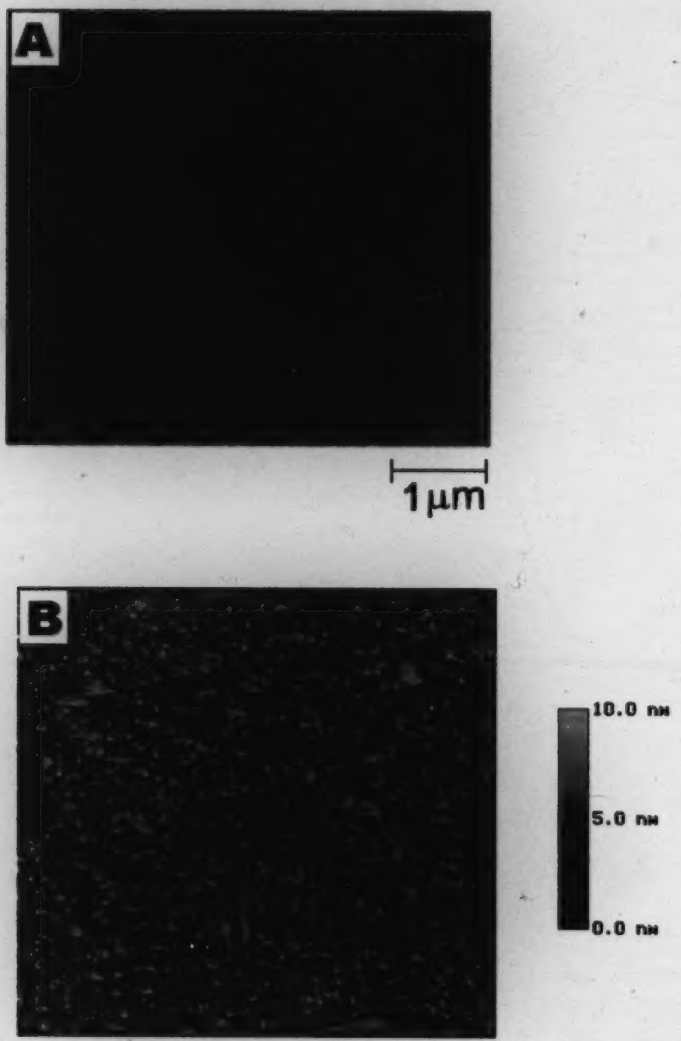

Figure 4.6: 5 × 5 μm SFM topographic images of a HOPG substrate (A) Surface modified by one cycle in 5 mM DDEA (0.1 M Bu_4NBF_4/CH_3CN). (B) Same surface after adsorbing 20 μg/mL BFG for one hour. (z-scale = 10 nm).

The aggregates are less densely packed and many are larger in size when compared to those found at the NB modified HOPG surface (Fig. 4.4). The aggregates range in height between 2 to 5 nm. At a pH of 7.4, the hydrophobic DEA film is neutral. Like most proteins, fibrinogen is usually adsorbed more on hydrophobic surfaces. It is therefore expected that there will be a favorable interaction between the fibrinogen and the DEA film. The measured height is less than the expected width of a single BFG molecule (4-6) nm possibly because of structural rearrangement. It is thought that the D-domains of fibrinogen change conformation to maximize hydrophobic interactions [19].

Figure 4.7-A is a 5 x 5 μm SFM topographic image of a HOPG substrate collected in 1 mM PBS after modification by 1 cycle of 5 mM PAA in 0.1 M Bu_4NBF_4/CH_3CN solution. The surface is comprised of segregated regions that consist of modified regions and unmodified regions exposing graphite basal plane. Figure 4.7-B shows the same surface after adsorption of 20 μg/ml BFG for one hour. The surface morphology is also comprised of macromolecular protein complexes. The size of the aggregates is different in the modified and unmodified regions. The aggregates range in height between 6 to 10 nm on the PAA modified sections and between 3 to 7 nm on the unmodified sections. The aggregate heights on the unmodified regions compare well with the heights observed in Figure 4.4 which showed the nature of the BFG on an unmodified HOPG surface. The pKa of PAA is 4.3. Hence, at a pH of 7.4, the surface-bound carboxylate groups are negatively charged [35], while fibrinogen has a net charge of about –7 [19]. Due

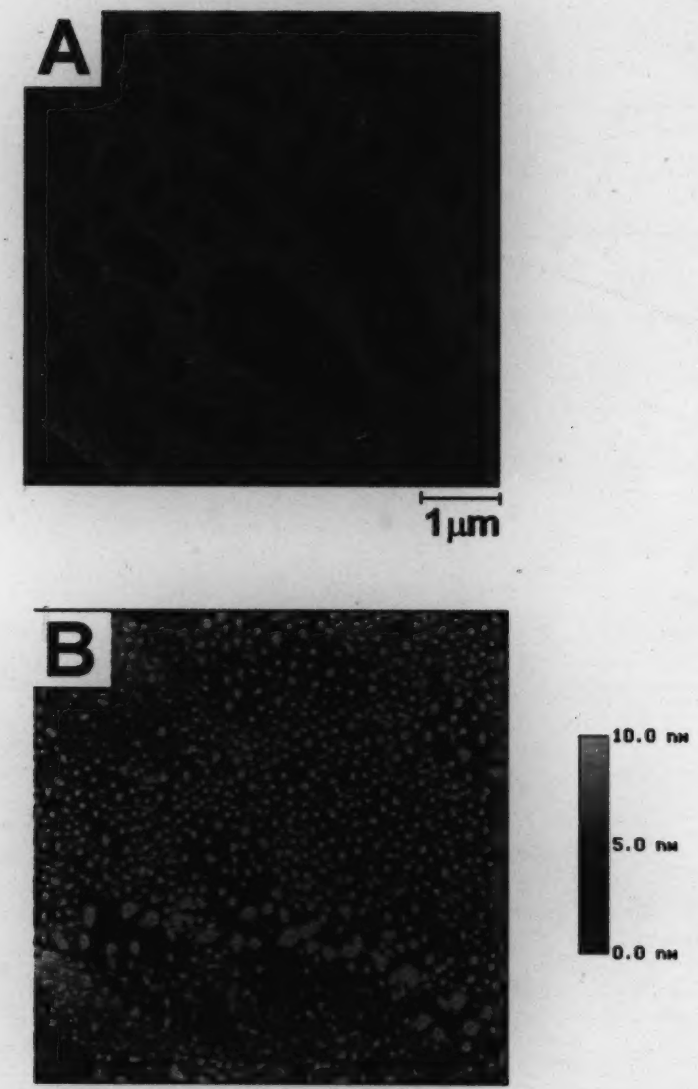

Figure 4.7: 5 × 5 µm SFM topographic images of a HOPG substrate. (A) Surface modified by one cycle in 5 mM PAA (0.1 M Bu_4NBF_4/CH_3CN). (B) Same surface after adsorbing 20 µg/mL BFG for one hour. (z-scale = 10 nm).

to electrostatic repulsion between the protein and the surface, inter-protein interactions are favored resulting in formation of the observed aggregates. The aggregates formed on the unmodified regions are larger by a factor of 2 when compared to those at the modified regions. This results from the favorable interactions between the fibrinogen and the exposed hydrophobic HOPG regions. It has been postulated that the D-domains of fibrinogen change conformation to maximize hydrophobic interactions [19].

To obtain an overall view of the differences in protein aggregates formed on the three surfaces, the size and density of aggregates formed on each surface were determined. Table 4.1 compares the aggregate diameter, aggregate height, and particle density of BFG on an unmodified HOPG surface as well as on the three modified surfaces. The size and the shape of the tip play a major role in defining the area of microcontact between the tip and the sample [36]. Although the presented data include a degree of tip convolution, data with similar features was obtained using different tips on the respective surfaces. This shows that the major factor controlling the shape and size of the protein aggregates was the underlying surface. The highest particle density of 46 particles per μm^2 was observed on the NB modified surface. More strand-like structures were observed on the DDEA modified surface giving a particle density of less than 5 particles per μm^2. In summary, the differences obtained in the number and size of the protein aggregates formed on the different surfaces can be attributed to the influence each

	Aggregate Diameter (nm)	Aggregate Height (nm)	Particle density / (μm^2)
	178±23	6.7±1.7	12±2
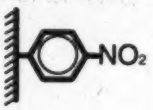	72±13	9.3±2.8	46±2
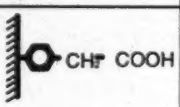	84±17 (Unmodified: 160 nm)	6.9±1.7	36±4
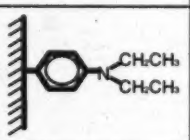	167±36	3.1±1.5	<5

Table 4.1: Results of SFM studies comparing protein aggregate size, number and density on an unmodified HOPG surface and on HOPG surfaces modified by one cycle in 5 mM solutions of NB, PAA, and DDEA in (0.1 M Bu_4NBF_4/CH_3CN) respectively.

surface has on the protein conformation and orientation. The hydrophilic or hydrophobic nature of the surface plays an integral part in determining the nature of the adsorbed protein.

The ability to control the adsorption of proteins to carbon surfaces is vital to the development of more compatible implant devices. Figure 4.8 is a photographic image of a full size commercial carbon heart valve fabricated from LTIC. The valves are more widely used than those made from animal tissue as they offer improved durability and alleviate clotting problems that have plagued development of heart valves for a decade. To date approximately 2000 implants of the LTIC fabricated heart valve have being carried out worldwide [20].

Using our expertise in modifying carbon surfaces, I extended my aryl modification scheme to an actual carbon heart valve. Figure 4.9 is a cyclic voltammogram corresponding to the reduction of 5 mM PAA in 0.1 M Bu_4NBF_4/CH_3CN on a LTIC surface. As was the case on GC and HOPG surfaces, a chemically irreversible wave was observed that corresponds to the reduction of PAA to phenylacetic acid radical. The observation of the irreversible wave suggests that the generated radical attaches to the heart valve surface in the same manner as was shown for HOPG and GC surfaces in Chapters II and III. This is an important initial step that shows the above method should lead to modulation of protein adsorption on LTIC as was shown for HOPG surfaces.

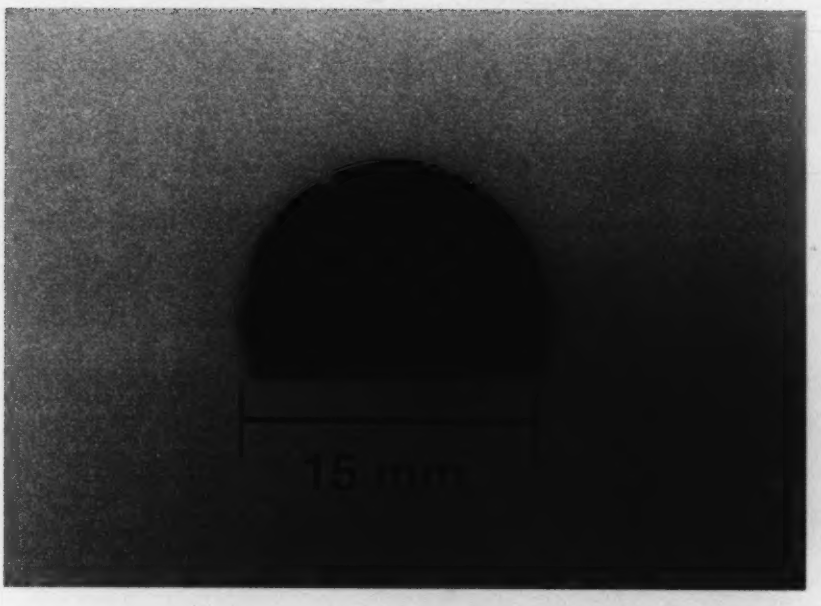

Figure 4.8: Photograph of an actual size carbon heart valve made from LTIC

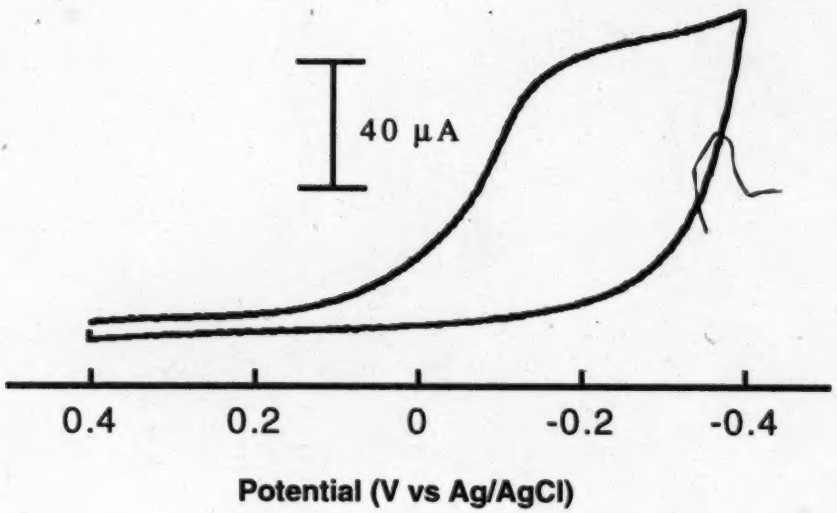

Figure 4.9: Cyclic voltammogram for the reduction of 5 mM PAA (0.1 M Bu_4NBF_4/CH_3CN on a heart valve fabricated from LTIC

In order to compare the surface morphology of LTIC with that of GC, I used SFM to study the surface properties of a LTIC substrate. Figure 4.10-A is a 10 x 10 μm^2 topographic image of a heart valve leaflet fabricated from LTIC. The leaflet was imaged as received without prior polishing. Figure 4.10-B is a 10 x 10 μm^2 topographic image of a polished GC electrode. The heart valve surface morphology bears some resemblance to that of an unpolished GC substrate. It consists of irregularly defined high topographic regions (lighter contrast) and low topographic regions (darker contrast). The GC surface exhibits the same features but appears much smoother when compared to the LTIC surface on the same scale. The similarities in surface morphology between the LTIC and GC surfaces are not surprising in that both are made by the pyrolysis of hydrocarbons [21, 37]. It would be difficult to study differences in protein conformations adsorbed on these surfaces using SFM due to their rough nature. Such studies can be carried out by infrared spectroscopy. Results from these types of studies will be presented in Chapter 5.

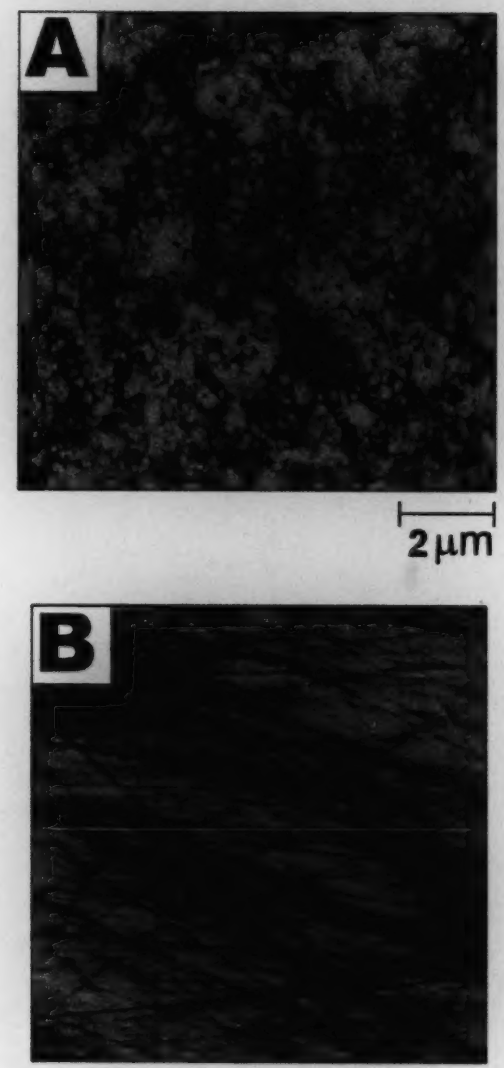

Figure 4.10: 10 × 10 μm SFM topographic mages. (A) A LTIC substrate (B) GC electrode z-scale = 10 nm for both images.

Conclusions

Using SFM, I have shown that the morphology of fibrinogen films depends on the nature of the substrate. Changing the chemistry of the carbon surface through chemical modification changes the conformation and orientation of the adsorbed protein as shown by the differences in physical features. I have been able to extend the modification scheme used on GC and HOPG surfaces to modify a heart valve made from LTIC. The extension of this easy and versatile modification scheme to LTIC, a material that shows a fair degree of biocompatibility, may ultimately lead to the production of a more biocompatible material.

References

1. H. Maeda, T. Okada, Y. Matsumoto, K. Katayama, Y. Yamauchi, and H. Ohmori, *Anal. Sci.* 15: 633 (1999).

2. K. L. Prime and G. M. Whitesides, *J. Am. Chem. Soc.* 115: 10714 (1993).

3. P. H. Grunze, R. Dahint, G. M. Whitesides, and P. E. Laibinis, *J. Phys. Chem. B* 102: 426 (1998).

4. P. Pantano, H. Morton, and W. G. Kuhr, *J. Am. Chem. Soc.* 113: 1833 (1991).

5. P. Pantano and W. G. Kuhr, *Anal. Chem.* 65: 623 (1993).

6. H. Maeda, M. Itami, K. Katayama, Y. Yamauchi, and H. Ohmori, *Anal. Sci.* 13: 721 (1997).

7. T. A. Horbett and J. L. Brash, in *Proteins at Interfaces: Physicochemical and Biochemical Studies* (J. L. Brash and T. A. Horbett, eds.), American Chemical Society, Washington, DC, 1987, p. 1.

8. J. E. Lee and S. S. Saavedra, in *Proteins at Interfaces II: Fundamentals and Applications* (J. L. Brash and T. A. Horbett, eds.), American Chemical Society, Washington, DC, 1985, p. 1.

9. T. C. Ta and M. T. McDermott, *Anal. Chem.* 72: 2627 (2000).

10. T. C. Ta, M. T. Sykes, and M. T. McDermott, *Langmuir* 14: 2435 (1998).

11. M. D. Garrison, T. C. McDevitt, R. Luginbuhl, C. M. Giachelli, P. Stayton, and B. D. Ratner, *Ultramicroscopy* 82: 193 (2000).

12. J. Tamayo, M. Miles, A. Thein, and P. Soothill, *J. Struct. Biol.* 128: 200 (1999).

13. K. Feldman, G. Hahner, N. D. Spencer, P. Harder, and M. Grunze, *J. Am. Chem. Soc.* 121: 10134 (1999).

14. T. B. McPherson, H. S. Shim, and K. Park, *J. Biomed. Mater Res.* 38: 289 (1997).

15. S. O. Vansteenkiste, S. I. Corneillie, E. H. Schacht, X. Chen, M. C. Davies, M. Moens, and L. Van Vaeck, *Langmuir* 16: 3330 (2000).

16. A. J. Downard, A. D. Roddick, and A. M. Bond, *Anal. Chim. Acta* 317: 303 (1995).

17. A. J. Downard and A. D. Roddick, *Electroanalysis* 7: 376 (1995).

18. C. Bourdillon, M. Delamar, C. Demaille, R. Hitmi, J. Moiroux, and J. Pinson, *J. Electroanal. Chem.* 336: 113 (1992).

19. L. Feng and J. D. Andrade, in *Proteins at Interfaces II: Fundamentals and Applications* (T. A. Horbett and J. L. Brash, eds.), American Chemical Society, Washington, DC, 1995, p. 66.

20. Medical Carbon Research Institute Web Site, (www.mcritx.com, accessed December 2000).

21. L. Feng and J. D. Andrade, *J. Biomed. Mater. Res.* 28: 735 (1994).

22. M. F. W. Dunker, E. B. Starkey, and G. L. Jenkins, *J. Am. Chem. Soc.* 58: 2308 (1936).

23. H. Chang and A. J. Bard, *Langmuir* 7: 1143 (1991).

24. D. R. Baselt and J. D. Baldeschwieler, *J. Vac. Sci. Technol. B* 10: 2316 (1992).

25. M. T. McDermott and R. L. McCreery, *Langmuir* 10: 4307 (1994).

26. J. Lahiri, E. Ostuni, and G. M. Whitesides, Langmuir 15: 2055 (1999).

27. M. C. Porte-Durrieu, G. N'Kaoua, B. Brouillaud, D. Ricci, H. Grattarola, and C. Baquey, *Colloid and Surfaces B: Biointerfaces* 17: 205 (2000).

28. D. R. Lide, ed., *CRC Handbook of Chemistry and Physics, 81st ed.*, CRC Press LLC, Boca Raton, FL, 2000.

29. E. W. van der Vegte and G. Hadziioannou, *J. Phys. Chem. B* 101: 9563 (1997).

30. D. V. Vezenov, A. Noy, L. F. Rozsnyai, and C. M. Liber, *J. Am. Chem. Soc.* 119: 2006 (1997).

31. H. Nygren and M. Stenberg, *J. Biomed. Mater. Res.* 22: 1 (1988).

32. B. Lipnski, S. M. Federman, and A. Krdewski, *Thrombosis Res.* 78: 461 (1995).

33. C. Saby, B. Ortiz, G. Y. Champagne, and D. Belanger, *Langmuir* 13: 6805 (1997).

34. Y.-C. Liu and R. L. McCreery, *J. Am. Chem. Soc.* 117: 11254 (1995).

35. A. Noy, D. V. Vezenov, and C. M. Lieber, *Annu. Rev. Mater. Sci.* 27: 381 (1997).

36. H. Takano, J. R. Kenseth, S. Wong, J. C. O'Brien, and M. D. Porter, *Chem. Rev.* 99: 2845 (1999).

37. R. L. McCreery, in *Electronalytical Chemistry*, Vol. 17 (A. J. Bard, ed.), Marcel Dekker, New York, 1991, p. 221.

Chapter V

Application of IRRAS to Study the Effect of Electrochemical Modification of Glassy Carbon Surfaces on Protein Adsorption

Introduction

In this chapter, I present infrared reflectance absorbance spectroscopy (IRRAS) descriptions of the adsorption of human fibrinogen (HFG) on modified carbon. Glassy carbon (GC) is used as a model material. It closely resembles low temperature isotropic carbon, a common artificial heart valve. Prior to adsorbing the proteins, the surfaces were modified by covalently attaching thin films bearing different functional groups. For this purpose, a recently discovered method that utilizes reduction of diazonium salts was used [1]. Protein adsorption on the modified surfaces was compared to that on a polished GC surface.

Quantitative and qualitative studies of surface-adsorbed proteins have been carried out mostly using electron microscopy, ellipsometry, Raman spectroscopy, radiolabelling techniques and ultraviolet fluorimetry [2]. However, with the advent of Fourier transform techniques, several reports that utilize IRRAS to probe the molecular nature of surfaces are currently available. For example, Sarver and Krueger have analyzed the conformation of protein deposited on polyethylene films using IRRAS [3]. The method produced estimates of protein secondary structure on relatively small quantities of protein in the range of 80 to 200 μg.

Few studies have applied IRRAS for such characterizations at carbon-based surfaces [4, 5]. This is a consequence of the inherent complexities of the experiment and the resulting spectra due to the lower reflectivity of carbon-based electrodes relative to metals. The low reflectivity reduces the sensitivity of the method. However, FTIR combined with insights from electromagnetic theory for optimizing sensitivity has led to the application of external-reflection IR on surfaces with low reflectivity [6, 7].

Because protein adsorption is of importance in determining biocompatibility, there is great need to study the molecular level interactions which take place when blood or blood components are exposed to various surfaces. Spectroscopic methods such as circular dichroism [8] and infrared spectroscopy (IR) in various configurations (*i.e.* attenuated total reflectance, reflectance adsorption) have been shown to be invaluable tools for the study of these important molecular level events [3]. Infrared spectroscopy is especially valuable because large amounts of chemical information are contained in the IR spectrum and detailed structural information has been accumulated in recent years produced by a number of various modifications of IR measurements, including reflection absorption spectroscopy. High resolution, high throughput, and the multiplex advantage of FTIR, combined with powerful-computer-supported data acquisition and handling, have introduced further advances in the study of vibrational species [9]. A recent review has shown the application of IR to problems in human health, which include studies of diseases, and drug delivery

[10]. Absorption band frequency, intensity and shape can reveal information regarding protein conformation, including the types and amounts of various secondary structures [11]. For example, the interaction of proteins with a surface can shift absorbance frequencies to higher energy as a result of protein denaturation. The intensity of amide II bands has been used to quantify the amount of protein present at the interface and peak shape analysis of amide I has been used for assigning protein secondary structure or conformation [12, 13].

This chapter will present demonstrate the ability to study adsorbed protein conformation on carbon surfaces with IRRAS. Most artificial implants are made from low temperature isotropic carbon (LTIC). In these studies, we employ GC to mimic the structure of LTIC. Electrochemical reduction of diazonium salts is used to chemically modify the GC surfaces. IRRAS is used to examine protein adsorption onto the modified GC and to quantitate antibody binding. It is hoped that these types of studies will eventually lead towards the use of diazonium attachment as a modification method for carbon biomaterials.

Experimental

Reagents and Materials. 4-diazo-N,N- diethylaniline fluoroborate (DDEA), and tetrabutyl ammonium tetrafluoroborate (Bu_4NBF_4) were obtained from Aldrich and used as received. 4-phenylacetic acid tetrafluoroborate was synthesized from 4-aminophenylacetic acid (Aldrich) according to the procedure described by Dunker *et al.* [14]. Reagent grade Acetonitrile (CH_3CN) was

obtained from Fisher and was used as received. All diazonium salt solutions were prepared in acetonitrile in 0.1 M Bu_4NBF_4 as the supporting electrolyte Fraction I human fibrinogen (HFG) was obtained from Sigma. Antibody to HFG (anti-HFG) from goat serum and antibody to fibronectin (anti-FN) were obtained from ICN biomedical (Aurora, OH). Protein concentrations were determined based on dry weight and diluted using 1 mM phosphate buffered saline (PBS), prepared with reagent grade 0.2 mM KH_2PO_4 and 0.8 mM Na_2HPO_4, 1 mM KCl and 10 mM NaCl. 20 µg/mL of HFG was used while 160 µg/mL of anti-HFG and anti-FN were used. Distilled/deionized water (18 MΩ/cm) was used in all solution preparations.

Electrode Preparation. The GC electrodes used for IRRAS (Tokai GC-20, Electrosynthesis Company, NY) consisted of 3 cm x 6 cm x 3 mm plates. The backside of these plates were coated with a thick film of poly(ethylene)/poly(vinylacetate) 60:40 (Aldrich) to block electroactivity. Electrode surfaces were prepared by polishing with successive slurries of 1, 0.3, and 0.05 µm alumina in nanopure water on microcloth (Buehler). The electrodes were sonicated for 10 min in distilled/deionized water between each size of the alumina slurries.

IRRAS Spectroscopy Studies. IRRAS spectra were obtained on an ATI Mattson Infinity Series FTIR spectrometer (Madison, WI) equipped with an external sample module and liquid nitrogen cooled mercury-cadmium-telluride (MCT) detector. Spectra were taken at 4 cm^{-1} resolution with an interferometer

mirror speed of 50 kHz. Typically 1000 scans were averaged to yield spectra with an acceptable signal-to-noise ratio. The interferrograms were Fourier transformed using triangular apodization. Reference spectra were obtained by use of an unmodified GC substrate. The p-polarized light was incident at an angle of 60° to maximize the mean-square electric field (MSEF) [15].

Results and Discussion

In the following sections, results obtained by use of IRRAS to study the effect of different carbon surfaces on protein adsorption are presented. I will compare spectra obtained after adsorbing HFG on polished GC surfaces with spectra obtained on GC surfaces following modification by 5 mM PAA, and by 5 mM DDEA solutions. Results of the effect of adsorbed protein to antibfibrinogen (anti-HFG) binding will also be presented.

Proteins and peptides exhibit characteristic bands in the 1500 to 1700 cm^{-1} spectral range, which are the direct results of vibrations in the peptide linkages. Specifically, the amide I band (C=O stretch) appears in the region from 1650 to 1680 cm^{-1} and the amide II band (combination of C-N stretch and N-H bend) is generally located in the vicinity of 1550 cm^{-1}. These bands typically exhibit high intensity and are useful as a diagnostic of adsorbed proteins [16-19]. Figure 5.1 contains IRRAS spectra from 2000 to 1000 cm^{-1} for three different GC surfaces. Spectrum A is that of a polished GC surface. A polished GC surface consists of a graphitic oxide layer which contains bands due to C-OH, C-O, and C=O vibrations

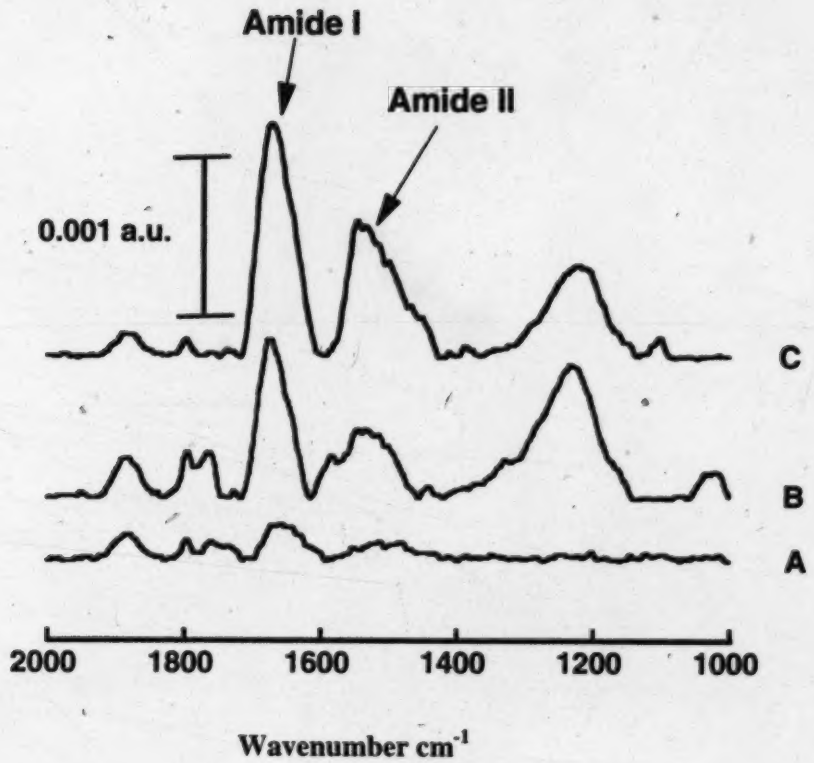

Figure 5.1: IRRAS spectra of various carbon surfaces. Spectrum A is of a polished GC. Spectrum B is of a GC surface after adsorbing HFG for one hour. Spectrum C is of a GC surface modified by a five minute potential step in 5 mM PAA (0.1 M Bu_4NBF_4/CH_3CN, then adsorbing 20 μg/mL HFG for one hour.

at 1070, 1400, and 1750 cm^{-1} respectively [20]. Spectrum B results following adsorption of 20 μg/ml HFG on a polished GC surface for one hour. Strong absorbencies corresponding to amide I (ν_{aI} = 1672 cm^{-1}) and amide II bands (ν_{aII} = 1546 cm^{-1}) are observed, diagnostic of HFG adsorption to the GC surface. This observation is consistent with previous measurements of fibrinogen adsorption on hydrophilic surfaces [12].

The spectroscopic results describing the interaction of HFG with a carboxylate-terminated monolayer are contained in spectrum C of Figure 5.1. The appearance of amide I band at 1672 cm^{-1} and amide II at 1546 cm^{-1} is noted. Most FTIR analysis of adsorbed proteins have been carried out on gold and other metal surfaces [9, 12]. The amide I and amide II peaks occur in the same region as observed in our results. The absorbance of the amide II band is linearly related to the amount of protein bound to the surface [21]. The amide II peak height for the polished GC surface is 0.0010 a.u. compared to 0.0015 a.u. for the PAA terminated surface. The data indicates almost equal affinity for protein adsorption for the PAA terminated surface when compared to the polished GC surface.

The frequency of the amide I band is changed upon adsorption to solid surfaces in relation to the same bands in the aqueous and solid phases. Blue shifts of about 10 to 40 cm^{-1} are observed, suggesting a conformational change upon adsorption [12, 22]. This shift can be used to supply qualitative details on the state of adsorbed protein. In Figure 5.1 the peak position of the amide I band in the polished (ν_{aI} = 1669 cm^{-1}), and the PAA (ν_{aI} = 1668 cm^{-1}) modified surfaces

spectra is blue shifted from its position for solution dissolved or solid HFG (ν_{al} = 1650 cm^{-1}) implying a degree of adsorption-induced conformation changes [23].

Peak positions for the amide I and amide II peaks were compared from spectra obtained at various GC surfaces. Table 5.1 shows Amide I and Amide II peak position of HFG adsorbed on various GC surfaces. Surfaces were modified with diethylaniline (DEA) or with PAA films. At all the three carbon surfaces, amide I and amide II peaks were found to be at approximately 1670 cm^{-1} and 1550 cm^{-1} respectively. These values agree with literature reports on proteins adsorbed on various surfaces [16, 19]. The amide I peak position for a protein in a native aqueous phase is ~ 1650 cm^{-1}. A blue shift in peak position is observed upon adsorption at all the three carbon surfaces. This shift has been attributed to a change in protein conformation upon adsorption [22].

Owing to their high specificity, antibodies immobilized on various supports have been widely used for different purposes such as purification, diagnostic immunoassays and immunosensors. In all cases the relative strength of the antibody-antigen interactions were utilized [24, 25]. Figure 5.2 contains IRRAS spectra from 1000 to 2000 cm^{-1} of a GC surface modified with a 5 min potential step at –0.6 V in 5 mM PAA. Spectrum A results after exposure of the GC surface to 20 µg/mL of HFG in PBS for one hour. After obtaining Spectrum A, the same surface was exposed to 160 µg/mL anti-HFG in PBS for two hours to obtain

Amide I and Amide II Peak Positions for HFG on Various Carbon Surfaces			
	Polished GC	**DDEA Modified Surface**	**PAA Modified Surface**
Amide I	1669 ± 4	1668 ± 3	1671 ± 3
Amide II	1545 ± 4	1549 ± 1	1550 ± 3

Table 5.1. Table of Amide I and Amide II peak position of HFG adsorbed on various GC surfaces. Surfaces were modified with 5 mM of DDEA or with 5 mM of PAA by a Potential step for 5 minutes. Values are compared with those at a polished GC surface.

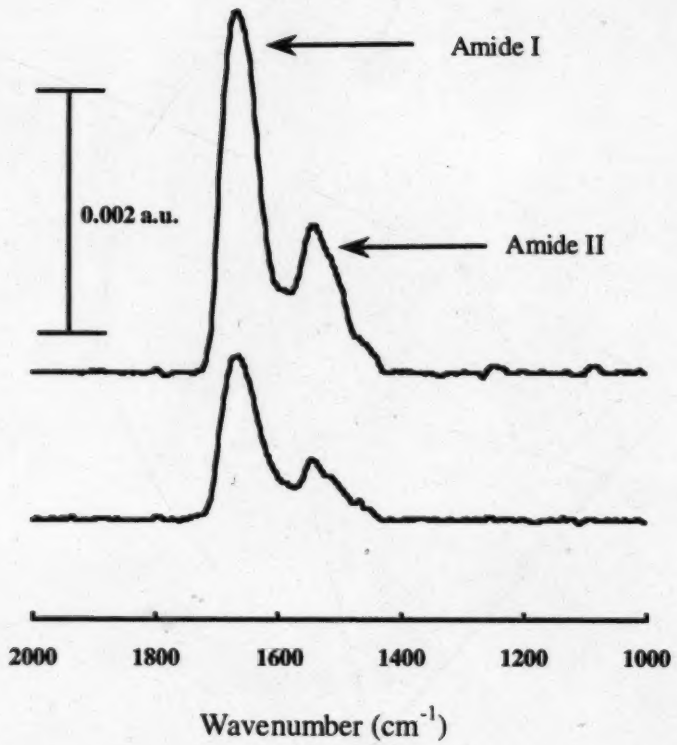

Figure 5.2: IRRAS spectra of HFG on GC surfaces modified with a potential step at –0.6 V in a solution of 5 mM PAA in 0.1 M Bu_4NBF_4 for 5 min. Spectrum A is after adsorption of 20 µg/mL of HFG in PBS for one hour. Spectrum B is after adsorption of anti-HFG in PBS for 2 hours.

Spectrum B. In both spectra, the characteristic amide I and amide II bands were observed. The absorbance of amide II bands is linearly related to the amount of protein bound to the surface [3]. An increase in the absorbance of the amide II band is noted in Spectrum B after adsorption of the anti-HFG. As expected from the favorable antigen-antibody binding, the increase in the amide II intensity corresponds to an increase in the amount of protein adsorbed on the surface.

Antibody binding is a widely accepted method to probe differences in protein conformation [26]. Antibody binding was therefore used to investigate whether HFG binds with different conformations on GC surfaces modified with DEA and PAA films. Figure 5.3 is a bar graph of corrected specific antibody binding as a function of surface chemistry onto which HFG was previously adsorbed. The amount of adsorbed HFG, as well as those of specific and non-specific binding, was based on intensities of amide II bands generated by IRRAS. The non-specific binding was corrected for by adsorbing antifibronectin (anti-FN) on surfaces already exposed to HFG. Bar 1 of Figure 5.3 shows the corrected % amide II increases due to anti-HFG binding on a GC surface modified with a 5 min potential step at – 1.0 V in a solution of 5 mM DDEA. Bar 2 of Figure 5.3 shows the same information on a GC surface modified with a 5 min potential step at – 0.6 V in a solution of 5 mM PAA. Percent increase due to specific binding was 48 ± 10 % and 34 ± 7 % for the DDEA and PAA modified surfaces respectively. Although the two means are not significantly different at the 95%

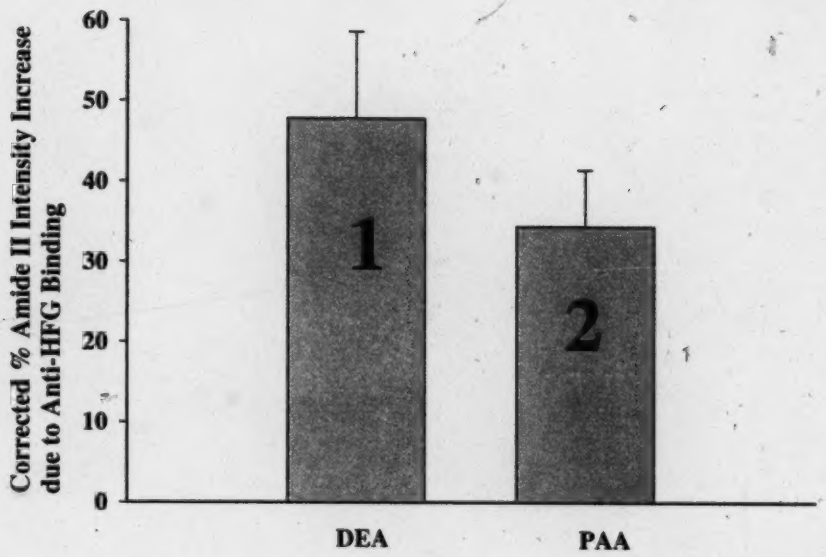

Figure 5.3: Bar graph depicting surface chemistry effect on amount of corrected specific binding of anti-HFG to adsorbed HFG. Bar Graph 1 is of a GC surface modified via a 5 min potential step with 5 mM DDEA in 0.1 M Bu_4NBF_4/CH_3CN at –1.0 V. Bar Graph 2 is of a GC surface modified via a 5 min potential step with 5 mM PAA in 0.1 M Bu_4NBF_4/CH_3CN at – 0.6 V.

confidence level, the small differences observed in the specific binding can be attributed to the different conformations of fibrinogen on surfaces with different chemistries. Similar studies have been carried out on gold surfaces modified with alkanethiol self-assembled monolayers (SAMs) of octadecanethiol and mercaptohexadecanoic acid [27]. Different amounts of antibody bound to adsorbed HFG on the two surfaces. These differences were attributed to differences in conformation of adsorbed HFG.

Amide I to amide II peaks ratios were next calculated for HFG adsorbed on the carbon surfaces. Table 5.2 contains data for amide I to amide II ratios of HFG adsorbed on GC surfaces modified with a 5 min potential step in 5 mM solutions of DDEA and PAA, and on a polished GC surface. Ratios of 1.8 ± 0.1 and 1.4 ± 0.1 were obtained on the DDEA and the PAA modified surfaces respectively. On the polished GC surface, a ratio of 2.2 ± 0.2 was obtained. The mean values between the PAA and the DEA modified surfaces are significant at the 95% confidence. Because the amide I and amide II peak heights are dependent on the interaction of the protein and the surface, the differences observed in the amide I to amide II peak ratios may also be attributed to different interactions between the HFG and the various chemically different surfaces. Amide I/amide II ratios are easily obtained using IRRAS. Therefore this method may eventually gain widespread usage in studying conformational differences of adsorbed protein. This method, unlike previously used IRRAS methods to study differences in

Amide I / Amide II Peak Ratios for HFG on Various Carbon Surfaces		
Polished GC	**DDEA Modified Surface**	**PAA Modified Surface**
2.2 ± 0.2	1.8 ± 0.1	1.4 ± 0.1

Table 5.2. Table of Amide I/Amide II ratio of HFG adsorbed on various GC surfaces. Surfaces were modified with 5 mM of DDEA or with 5 mM of PAA by a Potential step for 5 minutes. Values are compared to those at a polished GC surface.

protein conformation, does not involve extensive calculations or deconvolution of infrared spectra [3, 17].

Conclusions

In this chapter, IRRAS was used to determine conformational differences of proteins adsorbed on GC surfaces with different chemistries. Previous studies reported in the literature have been carried out on gold surfaces due to the inherent difficulties associated with infrared studies on carbon. Because carbon is used to manufacture prosthetic implants, this work presents an important initial step toward studying protein adsorption on a biomaterial using IRRAS. The ease and versatility of modifying carbon surfaces via the reduction of diazonium salts, makes the method easily adaptable to many biochemical applications. I have also demonstrated a quick and versatile method for determining relative protein conformational differences based simply on determining the amide I to amide II ratio. The method does not involve complex spectra deconvolution and is applicable to all proteins.

References

1. M. Delamar, R. Hitmi, J. Pinson, and J.-M. Saveant, *J. Am. Chem. Soc.* 114: 5883 (1992).

2. C. Werner and H. Jacobasch, *Int. J. Artif. Organs* 22: 160 (1999).

3. R. W. J. Sarver and W. C. Krueeger, *Anal. Biochem.* 212: 519 (1993).

4. M. D. Porter, D. H. Karweik, T. Kuwana, W. B. Theis, G. B. Norris, and T. O. Tiernan, *Appl. Spectrosc.* 38: 11 (1984).

5. M. Datta, J. J. Freeman, and R. E. W. Jansson, *Spectroscopy Letters* 18: 273 (1985).

6. M. D. Porter, *Anal. Chem.* 60: 1143A (1988).

7. R. G. Greenler, *J. Chem. Phys.* 44: 310 (1965).

8. R. W. Sarver and W. C. Krueger, *Anal. Biochem.* 199: 61 (1991).

9. M. Trojanowicz, *Anal. Lett.* 33: 1387 (2000).

10. J. K. Gillie, J. Hochlowski, and G. A. Arbuckle-Keil, *Anal. Chem.* 72: 71R (2000).

11. K. K. Chittur, D. J. Fink, T. B. Hutson, R. M. Genderau, R. J. Jakobsen, and R. I. Leiniger, in *Proteins at Interfaces: Physicochemical and Biochemical Studies* (J. L. Brash and T. A. Horbett, eds.), American Chemical Society, Washinton, DC, 1987, p. 362.

12. B. Liedberg, B. Ivarsson, P.-O. Hegg, and I. Lundstrom, *J. Colloid Interface Sci.* 114: 386 (1986).

13. S. Noinville-Servagent, M. Revault, H. Quiquampoix, and M.-H. Baron, *J. Colloid. Interface Sci.* 221: 273 (2000).

14. M. F. W. Dunker, E. B. Starkey, and G. L. Jenkins, *J. Am. Chem. Soc.* 58: 2308 (1936).

15. M. D. Porter, T. B. Bright, and D. A. Allara, *Anal. Chem.* 58: 2461 (1986).

16. T. C. Ta and M. T. McDermott, *Anal. Chem.* 72: 2627 (2000).

17. R. W. Sarver and W. C. Krueger, *Anal. Biochem.* 194: 89 (1991).

18. N. N. Kalnin, I. A. Baikalov, and S. Y. Venyaminov, *Biopolymers* 30: 1273 (1990).

19. R. J. Jakobsen and F. M. Wasacz, *Appl. Spectrosc.* 44: 1478 (1990).

20. R. M. Ianniello, H. J. Wieck, and A. M. Yacynych, *Anal. Chem.* 55: 2067 (1983).

21. C. E. Giacomelli, M. G. E. G. Bremer, and W. Norde, *J. Colloid. Interface Sci.* 220: 13 (1999).

22. B. Liedberg, B. Ivarsson, I. Lundstrom, and W. R. Salaneck, *Progr. Colloid & Polymer Sci.* 70: 67 (1985).

23. B. Liedberg, B. Ivarsson, and I. Lundstrom, *J. Biochem. Biophys. Met.* 9: 233 (1984).

24. B. Lu, M. R. Smyth, and R. O'Kennedy, *Analyst* 121: 29R (1996).

25. M. E. Kelly-Browning, K. Wadu-Mesthrige, V. Hari, and G. Y. Liu, *Langmuir* 13: 343 (1997).

26. K. L. Egodage, B. S. de Silva, and G. S. Wilson, *J. Am. Chem. Soc.* 119: 5295 (1997).

27. C. T. Ta, *Ph.D. Thesis, Department of Chemistry, University of Alberta* (2001).

Chapter VI

Electrochemical Studies of Carbon Films from Pyrolyzed Photoresist and their Application as Model Biomaterials.

Introduction

This chapter describes the preparation of carbon films by pyrolysis of photoresist. The films were pyrolysed from a positive photoresist and will be referred to in this chapter as photoresist-derived carbon (PDC) films. Electrochemical, scanning force microscopy (SFM), infrared reflectance absorbance spectroscopy (IRRAS), and Raman spectroscopy were used to characterize the resulting surfaces. I present my initial efforts to study the effect of modifying the PDC films via electrochemical reduction on controlling protein adsorption. My efforts are geared towards the application of PDC as a model carbon substrate for protein adsorption.

The use of photoresist in integrated circuit (IC) manufacture has mainly been limited to photolithographic applications. Patterns of dielectric, semiconductive, and conductive films have been defined through several steps, including photoresist application and patterning, etching of the underlying film, and removal of the photoresist mask. The direct lithographic definition of these materials would offer significant savings in the cost, as well as ease in the manufacturing of IC's. The first example of fabricating carbon films by pyrolyzing photoresist was reported by Lyons *et al.* [1]. Control of the feature dimensions was achieved by two steps, UV irradiation followed by increasing the

pyrolysis temperature. Thereafter, Lyons demonstrated the potential of direct lithography of carbon for IC manufacture [2]. Recently several studies have been initiated to evaluate thin carbon films as electrode materials and in microelectromechanical systems (MEMS) devices. Most of the focus is on the use of pyrolized photoresist to form carbon electrodes that have potential applications in batteries, electrochemical sensors, capacitors, and MEMS. The advantage of starting with a photoresist is that there is available a wealth of knowledge on forming well-defined microstructures by photolithographic techniques. After the photoresist microstructures are formed, they can be pyrolyzed to produce carbon microstructures which can then serve as microelectrodes. Several studies have been carried out to gauge the utility of pyrolyzed carbon microelectrodes. Kostecki *et al.* demonstrated the use of these microelectrodes to manufacture a carbon interdigitated electrode [3]. An iodine-iodine redox reaction was used to demonstrate the performance of the electrode. Kinoshita *et al.* demonstrated the development of a carbon-based lithium microbattery [4]. The microelectrodes were made by pyrolyzing photoresist. A cell voltage of about 3.0 V was obtainable from the microbattery.

The ease of fabricating smooth PDC films with similar properties to more complex carbon biomaterials, prompted me to employ these substrates for protein adsorption studies. In this chapter, I report my SFM and IRRAS studies of protein adsorption on PDC films. SFM has been widely used both in academic and industrial research for imaging of biological samples [5-7]. A lot of research using

IRRAS has been carried out to provide structural information of adsorbed proteins on metal substrates. Few studies have applied IRRAS for such characterizations at carbon-based surfaces. This is a consequence of the inherent complexities of the experiment and the resulting spectra due to the lower reflectivity of carbon-based electrodes relative to metals. The low reflectivity reduces the sensitivity of the method [8, 9].

The importance of surface chemistry to the electrochemical behavior of carbon electrodes is well established and has been reviewed extensively [10]. Redox systems vary greatly in their sensitivity to surface structure and, therefore, to surface history [11-13]. Redox systems have been classified to some degree, according to their electron-transfer kinetics. Classes include outer sphere systems e.g., $Ru(NH_3)_3^{+3/+2}$ which are insensitive to surface modification, but have been shown to act as an indicator of thick films or insulators, and systems requiring a non-oxide surface site e.g., $Fe(CN)_6^{-3/-4}$ but are decelerated when an intentional monolayer is present. Others like $Eu_{aq}^{+3/+2}$ are catalyzed by specific surface oxides [14, 15]. These well-defined redox systems will be used to characterize the PDC films before and after modification of the surfaces. The PDC films were modified via electrochemical reduction of diazonium salts [16]. The method is simple, flexible, and allows the grafting of functionalized aryl groups. As a result, surfaces with different chemistries can be easily tailored. The effect of the modified surfaces on protein adsorption and to electron-transfer kinetics was investigated. My findings show that different terminated aryl groups bound to the

surface produced different amounts of adsorbed protein. The electron-transfer blocking properties of the films were dependent on the chemical nature of the grafted aryl groups.

Experimental

Reagents and Materials. 4-diazo-N,N-diethylaniline fluoroborate (DDEA), and tetrabutyl ammonium tetrafluoroborate (Bu_4NBF_4) were obtained from Aldrich. 4-Nitro benzenediazonium tetrafluoroborate (NB) was obtained from Sigma. 4-phenylacetic acid diazonium tetrafluoroborate was synthesized from 4- aminophenylacetic acid (Aldrich) according to the procedure described by Dunker *et al.* [17]. Reagent grade Acetonitrile (CH_3CN) was obtained from Fisher. The redox systems studied were as follows: $Ru(NH_3)_6^{3+}$(aq) in 1 M KCl and $Fe(CN)_6^{3-}$ (aq) in 1 M KCl were prepared at 1mM concentrations from $Ru(NH_3)_3Cl_3$ (Strem Chemicals, Newburyport, MA) and $K_3Fe(CN)_6$ (Caledon Laboratories Ltd., Ontario, Canada) respectively. Eu^{3+}(aq) in 0.2 M $NaClO_4$ solution was prepared at 5 mM concentrations from $Eu(NO_3).5H_2O$ (Aldrich). All reagents were used as received. Fraction I human fibrinogen (HFG), and Fraction V bovine serum albumin (BSA) with 99% clottable protein were obtained from Sigma. Protein concentrations were determined based on dry weight and diluted using 1 mM phosphate buffered saline (PBS), prepared with reagent grade 0.2 mM KH_2PO_4 and 0.8 mM Na_2HPO_4, 1 mM KCl and 10 mM NaCl. For IRRAS studies, 1.5 x 1.5 cm PDC substrates were used, while 1 x 1 cm pieces were used for SFM

studies. Distilled/deionized water (18 MΩ/cm) was used in all solution preparations. All solutions were purged with pure argon for 20 minutes before use.

SFM Imaging. SFM images were obtained with a Nanoscope III multimode microscope (Digital Instruments, Santa Barbara, CA). Scanning was performed in contact mode with Si_3N_4 cantilevers, k ~ 0.6 N/m (Digital Instruments, Nanoprobes), both in ambient conditions and in a fluid cell. All *in situ* images were collected in 1 mM PBS. All protein solutions that were to be introduced into the microscope fluid cell were filtered with 0.22 μm millex-GV low protein-binding filter (Millipore, Bedford, MA) just before use. Topographic and lateral force images were collected simultaneously. Images were software flattened and are shown unfiltered.

IRRAS and Raman spectroscopy Studies. IRRAS spectra were obtained on an ATI Mattson Infinity Series FTIR spectrometer (Madison, WI) equipped with an external sample module and liquid nitrogen cooled mercury-cadmium-telluride (MCT) detector. Spectra were taken at 4 cm^{-1} resolution with an interferometer mirror speed of 50 kHz. Typically 1000 scans were averaged to yield spectra with an acceptable signal-to-noise ratio. The interferrograms were Fourier transformed using triangular apodization. Reference spectra were obtained by use of an unmodified PDC substrate. Raman spectra were obtained by a Princeton Instruments spectrometer with a coherent I-400 argon ion laser

(514 nm) and fitted with a liquid nitrogen cooled CCD detector coupled to the first half of a Spex 1401 monochromator.

Carbon film preparation. A positive photoresist, HPR 504, (Arch Chemicals) was used to form conductive carbon films. Silicon wafers were cut into approximately 1.0 x 1.0 cm or into 2.5 x 2.5 cm pieces using a diamond tip. The larger substrates were used for IRRAS studies. The pieces were then dipped in a 10:1 buffered oxide etch (BOE, 10:1 HF and Ammonium Bifluoride) solution for 30 s. They were then rinsed with water and dried by blowing with N_2 before being spin-coated with a thin layer of photoresist. The photoresist was applied manually on the silicon substrates. The photoresist was spread at 500 rpm for 10 s before spinning at 4000 rpm for 40 s in a spin coater (Solitec model 5110-CD, San Jose, CA). About 5 to 7 applications were needed to produce a final film thickness of about 5-10 μm before pyrolysis. It was noted that the final thickness of the photoresist was instrumental in the quality of carbon films obtained. Less than 5 μm thick photoresist always resulted in cracked films after pyrolysis. Pyrolysis occurred in a tube furnace fitted with a quartz tube. Prior to starting the heating cycle, the tube furnace was purged by forming gas (95% N_2, 5% H_2) for about 30 min. The purging step was necessary to remove all the air from the tube. This was because traces of oxygen in the tube adversely affected the final structure of the film. This effect is discussed in the Results and Discussion section. The photoresist films were carbonized by heating in forming gas at 1000°C. The

forming gas was flowing at about 200 cubic centimeters per minute. Samples were heated at 120°C/hour, and held at the maximum temperature for 60 min before cooling. The pyrolyzed samples were cooled to room temperature in the pyrolysis atmosphere before exposure to air. Failure to do this resulted in cracks forming on the film surface.

Electrochemical measurements. Cyclic voltammetric measurements were performed in a standard three-electrode cell or in an ordinary beaker for the 1.5 x 1.5 cm PDC electrodes used for infra-red spectroscopy. A platinum auxiliary electrode and a Ag/AgCl reference electrode were used. The cell was connected to a model AFCBP1 (Pine Instruments, Grove City, PA) potentiostat. Data was recorded with PineChem (version 2.5.2) software.

Results and Discussion.

The experiments described in the following sections deal with the preparation, characterization, electrochemical behavior, and utilization of carbon films made from a positive photoresist. I utilized scanning force microscopy (SFM) and Raman spectroscopy to study the surface morphology and microstructure of the films. Several benchmark redox probes were then used to gauge the electrochemical performance of the electrodes. Protein adsorption on the carbon films was studied using SFM and infrared reflectance absorbance spectroscopy (IRRAS). The carbon films were then chemically modified via

electrochemical reduction of diazonium salts. The effect of the resulting surface on protein adsorption was investigated using IRRAS.

Figure 6.1 shows photographs of PDC films. Figure 6.1-A is of a well formed PDC film substrate. The surface appears smooth and shiny to the naked eye with no evidence of the carbon film lifting off the silicon substrate. Figure 6.1-B is of a poorly formed PDC film substrate. The carbon film in this case does not adhere firmly to the silicon substrate. Many regions of the films have lifted off the silicon substrate exposing bare regions of the silicon surface. The film distortion was found to occur soon after removing the PDC substrates from the oven. In some cases, the film distortion occurred after the film was exposed to solution. My experience and that of others [18] shows that these poorly formed films are as a result of air leaks in the oven system. The photographs of these films are included in this chapter as a guide to future workers to the physical appearance of the carbon films.

I next studied the morphology of well-formed PDC films using SFM. Figure 6.2 is a 10 x 10 μm SFM image of a pyrolysed photoresist carbon film. The topographic image A is featureless with no evidence of segregated high and low regions as evidenced in a glassy carbon surface [19, 20]. The corresponding lateral force image B, also shows a fairly uniform friction contrast throughout the surface. These type of film surfaces have been thoroughly characterized using a variety of methods that included SFM, transmission electron microscopy (TEM), and Raman spectroscopy [21]. In all cases, the surfaces were observed to be

Figure 6.1: Photographs of PDC film substrates. (A): Photo shows a well formed film surface. The surface appears shiny and featureless to the naked eye. (B): Photo shows a poorly formed film. The film can be seen lifting off the silicon substrate just after removing it from the oven.

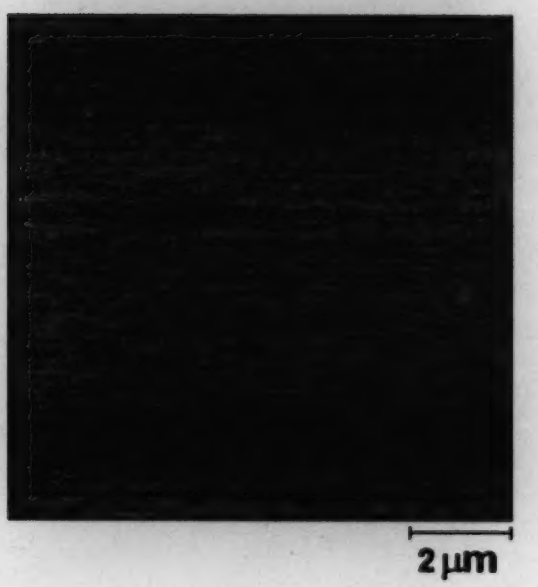

Figure 6.2: 10×10 μm SFM images of a PDC substrate obtained in 1 mM PBS. (A): Topographic image (z-scale = 10 nm). (B): Corresponding lateral force image (z-scale = 0.2 V).

smooth with no observable features. Compared to other carbon electrodes, the smoothness of PDC films is exceptional, approaching that of the atomically smooth highly oriented pyrolytic graphite (HOPG), whose root mean square (rms) roughness value as determined by scanning tunneling microscopy (STM), is 0.24 nm [11]. Reported roughness for glassy carbon (GC) ranges from 4.1 ± 0.1 nm from STM [22] to 44 ± 6 nm from SFM [23]. PDC films used in this work had rms roughness of 0.38 ± 0.06 nm. This is in agreement with values reported in the literature for smooth PDC films [21].

The nature of the graphitic microstructure of the carbon films was obtained by use of Raman spectroscopy studies. Raman spectra of the PDC film were acquired to assess the development of the characteristic sp^2 carbon bands at ~ 1360 (D) and ~ 1580 (E_{2g}) cm^{-1}. The D and E_{2g} bands have been studied extensively and their peak ratio (D/E_{2g}) has been correlated with disorder of the sp^2 carbon matrix [10, 24]. A larger D/E_{2g} ratio correlates with smaller graphite crystallite size (L_a), and indicates greater disorder. Figure 6.3 is a Raman spectrum of a PDC substrate. The "D" band occurred at 1330 cm^{-1} while the "E_{2g}" band occurred at 1580 cm^{-1}. The D/E_{2g} intensity ratio was found to be 0.94. Fractured GC has been found to have an intensity ratio of 1.2, implying the presence of a greater number of exposed edge planes and smaller microcrystallites. Figure 6.3 indicates that the microcrystallite size of the PDC films is in between those of HOPG and GC electrodes [21, 25]. The surfaces were then modified via electrochemical

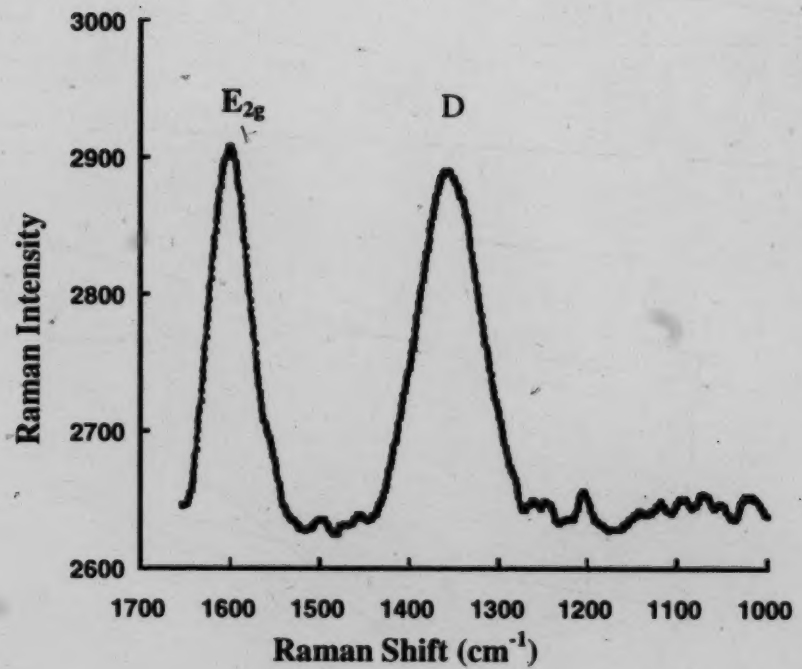

Figure 6.3: Raman spectra (515 nm) of a PDC film substrate.

reduction of diazonium salts. Figure 6.4 is a cyclic voltammogram for the reduction of 5 mM of 4-phenylacetic acid tetrafluoroborate (PAA) in 0.1 M tetrabutylammonium tetrafluoroborate in acetonitrile (Bu_4NBF_4/CH_3CN) on a PDC surface. The chemically irreversible cathodic wave corresponds to the reduction of PAA to a phenylacetic acid radical. The wave is similar to those obtained for the reduction of diazonium salts on GC and HOPG surfaces [26, 27]. Because of the ease of synthesizing diazonium salts bearing different functional groups, the PDC films can be modified by attaching different aryl groups to the surface using electrochemical reduction of diazonium salts. In the following sections, I present results of some applications of the modified surfaces, including controlling protein adsorption.

Electrode kinetics at carbon surfaces have been studied extensively [10, 28]. In general, carbon electrode surfaces are ill-defined on the atomic level, and electron-transfer rates are strongly dependent of surface history. In this work, I have used $Fe(CN)_6^{3-/4-}$, $Ru(NH_3)_6^{2+/3+}$, and $Eu_{aq}^{2+/3+}$ redox systems to study electron-transfer rates on PDC films. The effect of electrochemical modification of the PDC films on electron-transfer of the three redox systems was also investigated. Figure 6.5 contains cyclic voltammetric current-potential curves for 1 mM $Fe(CN)_6^{3-/4-}$ (1 M KCl). Curve A of Figure 6.5 is the voltammogram at an unmodified PDC substrate. The value for the voltammetric peak separation (ΔE_p) of 90 mV in curve A of Figure 6.5 is a diagnostic of a carbon surface

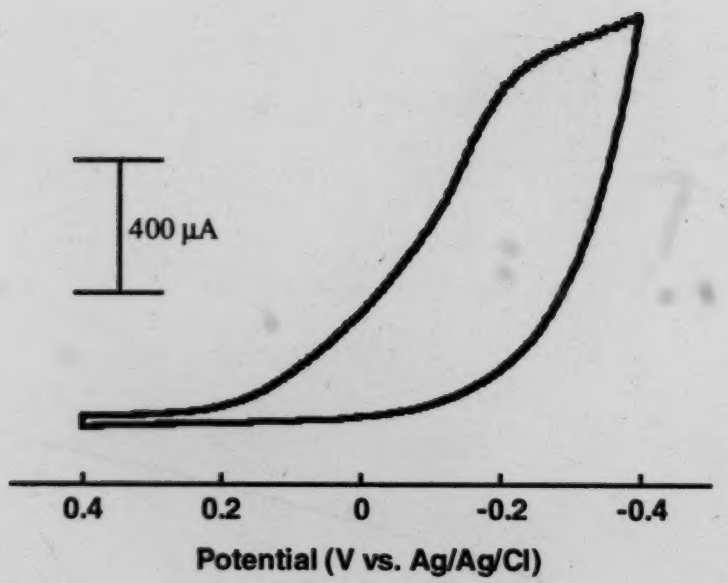

Figure 6.4: Cyclic voltammogram for the reduction of 5 mM PAA in (0.1 M Bu_4NBF_4/CH_3CN) on a PDC surface. Scan rate: 100 mV/s.

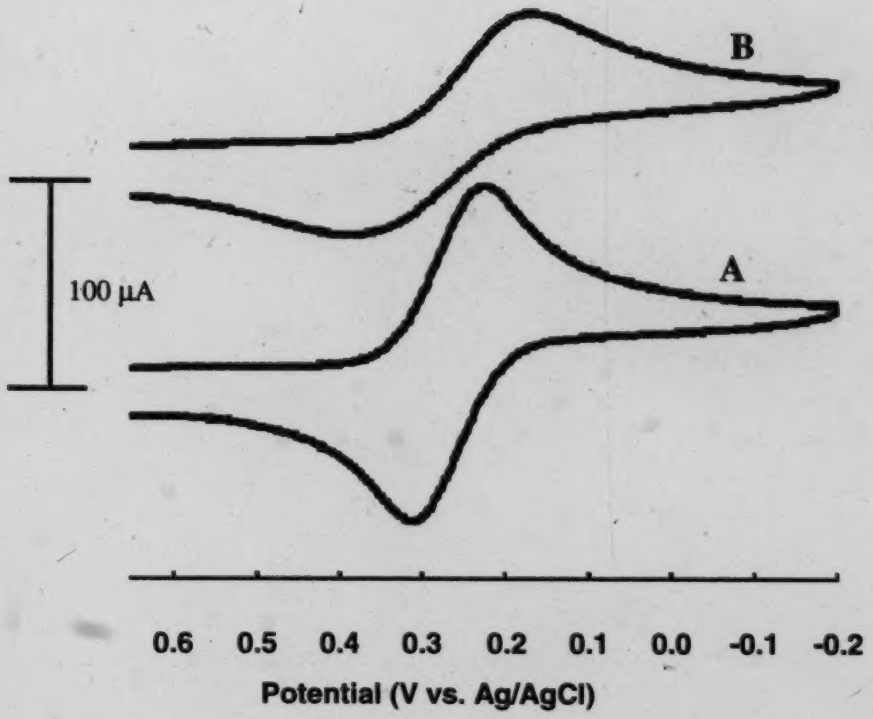

Figure 6.5: Cyclic voltammetry of 1 mM $Fe(CN)_6^{3-/4-}$ (1 M KCl) on PDC. Curve (A) corresponds to an unmodified PDC substrate. Curve (B) is on a PDC substrate modified with one cycle in 5 mM DDEA (0.1 M Bu_4NBF_4/CH_3CN).

exhibiting reasonable electron-transfer rate. The heterogeneous electron-transfer rate of $Fe(CN)_6^{3-/4-}$ has been correlated with carbon electrode microstructure, and increases with increasing edge plane density [29]. For example, the basal plane of highly ordered pyrolytic graphite (HOPG) exhibits slow electron-transfer rate while GC and edge plane HOPG which have a higher density of edge sites exhibit much faster electron-transfer rates [13]. After this voltammogram was collected, the cell was rinsed and filled with 5 mM DDEA. The potential was cycled once in the manner of Figure 6.4 to induce the deposition of diethylaniline (DEA). Curve B of Figure 6.5 is the $Fe(CN)_6^{3-/4-}$ voltammogram on the resultant PDC film surface. The measured ΔE_p value of 220 mV reflects a significant decrease in the electron-transfer rate from the unmodified electrode due to blocking by the bound DEA film. Similar results have been obtained on studies carried out on HOPG surfaces [27].

Studies were then carried out using the $Ru(NH_3)_6^{2+/3+}$ redox system. Curve A of Figure 6.6 is the voltammogram at an unmodified PDC substrate. In this case, the value of ΔE_p was also 90 mV. This shows that the redox system exhibits reasonable electron-transfer rate on the PDC surface. The surface was then modified in the same manner as described above. Curve B of Figure 6.6 is the $Ru(NH_3)_6^{2+/3+}$ voltammogram on the resultant PDC modified surface. The measured ΔE_p value of 160 mV reflects a fairly significant decrease in the electron-transfer rate from the unmodified electrode. However, the decrease in

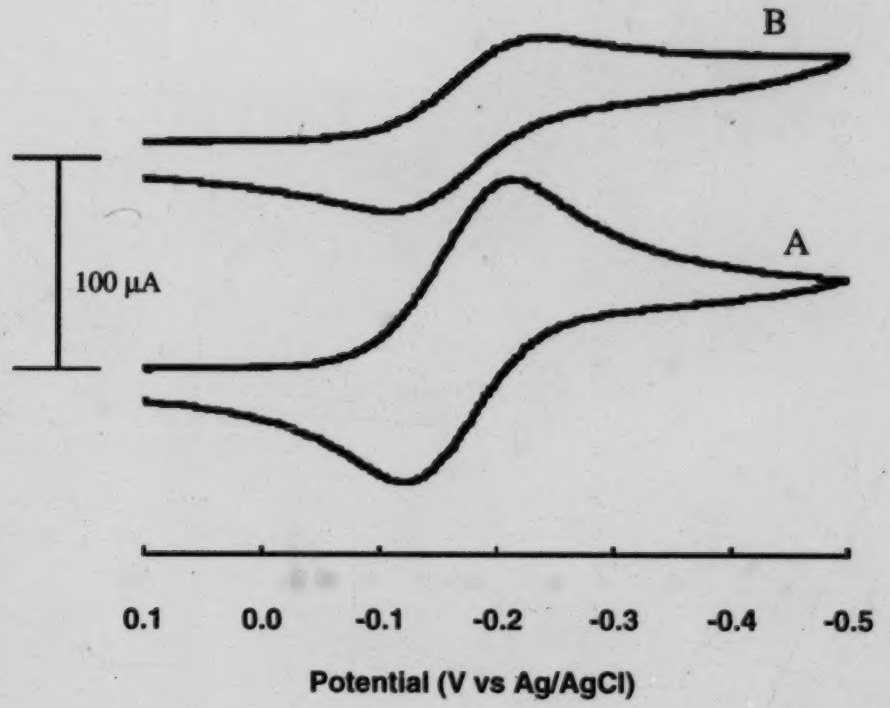

Figure 6.6: Cyclic voltammetry of 1 mM $Ru(NH_3)_6^{2+/3+}$ (1 M KCl) on PDC. Curve (A) corresponds to an unmodified PDC substrate. Curve (B) is on a PDC substrate modified with one cycle in 5 mM DDEA (0.1 M Bu_4NBF_4/CH_3CN).

electron-transfer rate as shown by the ΔE_p value is smaller than that of the $Fe(CN)_6^{3-/4-}$ redox system. This is because the $Ru(NH_3)_6^{2+/3+}$ redox system is an outer-sphere system that shows minor kinetic effects of surface modification even when a compact organic monolayer is chemisorbed to the surface [30]. The electron-rate was reduced only by an amount consistent with electron tunneling through the monolayer.

I then studied the effect of the surface modification on the $Eu_{aq}^{2+/3+}$ redox system. Curve A of Figure 6.7 is the voltammogram at an unmodified PDC substrate. The ΔE_p value of 580 mV obtained in curve a of Figure 6.7 is typical of the redox system on carbon surfaces with a low density of surface oxides [31]. The surface was then modified in the same manner as described for the $Fe(CN)_6^{3-/4-}$ redox system. Curve B of Figure 6.7 is the $Eu_{aq}^{2+/3+}$ voltammogram on the resultant PDC film surface. The measured ΔE_p value of 1400 mV reflects a very significant decrease in the electron-transfer rate from the unmodified electrode. Electron-transfer rate for aquated metal systems like $Eu_{aq}^{2+/3+}$ is governed by surface carbon-oxygen groups at carbon electrodes [31, 32]. The PDC films are low in carbon-oxygen groups initially. Hence the observed blocking behavior cannot be attributed to a reduction in these functionalities [21]. The behavior can be attributed to the presence of a spacer between the redox system and the electrode. Increased tunneling distance for electron-transfer due to the grafted film slows down the rate of electron-transfer [33]. In all cases, the

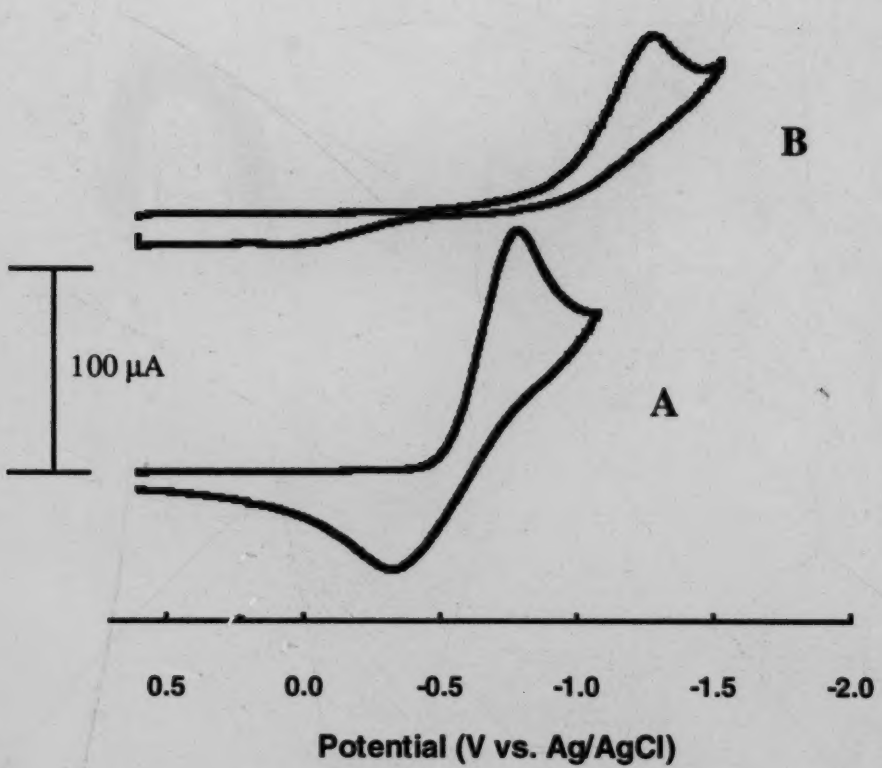

Figure 6.7: Cyclic voltammetry of 1 mM $Eu^{2+/3+}$ (1 M KCl) on PDC. Curve (A) corresponds to an unmodified PDC substrate. Curve (B) is on a PDC substrate modified with one cycle in 5 mM DDEA (0.1 M Bu_4NBF_4/CH_3CN).

electrochemical studies were carried out on PDC films that had minimum exposure to air. Background voltammograms with an uncoated silicon sample showed no voltammetric features.

Table 6.1 provides a summary of results from electrochemical characterizations of PDC surfaces modified by one potential cycle in 5 mM DDEA and 5 mM NB respectively. Data for both unmodified GC and PDC surfaces is also presented for comparison purposes. The ΔE_p values for $Fe(CN)_6^{3-/4-}$ and $Ru(NH_3)_6^{2+/3+}$ redox systems are comparable on both unmodified surfaces. However, the ΔE_p value for $Eu^{2+/3+}$ redox systems is about three times higher for GC when compared to PDC. These results imply that GC and PDC have similar surface microstructure but with the PDC electrodes having a lower density of surface oxides [14]. For the $Fe(CN)_6^{3-/4-}$ redox system, an average ΔE_p value of 341 mV was obtained for the surface modified with a NB film compared to 232 mV for the DDEA modified surface. It appears from these results that the NB modified surface blocks electron-transfer more effectively than the DEA modified surface. This may be due to the formation of a more compact layer. The electron-transfer rates for the $Ru(NH_3)_6^{2+/3+}$ on the two surfaces was found to be similar when the margin of error was taken into account. This result is not surprising since the $Ru(NH_3)_6^{2+/3+}$ redox system has been shown to be an outer sphere redox system [15]. An average ΔE_p of 1483 mV was obtained for the $Eu^{2+/3+}$ redox systems on the DDEA modified surface, while an average ΔE_p value of 1046 mV

Substrate	ΔE_p (mV)		
	$Fe(CN)_6^{3-/4-}$	$Ru(NH_3)_6^{3+/2+}$	$Eu^{3+/2+}$
Unmodified GC	78 ± 10	80 ± 9	203 ± 21
Unmodified PDC	87 ± 2	91 ± 4	611 ± 41
PDC modified with 5 mM DDEA	232 ± 13	162 ± 5	1483 ± 69
PDC modified with 5 mM NB	341 ± 23	119 ± 2	1046 ± 26

Table 6.1: Results from electrochemical characterizations of photoresist-derived carbon films. The surfaces were modified by one potential cycle in 5 mM of the corresponding diazonium salt. Scan rate was 100 mV/s for all systems. Potentials are versus Ag/AgCl reference electrode. For comparison, data for both unmodified GC and PDC substrates is also presented. Data is given for three trials each.

was obtained for the NB modified surface. In both cases, significant decrease in electron-transfer is observed when compared to the unmodified surfaces. Assuming similar film formation on the PDC surfaces, electron tunneling should occur faster through the less compact film [15]. The $Eu_{aq}^{2+/3+}$ redox system exhibits a faster electron-transfer rate on the NB modified surfaces either because the film formed was less compact, hence easier electron tunneling, or because of other interactions between the redox system and the grafted film. surface. For example, the suppression of the electrochemical response of $Fe(CN)_6^{3-/4-}$ redox system at GC surfaces modified with NB has been attributed to hydrophobicity of the film [34].

I next used SFM to characterize the PDC film structure after modifying the surface by attaching a DEA thin film via electrochemical reduction of DDEA. Figure 6.8 is comprised of 20 x 20 μm^2 SFM images of a PDC substrate following one deposition cycle in 5 mM DDEA. Part A of Figure 6.6 is the topographic image while part B is the corresponding lateral force image. Observed in the topographic image is a film of uniform height. Several 3-dimensional features are however apparent in several places which exhibit a larger height than the surrounding layer. These segregated spherical structures range in height from 3 to 14 nm. These types of features have been observed on highly oriented pyrolytic graphite (HOPG) and glassy carbon (GC) surfaces [27]. In Chapters II and III, their formation was attributed to a polymerization type reaction between the bound monolayer and the free radicals in solution. The surface exhibits a fairly uniform

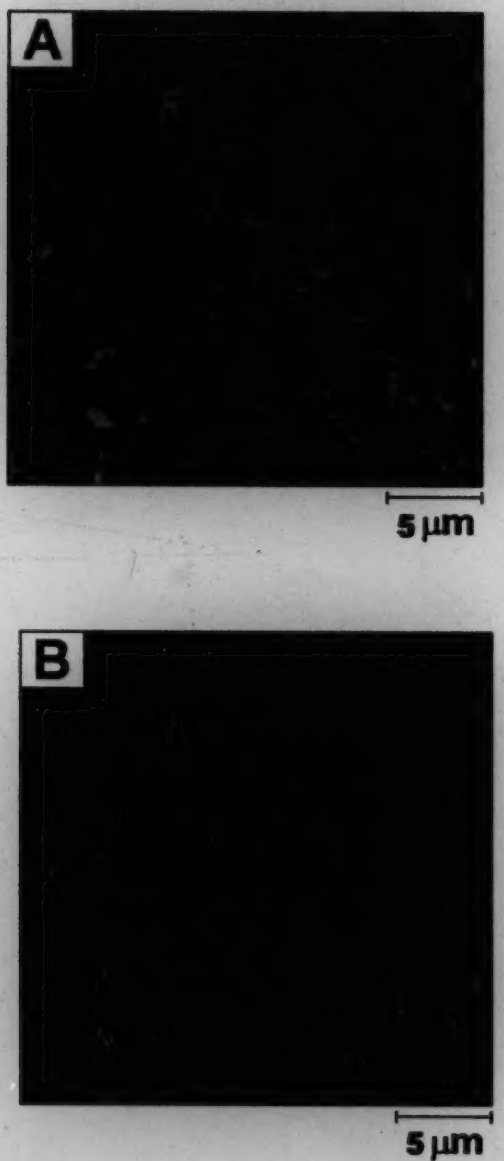

Figure 6.8: 20×20 µm SFM images of a PDC substrate obtained in ambient air. (A): Topographic image (z-scale = 20 nm). (B): Corresponding lateral force image (z-scale = 0.2 V).

frictional contrast as shown in part B of Figure 6.8. These observations are consistent with a uniform well-packed DEA layer bound to the PDC surface. The higher topographical features show a higher frictional contrast than the surrounding layer most likely due to a mechanical "tripping" of the tip [35].

When biomaterials are implanted in the human body, proteins adsorb on the biomaterial surface within a few seconds. Later, cells arrive at the surface, interacting with the adsorbed layer rather than with the biomaterial itself. The biocompatibility of a material is therefore affected by the initial event of protein adsorption, which then influences any further biological reaction. I believe PDC films will serve as a good model surface for more complex LTIC biomaterials in SFM studies. I report the results of my SFM studies on protein adsorption on a PDC film. Figure 6.9 is 20 x 20 μm^2 topographic image of a PDC substrate following adsorption of 20 µg/mL bovine serum albumin (BSA) in 1mM phosphate buffered saline (PBS) for one hour. The film morphology is comprised of many strand-like aggregates that measure between 3 and 6 nm in height. Tip-induced displacement of the protein film was observed. This shows that the protein aggregates were not stable to imaging at the normal forces of < 10 nN in PBS used in this study. Aggregates of BSA on various surfaces have been reported. For example, Sheller et al. have reported BSA aggregates with a thickness of ~ 3.6 nm on a methyl-terminated hydrophobic monolayer formed on silicon wafers [36]. Aggregates of BSA have also been observed on polystyrene substrates [37]. I note that the results presented in this chapter are preliminary and

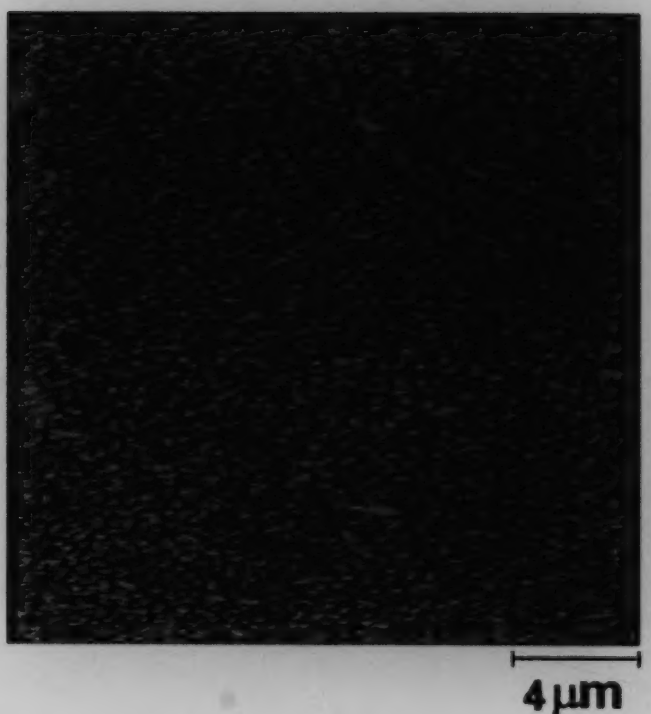

Figure 6.9: 20 × 20 µm SFM topographic image of a PDC substrate obtained in 1 mM PBS following adsorption 0f 20 µg/mL BSA for one hour. (z-scale = 15 nm).

more work needs to be done to effectively evaluate the effect of the PDC surfaces on protein adsorption.

Infrared reflectance absorbance spectroscopy (IRRAS) was employed to assess the structure of the adsorbed protein. Proteins and peptides exhibit characteristic bands in this spectral region, which are the direct result of vibrations in the peptide linkages. Specifically, the amide I band (C=O stretch) appears in the region from 1650 to 1680 cm^{-1} and the amide II (combination of C-N stretch and N-H bend) is generally locate in the vicinity of 1550 cm^{-1}. These bands typically exhibit high intensity and are useful as a diagnostic of adsorbed proteins [38]. Figure 6.10 contains IRRAS spectrum from 2000 to 1000 cm^{-1} of a PDC substrate after exposure to 20 μg/mL HFG for one hour. Strong absorbencies corresponding to amide I (ν_{aI} = 1671 cm^{-1}) and amide II bands (ν_{aII} = 1540 cm^{-1}) are observed, diagnostic of HFG adsorption to the PDC surface. The amide I band of dissolved or solid HFG is ~ 1650 cm^{-1}. Hence, my results imply a degree of adsorption-induced conformation changes [38]. My results are similar to those from studies of protein adsorption using IRRAS on gold surfaces. For example, Ta and McDermott have used IRRAS to correlate protein adsorption to hydrophobic and hydrophilic surfaces [39].

I next employed IRRAS to assess the amount of HFG adsorbed on DEA modified PDC surfaces. Spectrum A of Figure 6.11 corresponds to the PDC surface modified by a five minute potential step at – 1.0 V in 5 mM DDEA. In this case ν_{aI} was observed at 1679 cm^{-1}, while ν_{aII} was observed at 1530 cm^{-1}.

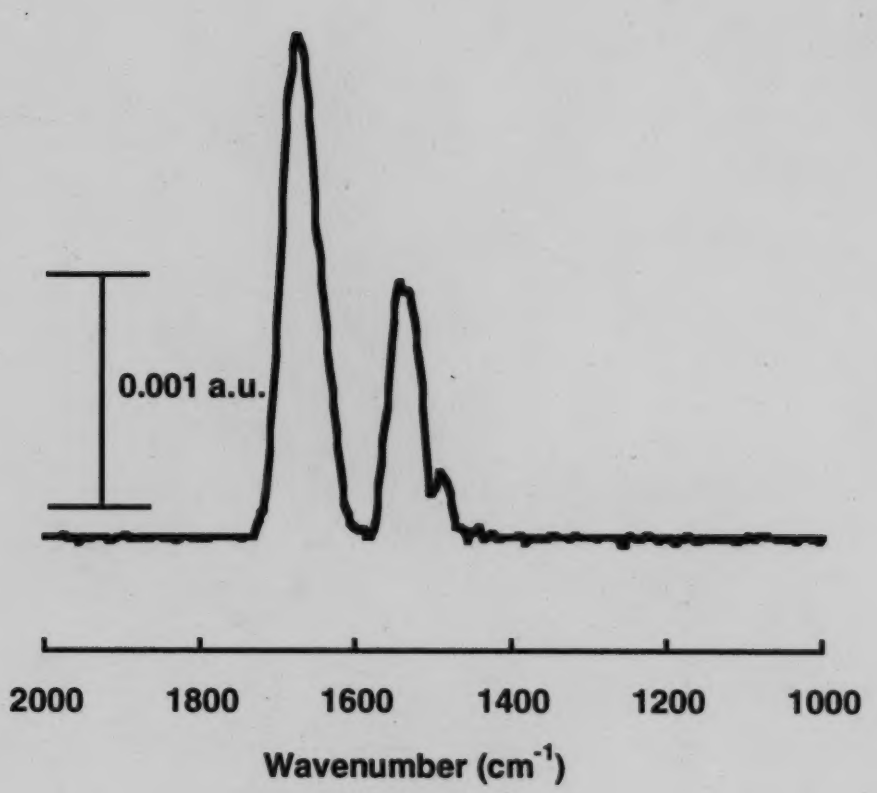

Figure 6.10: IRRAS spectra of a PDC substrate following adsorption of 20 µg/mL HFG in 1 mM PBS for one hour.

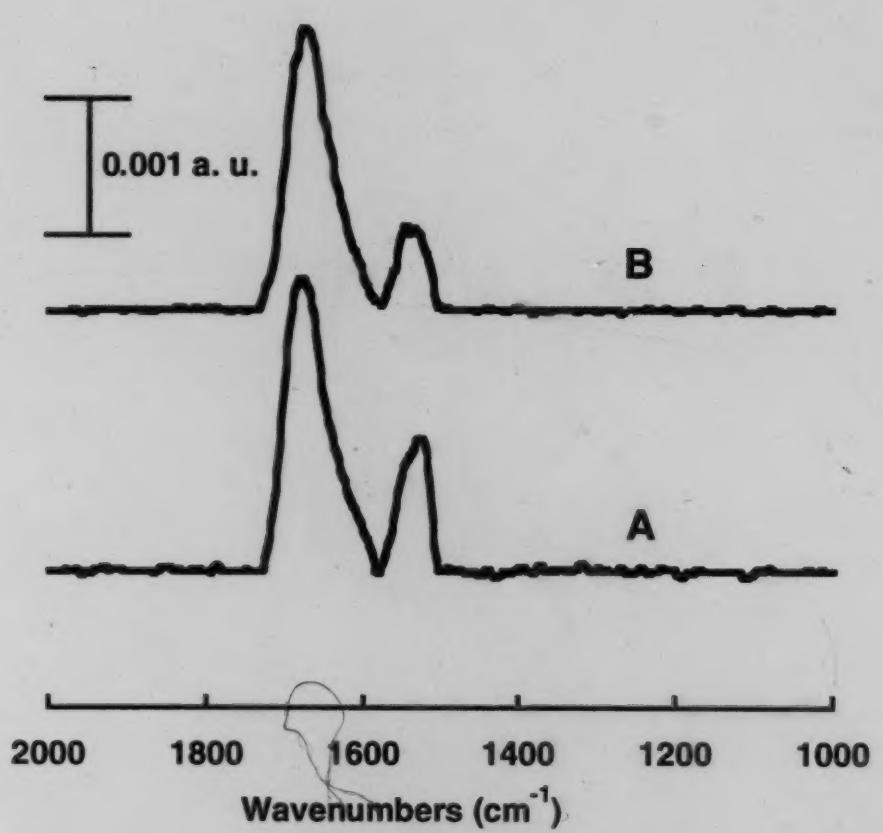

Figure 6.11: IRRAS spectra of a PDC substrate following adsorption of 20 µg/mL HFG in 1 mM PBS for one hour. (A): Surface modified via a 5 minutes potential step at – 1 0V in 5 mM DDEA (0.1 M Bu_4NBF_4/CH_3CN). (B): Surface modified via a 5 minutes potential step at – 1.0 V in 5 mM PAA (0.1 M Bu_4NBF_4/CH_3CN).

The position of the amide I band implies further denaturation of the protein upon adsorption on the modified surfaces. Spectrum B of Figure 6.9 corresponds to the PDC surface modified by a five minute potential step at – 1.0 V in 5 mM PAA. In this case ν_{aI} was observed at 1546 cm^{-1}, while ν_{aII} was observed at 1675 cm^{-1}. The absorbance of the amide II bands (A_{aII}) are related to the amount of protein bound to the surface and can be used to quantitate the binding of proteins to surfaces [38, 40]. In spectrum A of Figure 6.9, A_{aII} = 0.00098 a.u., while A_{aII} in spectrum B of Figure 6.9 is 0.00062 a.u. The A_{aII} band for the DEA modified surface is approximately one and a half times as high in intensity when compared to the A_{aII} for the PAA modified surface. The coverage of HFG is higher on the more hydrophobic DEA terminated surface when compared to the hydrophilic terminated PAA surface. Generally, proteins have been shown to adsorb more readily to hydrophobic surfaces [41]. Covalent modification of carbon surfaces with hydrophilic molecules have been shown to reduce protein adsorption [42].

Conclusions

I have demonstrated the fabrication of PDC carbon films from the pyrolysis of photoresist. The material was found to be suitable for electrochemistry, and its electron-transfer kinetics for several benchmark systems was comparable to that of GC. In addition, PDC surfaces may be fabricated lithographically, into microstructures or in any desired shapes or configurations. The ease and low cost of making the films makes mass production of PDC components feasible. The

ability to chemically modify the already well-defined surfaces via electrochemical reduction of diazonium salts affords the possibility of producing electrodes with tailor-made properties. I have also demonstrated the possibility of using the PDC surface as a model for carbon biomaterials. Protein adsorption on the surfaces showed the expected amide I and amide II bands. Because the PDC surfaces have just recently gained much interest as an alternative to the more widely used GC, there remains a lot to be done to fully understand the chemical and physical nature of the PDC films and to explore its application.

References

1. A. M. Lyons, L. P. Hale, and C. W. Wilkins, *J. Vac. Sci. Technol.* B 3 : 447 (1984).

2. A. M. Lyons, *J. Non-Crystalline Solids* 70: 99 (1985).

3. R. Kostecki, X. Song, and K. Kinoshita, *Electrochem. Solid-State Lett.* 2(9): 465 (1999).

4. K. Kinoshita, X. Song, J. Kim, and M. Inaba, *Journal of Power Sources* 81-82: 170 (1999).

5. T. C. Ta, M. T. Sykes, and M. T. McDermott, *Langmuir* 14: 2435 (1998).

6. J. Tamayo, M. Miles, A. Thein, and P. Soothill, *J. Struct. Biol.* 128: 200 (1999).

7. M. D. Garrison, T. C. McDevitt, R. Luginbuhl, C. M. Giachelli, P. Stayton, and B. D. Ratner, *Ultramicroscopy* 82: 193 (2000).

8. M. Datta, J. J. Freeman, and R. E. W. Jansson, *Spectroscopy Letters* 18: 273 (1985).

9. M. D. Porter, D. H. Karweik, T. Kuwana, W. B. Theis, G. B. Norris, and T. O. Tiernan, *Appl. Spectrosc.* 38(1): 11 (1984).

10. R. L. McCreery, in *Electronalytical Chemistry*, Vol. 17 (A. J. Bard, ed.), Marcel Dekker, New York, 1991, p. 221.

11. M. T. McDermott, K. Kneten, and R. L. McCreery, *J. Phys. Chem.* 96: 3124 (1992).

12. K. R. Kneten and R. L. McCreery, *Anal. Chem.* 64: 2518 (1992).

13. K. K. Cline, M. T. McDermott, and R. L. McCreery, *J. Phys. Chem.* 98: 5314 (1994).

14. P. Chen and R. L. McCreery, *Anal. Chem.* 68: 3958 (1996).

15. H.-H. Yang and R. L. McCreery, *Anal. Chem.* 71: 4081 (1999).

16. M. Delamar, R. Hitmi, J. Pinson, and J.-M. Saveant, *J. Am. Chem. Soc.* 114: 5883 (1992).

17. M. F. W. Dunker, E. B. Starkey, and G. L. Jenkins, *J. Am. Chem. Soc.* 58: 2308 (1936).

18. S. Ranganathan, , Personal Communication, 2000.

19. W. H. Smyrl, R. T. Atanasoski, L. Atanasoska, L. Hartshorn, M. Lien, K. Nygren, and E. A. Fletcher, *J. Electroanal. Chem.* 264: 301 (1989).

20. M. T. McDermott and R. L. McCreery, *Langmuir* 10: 4307 (1994).

21. S. Ranganathan, R. L. McCreery, S. M. Majji, and M. Madou, *J. Electrochem. Soc.* 147(1): 277 (2000).

22. M. T. McDermott, C. A. McDermott, and R. L. McCreery, *Anal. Chem* 65: 937 (1993).

23. Q. Chen and G. M. Swain, *Langmuir* 14: 7017 (1998).

24. R. J. Rice, N. M. Pontikos, and R. L. McCreery, *J. Am. Chem. Soc.* 112 (1990).

25. R. J. Bowling, R. T. Packard, and R. L. McCreery, *J. Am. Chem. Soc.* 111: 1217 (1989).

26. P. Allongue, M. Delamar, B. Desbat, O. Fagebaume, R. Hitmi, J. Pinson, and J.-M. Saveant, *J. Am. Chem. Soc.* 119: 201 (1997).

27. J. K. Kariuki and M. T. McDermott, *Langmuir* 15: 6534 (1999).

28. K. Kinoshita, *Carbon: Electrochemical and Physicochemical Properties*, Wiley, New York, 1988.

29. R. J. Rice and R. L. McCreery, *Anal. Chem.* 61: 1637 (1989).

30. P. Chen, M. A. Fryling, and R. L. McCreery, *Anal. Chem.* 67: 3115 (1995).

31. C. A. McDermott, K. R. Kneten, and R. L. McCreery, *J. Electrochem. Soc.* 140: 2593 (1993).

32. R. L. McCreery, K. K. Cline, C. A. McDermott, and M. T. McDermott, *Colloids Surfaces A* 93: 211 (1994).

33. C.-T. Kuo and R. L. McCreery, *Anal. Chem.* 71: 1553 (1999).

34. C. Saby, B. Ortiz, G. Y. Champagne, and D. Belanger, *Langmuir* 13: 6805 (1997).

35. G. Meyer and N. M. Amer, *Appl. Phys. Lett.* 56: 2100 (1990).

36. N. B. Sheller, S. Petrash, and M. D. Foster, *Langmuir* 14: 4535 (1998).

37. X. Chen, M. C. Davies, C. J. Roberts, S. J. B. Tendler, and P. M. Williams, *Langmuir* 13: 4106 (1997).

38. B. Liedberg, B. Ivarsson, and I. Lundstrom, *J. Biochem. Biophys. Met.* 9: 233 (1984).

39. T. C. Ta and M. T. McDermott, *Anal. Chem.* 72: 2627 (2000).

40. W. G. Pitt, S. H. Spiegelberg, and S. L. Cooper, in *Proteins at Interfaces: Physicochemical and Biochemical Studies* (J. L. Brash and T. A. Horbett, eds.), American Chemical Society, Washington DC, 1987, p. 324.

41. S. O. Vansteenkiste, S. I. Corneillie, E. H. Schacht, X. Chen, M. C. Davies, M. Moens, and L. Van Vaeck, *Langmuir* 16: 3330 (2000).

42. H. Maeda, T. Okada, Y. Matsumoto, K. Katayama, Y. Yamauchi, and H. Ohmori, *Anal. Sci.* 15: 633 (1999).

Chapter VII

Conclusions and Future Work

Overall Conclusions

The first report of chemical modification of carbon surfaces by aryl radicals generated from the electrochemical reduction of diazonium salts was reported by Saveant *et al.*, in 1992 [1]. Since then, there have been numerous reports in the literature on the various applications of this method. A recent review by Downard summarizes these applications [2].

Carbon microstructure is one of the properties of carbon electrodes that affect their electrochemical reactivity. My research was geared towards exploring in greater detail the nucleation and growth of films formed from the reduction of diazonium salts on carbon surfaces with an aim to determine how the carbon microstructure affects film growth. I utilized electrochemical characterizations and infrared reflectance absorption spectroscopy (IRRAS) to provide a macroscopic picture of the development of films on various carbon surfaces. Scanning force microscopy (SFM) as well as scanning tunneling microscopy (STM) were used to probe the growth of the films at a microscopic scale. Another aspect of my research was to apply the thin films formed on the carbon surfaces towards controlling protein adsorption on the surfaces. I studied the nature of the interactions between different proteins and the carbon surfaces, with an aim of

making use of the ease and versatility of the derivatization method to fabricate more biocompatible carbon surfaces.

Electrochemical blocking and SFM imaging both indicated that aryl films formed on highly oriented pyrolytic graphite (HOPG) from the electrochemical reduction of diazonium salts initiate at cleavage steps. By use of STM, clear images of nucleation on the basal plane were seen. The nucleation likely occurred at sites that are distinct from the cleavage defects. These sites are likely atomic scale defects (i.e., vacancies) on the otherwise pristine basal plane. The structure of the completed film consisted of 3-dimensional features, which formed via a polymerization type reaction between the bound monolayer and the free radicals in solution. After thoroughly characterizing the films formed on HOPG surfaces, the study was extended to the more widely used glassy carbon (GC) surface. SFM and IRRAS studies showed that more than monolayer coverage could also be formed on GC surfaces at longer deposition times.

Photoresist derived carbon films (PDC) were also used in my research. The films were found to be suitable for electrochemistry, and their electron-transfer kinetics for several benchmark redox systems were comparable to those of GC electrodes. The surfaces were chemically modified via the electrochemical reduction of diazonium salts method. The ability to chemically modify the already well-defined surfaces affords the possibility of producing electrodes with tailor-made properties. The possibility of using the PDC surface as a model biomaterial

was demonstrated. Using IRRAS, adsorbed protein adsorbed on the surfaces showed the expected amide I and amide II bands.

Interaction of adsorbed protein with other carbon surfaces was also investigated. Using SFM, it was shown that the morphology of fibrinogen films depends on the nature of the substrate. Changing the chemistry of the carbon surface through chemical modification changes the conformation and orientation of the adsorbed protein as shown by the differences in physical features. I extended the modification scheme used on GC and HOPG surfaces to a heart valve made from low temperature isotropic carbon (LTIC). My results showed that the modification scheme could be successfully carried out on the LTIC surfaces. The extension of this easy and versatile modification scheme to LTIC, a material that shows a fair degree of biocompatibility, may ultimately lead to the production of a more biocompatible material.

Suggestions for Future Work

A few suggestions towards exploring further some aspects of my research will be put forward. Due to conflicting reports regarding the electrochemical blocking of the films, further work needs to be carried out to gain further insight of the nature of the films formed on the carbon electrodes. Further research is also needed to obtain more details on the mechanism behind the formation of multilayers on the carbon electrodes. This should involve formation of films

bearing different functional groups with a view of determining any effect of the functional groups on the film structure. It would be desirable if a combination of SFM and other surface analysis methods like ellipsometry could be employed to provide more details on the nature of film formation on carbon surfaces.

More research is also needed to fully determine the utility of these thin films toward controlling protein adsorption. Adsorption of different proteins on the films should be studied on various surfaces to fully understand the effect of these films on the adsorbed proteins.

It would be interesting to study the formation of mixed monolayers on carbon surfaces. This would involve grafting of films on the same surface that bear different functionalities. Such surfaces might be useful in fabrication of sensors. Preliminary results not reported in this work showed the possibility of grafting films with both hydrophobic and hydrophilic end groups.

Many covalent attachment schemes have been used to immobilize enzymes to electrode surface [3-6]. Most attempts have centered on coupling enzymes to a carbon surface via a cyanuric chloride [4] or carbodiimide linkage [5]. Attachment of enzymes to a carbon surface through avidin-biotin coupling has also been reported [7]. The attachment of functional groups on carbon via reduction of diazonium salts affords a versatile way of attaching biomolecules mainly through a carbodiimide linkage. In view of the importance of these types of reactions, there is a need to investigate the coupling of biomolecules on the modified carbon surfaces.

References

1. M. Delamar, R. Hitmi, J. Pinson, and J.-M. Saveant, *J. Am. Chem. Soc.* 114: 5883 (1992).

2. A. J. Downard, *Electroanalysis* 12: 1085 (2000).

3. A. W. C. Lin, P. Yeh, A. M. Yacynych, and T. Kuwana, *J. Electroanal. Chem.* 84: 411 (1977).

4. R. M. Ianniello and A. M. Yacynych, *Anal. Chem.* 53: 2090 (1981).

5. R. M. Ianniello, T. J. Lindsay, and A. M. Yacynych, *Anal. Chem.* 54: 1980 (1982).

6. C. Bourdillon, J. P. Bourgeois, and D. Thomas, *J. Am. Chem. Soc.* 102: 4231 (1980).

7. P. Pantano, H. Morton, and W. G. Kuhr, *J. Am. Chem. Soc.* 113: 1833 (1991).